2014

Surface stress detection and mechanism study with microcantilever based sensor for biomolecular monolayers

Yue Zhao
Iowa State University

Surface stress detection and mechanism study with microcantilever based sensor for biomolecular monolayers

by

Yue Zhao

A dissertation submitted to the graduate faculty

in partial fulfillment of the requirements for the degree of

DOCTOR OF PHILOSOPHY

Major: Mechanical Engineering

Program of Study Committee:
Pranav Shrotriya, Major Professor
Sriram Sundararjan
Shankar Subramaniam
Marit Nilsen-Hamilton
Monica Lamm

Iowa State University

Ames, Iowa

2014

TABLE OF CONTENTS

Page

ACKNOWLEDGEMENTS iv

ABSTRACT v

CHAPTER 1 OVERVIEW 1

CHAPTER 2 LITERATURE REVIEW 3
- Micro-Cantilever Based Sensor 3
- Differential Interferometer and Sensor Configurations 5
- DNA Hybridization Induced Cantilever Deflection 8
- Mechanism Exploration and Simulation Approaches 10

CHAPTER 3 DETECTION OF CANTILEVERDEFLECTION DUE TO MALACHITE GREEN/APTAMER BINDING 15
- Abstract 15
- Introduction 15
- Materials and Methods 17
- Experimental Procedures 20
- Results 21
- Discussions 23
- Conclusion 27

CHAPTER 4. MECHANISM STUDY ON CANTILEVER DEFLECTION DUE TO ALKANETHIOL SELF-ASSEMBLED MONOLAYER IMMOBILIZATION ON CANTILEVER SURFACE 29
- Abstract 29
- Introduction 30
- Surface Stress Measurement 33
- Experimental Results 36
- Overall Energy of the System due to SAM adsorption 39
- Energy Models Associated with Alkanethiol SAM layer 40
- Energy Models Associated with Gold Substrate 41
- Simulation Models and Surface Stress Predictions 43
- Modeling Results and Discussions 46
- Comparison of Numerical Predictions with Experimental Reports 51
- Conclusions 52

CHAPTER 5. CANTILEVER DEFLECTION ASSOCIATED WITH HYBRIDIZATION OF MONOMOLECULAR DNA FILM 54
- Abstract 54

Introduction 55
Theoretical Model 59
Initial DNA Ensembles 64
Cantilever Bending Computation 66
Simulation Results and Discussions 68
Comparison of Numerical Prediction with Experimental Reports 74
Conclusions 77
Acknowledgements 78

CHAPTER 6. INFLUENCES MOLECULAR CONFIGURATION AND CONFORMATION ON CANTILEVER DEFLECTION ASSOCIATED WITH DNA HYBRIDIZATION 79
Introduction 79
Experimental Observations 81
Distributions and Configurations of Hybridized DNA 84
Energy Models and Cantilever Bending Predictions 87
Model Results 93
Comparison of Numerical Prediction with Experimental Reports 99
Conclusions 102

CHAPTER 7. CONCLUSIONS 104

BIBLIOGRAPHY 108

ACKNOWLEDGEMENTS

First and foremost, I would like to thank my advisor Professor Pranav Shrotriya for his guidance, help and patience during the journey of this project. Without his support, the work could not have been accomplished.

I would also like to express my gratitude and appreciation to all my committee members: Professor Sriram Sundararajan, Professor Shankar Subramaniam, Professor Marit Nilsen-Hamilton and Professor Monica Lamm for serving on my POS committee and providing me with all the valuable inputs for my research.

My thanks extend to all professors and colleagues in the project, particularly to Professor Marit Nilsen-Hamilton and Professor Baskar Ganapathysubramanian, Dr. Lee Bendickson, Kyungho Kang, Lijie Zhai, Tianjiao Wang, and Zhichen Zhu for many useful discussions, technical and otherwise.

I would also like to thank all the lab colleagues, former and present: Kyungho Kang, Dinesh Karyana-Sundaram, Janice Marquardt, Xiao Ma, Zhuoru Wu, Nazita Taghavi, Zhichen Zhu, Zhao Wang, Manan Sevak, and Norma Granados with whom I share and discuss a lot of professional and personal stories.

I would like to thank my family for their support and love. Finally, my most sincere thanks go to my parents, Minghui Pan and Yongjiu Zhao who carried me through these years.

ABSTRACT

Specific aims of this study are to investigate the mechanism that governs the surface stress generation with hybridization of single stranded DNA (ssDNA) molecules immobilized on micro-cantilevers. The hybridization of DNA on cantilever surfaces leads to configurational change, charge redistribution, and steric hindrance between neighboring hybridized molecules, which result in surface stress change and measureable cantilever deformation. Differential interferometer with two adjacent micro-cantilevers (a sensing/reference pair) was investigated to measure the cantilever deformation. The sensing principle is that binding/reaction of specific chemical or biological species on the sensing cantilever transduces to mechanical deformation. The differential bending of the sensing cantilever respect to the reference cantilever ensures that measured response is insensitive to environmental disturbances. In order to improve the sensitivity for sensing system, new approach of immobilization was utilized to enhance the deformation of the cantilever surface. Immobilization of receptor molecules was modified to use ssDNA with thiol-groups on both 3' and 5' ends; therefore both ends of the ssDNA molecules were immobilized to the gold surface and cause stronger surface interactions. To confirm the improvement of the sensitivity of the system, surface stress change associated with hybridization of ssDNA and malachite green-aptamer binding was measured.

To explore the mechanism under the surface stress change associated with ssDNA hybridization. A general beam bending model was established based on the minimization of the total energy of the system. The energy consisted of the bending energy of the cantilever and the in-film energy due to the hybridization of ssDNA on the surface. Different stages of

immobilization were proposed according to the different immobilization densities and immobilization approaches, the in-film energy associated with each stage was investigated. Numerical predictions are carried out with different stages and compared to the experimental observations, and the findings confirmed the capability of the beam bending model to use in surface stress predictions.

CHAPTER 1. OVERVIEW

A general simulation model is established to investigate the mechanism underlying the surface stress generation induced by the receptor-ligand binding. The model is based on the energy minimization of a beam bending model, and hybridization of ssDNA molecules are utilized as the verification of the model. The principle of the model is that the immobilized DNA molecules would lead to pairwise or pointwise molecular interactions after the hybridization, and the interactions will cause repulsions or surface reconstructions on the cantilever surface and bend the cantilever consequently. The interactions might include hydration forces, electrostatic repulsions, and interactions due to surface charge redistribution. The strength of the interactions is affected by the immobilization density, hybridization efficiency, molecular configuration, and ionic strength in the solution.

Ultimate goal of this study is to achieve the mechanism based understanding of the surface stress generation due to the hybridization of the ssDNA molecules and the influence of parameters that controls the magnitude of the cantilever deformation. The knowledge of the mechanism of surface stress generation would lead to more accurate and reliable predictions of similar sensors with receptor-ligand binding, and help to investigate surface stress sensors with higher sensitivity and greater reliability. In order to achieve this goal, we established a general beam bending model to simulate the micro-cantilever behavior associated with the DNA hybridization, and verified the model with the comparison of experimental observations. These objectives were achieved through successful completion of tasks as follow:

1) Establish the general energy model for simulation
2) Investigate the different types of interactions due to the DNA hybridization on the

cantilever surface associated with different immobilization approaches and immobilization densities.

3) Study the influence on the distribution of the ssDNA molecules on the cantilever surface and the hybridization efficiencies.

4) Predict the surface stress change of the micro-cantilever with different immobilization methods, immobilization densities, distribution of the DNA molecules, and the hybridization efficiencies, and verify the model by comparing the predictions with the experimental reports.

My contributions to the work and publications:

1) Detection of cantilever deflection due to malachite green/aptamer binding: worked with Zhao.

2) Mechanism study on cantilever deflection due to alkanethiol self-assembled monolayer immobilization on cantilever surface: worked with Kyungho.

3) Cantilever deflection associated with hybridization of monomolecular DNA film.

4) Cantilever deflection associated with hybridization of DNA hybridization with low densities and alternative immobilization approach.

5) Influence of receptor immobilization on threshold sensitivity of micro-cantilever sensors: applications to DNA hybridization, worked with Kyungho Kang.

6) An RNA aptamer-based microcantilever sensor to detect the inflammatory marker, mouse lipocalin-2, worked with Lijie Zhai, Tianjiao Wang, and Kyungho Kang.

CHAPTER 2. LITERATURE REVIEW

Microcantilever Based Sensor

In 1994, Thundat and his colleagues (Thundat, Warmack et al. 1994) made the seminal observation that Atomic Force Microscope (AFM) cantilevers deflect due to changes in relative humidity and thus opened a myriad of possibilities for the use of AFM cantilevers for chemical and biological sensing. They predicted possibilities of adsorbate detection of the order of picograms and immediately followed up with another study in which they detected mercury adsorption on cantilever from mercury vapor in air with picogram resolution (Thundat, Warmack et al. 1994, Thundat, Wachter et al. 1995). Also, Berger et al.(Berger, Delamarche et al. 1997) measured differential surface stress induced by formation of alkanethiol self-assembled monolayers (SAMs) on gold coated microcantilever. Godin et al.(Godin, Williams et al. 2004)reported that surface stress development is dependent on the grain size of the gold film and elucidated the transition phases during SAM formation. The thickness of the SAM also affects the magnitude of the measurements as well as sensing performance (White, Phares et al. 2008).

Microcantilever based sensors have been successfully utilized for biomolecular recognitions. Fritz et al. (Fritz, Baller et al. 2000) monitored hybridization of single-stranded DNAs (ssDNAs). They measured surface stress of 5 mN/m and actuation force of 300 pN due to single base mismatch between 12-mer and 16-mer oligonucleotides. Moulin et al. (Moulin, O'Shea et al. 1999)conducted surface stress measurements of immunoglobulin G (IgG) and albumin (BSA) and found that the strength of surface stress change is time dependent.

Majumdar and coworkers (Biswal, Raorane et al. 2006, Stachowiak, Yue et al. 2006) reported a series of works on label-free microcantilever sensor for biological detections.

Stachowiak et al. (Stachowiak, Yue et al. 2006) investigated the efficiency of DNA hybridization in various ionic strength and dependence on the grafting density as well as the length of the DNA. They found that surface grafting density of ssDNAs can be controlled by changing the DNA chain length and ionic strength. Inversely, Biswal et al.(Biswal, Raorane et al. 2006) measured surface stress changes associated with dehybridization of double-stranded DNA (dsDNA). They observed the response of melting and diffusing dsDNAs away from the cantilever as a function of salt concentration and length of oligonucleotides. They confirmed that increasing salt concentration and oligonucleotide length result in an increase in the melting temperature. They even extended their sensing platform to two-dimensional microcantilever sensor for high-throughput multiplexed chemical and biomolecular analysis. Several cantilevers are fabricated in parallel and each cantilever is functionalized for a specific target molecule. Through this process, they provided that the two-dimensional multiplexed microcantilever sensor can detect many target molecules. With the new sensor platform, they measured surface stress changes in the responses of DNA immobilization on gold surface(Yue, Lin et al. 2004), toluene and water vapor in vapor phase(Lim, Raorane et al. 2006), Prostate specific antigen (PSA)(Yue, Stachowiak et al. 2008) as low as 1 ng/mL which corresponds to 2 mN/m of surface stress change.

Maraldo et al. (Maraldo, Garcia et al. 2007) performed the prostate cancer detection through prostate cancer biomarker (α-methylacyl-CoA racemase; AMACR) directly in patient urine. They demonstrated the function of microcantilever sensors as a feasible application of cancer detection. There have been many other applications to oligonucleotide hybridization (Hansen, Ji et al. 2001, McKendry, Zhang et al. 2002, Stachowiak, Yue et al. 2006, Zhang, Lang et al. 2006), receptor-ligand (Thaysen, Yalcinkaya et al. 2002, Marie, Thaysen et al. 2003,

Savran, Burg et al. 2003, Savran, Knudsen et al. 2004, Mukhopadhyay, Sumbayev et al. 2005), and antigen-antibody interaction (Raiteri, Nelles et al. 1999, Raiteri, Grattarola et al. 2001, Grogan, Raiteri et al. 2002, Dutta, Tipple et al. 2003).

Differential Interferometer and Sensor Configurations

In majority of the current state of art sensors, molecule absorption induced surface stress change is inferred from the deflection of a single or multiple laser beams reflected from the sensing surface. A large optical path is required between sensitized surface and position sensitive detectors to achieve high sensitivity in surface stress measurement. Deflection of two laser beams reflected each from sensing and reference cantilevers may also be used for differential surface stress measurement but that setup may suffer from the following drawbacks: measured sensitivity is again proportional to the distance between a cantilever and a photodetector; and measured response is determined by subtracting the two signals, which may lead to resolution losses.

The micro-cantilever based detection assay was performed with a differential interferometer. In the study, a pair of gold coated sample/reference micro-cantilevers was used. The sample cantilever was immobilized with thiolated aptamers, while the reference cantilever was immobilized with an irrelevant thiolated DNA oligo. In the sensing system, two laser beams were generated and hit on the sample and reference cantilevers respectively. The reflected signals were collected and interfered, and the intensity of the interfered fringe pattern was monitored.

When the solution of the target molecules was introduced to the cantilever pair, a differential surface stress change was generated during the receptor-ligand binding, and a

differential cantilever deflection Δl was induced. As a result, the path length difference travelled by the two reflected laser beam were shifted by a value of $2\Delta l$, and a corresponding phase change of $2\Delta l/\lambda$ was observed. The intensity of the interfered fringe was monitored and recorded during the whole procedure of introduction of the target molecules till the signal got stable. By analyzing the interfered signal, the differential deflections and surface stress changes could be calculated.

In details, the sensor system works with two mutually orthogonal polarization state: p state with polarization in-plane and the s state which is perpendicular to p. The laser beam starts with a linear polarizer at 45° relative to p and s states, and goes through Soleil Babinet compensator which shifts the phase between s and p states. After the beam splitter, the beam is divided into a reference (p state) and sensing (s state) parts, and hit on the cantilever pair after the focusing lenses.

Both beams are back-reflected from the cantilevers and the sensing beam will travel path length $2\Delta l$ more than the reference beam. The two reflected beams will travel backwards, merge into one through the beam displacer, and the merged beam is reflected by the beam splitter.

A Wollaston prism is placed at 45° relative to the merged reflective beam, and the intensity of the two beams coming out is detected and converted to electric signals I_1 and I_2 by two photodiodes. The photodiodes signals are

$$I_1 = \frac{1}{4}\left[I_s + I_p + 2\sqrt{I_s I_p}\cos\emptyset\right]$$
$$I_2 = \frac{1}{4}\left[I_s + I_p - 2\sqrt{I_s I_p}\cos\varphi\right] \quad (1)$$

where I_s (I_p) is the light intensity of the reflected beams, φ is the phase difference between the reflected beams. As a result, we can monitor the change of the phase difference between reference and sensing beams by

$$\cos\varphi = k\frac{I_1 - I_2}{I_1 + I_2}, k = \left(I_s + I_p\right)/2\sqrt{I_s I_p} \qquad (2)$$

During the process of receptor-ligand binding, the signals were monitored recorded, and change of the phase difference $\Delta\varphi$ was calculated from equation (2), and the differential deflection was $\Delta l = \lambda\Delta\varphi/4\pi$ accordingly, and differential surface stress ($\Delta\sigma$) between the two cantilevers is determined using Stoney's formula (Stoney 1909).

$$\sigma = \frac{Eh^2}{6R(1-v)} \qquad (3)$$

where E is the Young's modulus and v is the Poisson's ratio; L and t are the effective length and thickness of the cantilever; l is the static deflection of the cantilever beam.

Micro-cantilevers are the heart of nanomechanical sensors to transducer molecular adsorption and reactions into mechanical response. Microcantilevers are made of silicon or silicon nitride where a thin gold film (10 - 200 nm) is deposited on one side by evaporating or sputtering in an ultrahigh vacuum (UHV). A thin layer of Cr or Ti (> 10nm) improves the adhesion between a gold layer and a solid silicon substrate. In the sensor system, two adjacent rectangular tipless silicon cantilevers (480 µm long, 80 µm wide, and 1 µm thick) with a top side coating of 5nm titanium and 30nm gold film. (Nanoworld, Switzerland) were used as sensing/reference pair. AFM cantilevers are batch produced with large variation of dimensions and mechanical properties from the manufacture's quote.

DNA Hybridization Induced Cantilever Deflection

Microcantilever based sensors are an intriguing new alternative for conventional chemical and biological sensors because of their extremely high sensitivity and miniature sensing elements. The sensing strategy involves coating one surface of a micromachined cantilever with a receptor species that has high affinity for the analyte molecule. Binding of the ligand on the sensitized surface induces a mechanical deformation of the microcantilevers thus transducing the surface chemical reaction into a measurable quantitative signal. Thundat and his colleagues (Thundat, Warmack et al. 1994) made the seminal observation that Atomic Force Microscope (AFM) cantilevers deflect due to changes in relative humidity and thus opened a myriad of possibilities for the use of AFM cantilevers for chemical and biological sensing. They predicted possibilities of adsorbate detection of the order of picograms and immediately followed up with another study in which they detected mercury adsorption on cantilever from mercury vapor in air with picogram resolution (Chen, Warmack et al. 1994, Allison, Thundat et al. 1995). Since these initial reports, microcantilever-based sensors have been investigated for sensing of chemicals(Tamayo, Humphris et al. 2001, Lavrik, Sepaniak et al. 2004), DNA hybridization (Fritz, Baller et al. 2000, Hansen, Ji et al. 2001, Wu, Ji et al. 2001, Alvarez, Carrascosa et al. 2004, Stachowiak, Yue et al. 2006, Kang, Nilsen-Hamilton et al. 2008, Jin, Shin et al. 2009, Kang, Nilsen-Hamilton et al. 2009), explosives (Thundat, Pinnaduwage et al. 2004, Zuo, Li et al. 2007, Seena, Rajoriya et al. 2010), biomolecules (Ilic, Czaplewski et al. 2001, Raiteri, Grattarola et al. 2001, Wu, Datar et al. 2001, Arntz, Seelig et al. 2003), and markers for cancer (Hood, Heath et al. 2004, Ferrari 2005, Sengupta and Sasisekharan 2007).

DNA hybridization is a simple and prominent example of biomolecular recognition and detection, since it is fundamental to most biological process. Fritz et al. (Fritz, Baller et al. 2000)

monitored hybridization of surface immobilized single stranded DNA (ssDNA) with oligonucleotide length of 12 nt, and with 3 different concentration values of the target ssDNA molecules (80nM, 400nM, and 2000nM). Cantilever deflections of about 3 nm, 15 nm, and 21 nm were reported respectively. Cantilever deflection was also found to be different for hybridization of ssDNA with strands that had single base-pair mismatch, indicating that microcantilever based sensors have intrinsic sensitivity to detect single nucleotide polymorphisms. Since this work, cantilever deflection due to ssDNA hybridization has been utilized as an validation experiments for new techniques, and cantilever deflection signal up to ~100 nm have been reported for those experiments (Wu, Ji et al. 2001, McKendry, Zhang et al. 2002, Stachowiak, Yue et al. 2006, Kang, Nilsen-Hamilton et al. 2008, Kang, Nilsen-Hamilton et al. 2009).

Hansen et al. (Hansen, Ji et al. 2001) also demonstrated that hybridization induced cantilever deflection can be used to discriminate base-pair mismatches with 20- and 25-mer probe DNA molecules. They used 10-mer DNA oligonucleotides as complementary target molecules which contain one or two internal mismatches. The results showed that the number and position of mismatch pairs will affect the deflection of the cantilever.

Stachowiak and co-workers (Wu, Ji et al. 2001, Stachowiak, Yue et al. 2006) conducted experiments to investigate the influence of ssDNA strand length, immobilization density and hybridization efficiency on the hybridization induced microcantilever deformation. The salt concentrations in immobilization and hybridization buffer were varied to achieve different immobilization density and coverage of hybridized molecules, respectively. Changing the salt concentrations from 0 to 1000 mM resulted in an increase in immobilization density from 0.06 to 0.12 nm-2 and similar change of salt concentration in hybridization buffer resulted in an increase

of hybridization efficiency from 30% to 80%. Three different molecular lengths of 10 nt, 20 nt, and 30nt were used and both immobilization density and coverage of hybridized molecules decreased as the chain length increased. Hybridization induced cantilever deflections corresponding to different chain lengths, immobilization densities and hybridization efficiencies collapsed on to a single curve when expressed as a function of the coverage of hybridized chains. These results indicated that the effects of the immobilization density, hybridization efficiencies and chain length are coupled and the cantilever deflection primarily depends on the surface coverage of hybridized chains.

Kang (Kang 2011) reported the influence of receptor molecule immobilization on the surface stress changes associated with DNA hybridization. In order to investigate the influence of ssDNA immobilization on hybridization induced mechanical deformation, surface stress changes were measured for two different immobilization schemes of receptor DNA strands: one end tethered and both end tethered. The immobilization density of receptor molecules and were also measured and confirmed that in both immobilization schemes they had the same immobilization density of 1.9×10^{16} molecules/m^2. They confirmed the double thiolation method could improve the threshold sensitivity by orders of magnitude and measure target concentration as low as 2 nM, and had a surface stress change of 30 mM/m, while single thiolation cases can achieve the same surface stress at a target concentration of 100 nM.

Mechanism Exploration and Simulation Approaches

Although there have been extensive efforts to elucidate the origin of the biomolecular binding induced surface stress changes, consensus on the underlying mechanisms is still elusive due to complex molecular interactions. Compressive surface stresses are attributed due to an

expansion of a cantilever surface influenced by electrostatic repulsion of surface groups and increasing the number of negative charges on the surface. Alternatively, conformational changes of receptor molecules caused by hybridization or binding that result in formation of ordered structures may relax the repulsive steric interactions between disordered unbound molecules bending the cantilever upward to tensile direction. Therefore, when a surface bound with single-stranded oligonucleotides undergoes hybridization, conformational changes from a single strand to a rod-like double helix may result in initial tensile surface stress changes but as the hybridization proceeds the surface stress development changes sign to compressive stresses due to buildup of charge interactions among neighboring molecules. Conformational changes and electrostatic and hydrophobic forces are dependent on individual ligand/receptor pair, so the transition point and dominant phenomena is difficult to identify (Fritz 2008).

Wu et al.(Wu, Ji et al. 2001) introduced thermodynamic principles to explain the nanomechanical motion of the cantilever during DNA immobilization and hybridization. In addition to the electrostatic repulsive force between neighboring DNA chains, they argued that the origin of cantilever bending is due to a change in configurational entropy and intermolecular energetics induced by specific biomolecular interactions. When immobilized single-stranded DNAs interplay between neighboring chains, the configurational entropy decreases which lead to increase entropic driving force. The configurational entropy of single-stranded DNA is highest in a free solution, but forming double stranded DNAs during DNA hybridization reduces this entropic driving force balanced by the strain energy of bending the cantilever. Therefore, this curvature produces the cantilever bending up to tensile direction.

In order to explain the underlying mechanism for hybridization induced deflection, Fritz (Fritz 2008) hypothesized that the cantilever deflection is result of two competing mechanism:

electrostatic repulsion between negative charges on the DNA strands and relaxation of steric hindrance as disordered ssDNA transition to ordered DNA strands. The increase in negative charges during hybridization results in an expansion of the cantilever surface due to the electrostatic repulsion and consequently, bending of the cantilever. Alternatively, when surface bound single stranded oligonucleotide undergo hybridization, conformational changes from a disordered strand to rod-like double helix result in relaxation of the steric hindrance and contraction of the surface. The competing mechanisms were proposed to explain cantilever bending observed during hybridization experiments. During the initial phase of DNA hybridization the relaxation of steric hindrance leads to relaxation of cantilever bending but as the hybridization proceeds, the surface starts expanding due to buildup of charge interactions among neighboring molecules. However, it is important to note that the DNA hybridization experiments are performed in buffers with high salt concentrations. The positive ions in the solutions may shield the electrostatic repulsion between the strands and the magnitude of inter-chain repulsion may depend on the ionic composition of the hybridization buffer.

Besides the electrostatic effects, hydration forces between the chains may also lead to hybridization induced cantilever deflection (Strey, Parsegian et al. 1997, Strey, Parsegian et al. 1999, Hagan, Majumdar et al. 2002). To study the effect of the hydration forces, Mertens et al.(Mertens, Rogero et al. 2008) conducted experiments to investigate the influence of relative humidity on deflection of micro-cantilevers immobilized with ssDNA and double stranded DNA (dsDNA). Deflection of cantilevers with ssDNA and dsDNA strands increased to about 500 nm and 600 nm, respectively as the relative humidity was changed from 0 to 100%.These results indicate that hydration forces play an important part in determining cantilever deflection.

Hagan et al.(Hagan, Majumdar et al. 2002) modeled the hybridization induced cantilever deflections based on both electrostatic repulsions and hydration forces between DNA strands. The microcantilever was modeled as a membrane and the DNA strands were modeled as straight rods immobilized on the membrane surface. Repulsive interactions between the DNA strands lead to increase in their spacing and rotation of rods, resulting in cantilever bending. Cantilever deflections due to a high immobilization density of 0.17 chains/nm2 and hybridization efficiency of 100% were investigated. Based on the numerical results it was concluded that the cantilever deflection induced by uniformly distributed DNA strands is much smaller in magnitude compared to experimental observations. However, numerical prediction based on disordered arrangement of DNA strands and 100% hybridization efficiency was found to match the experimental observations.

Zhang et al. (Zhang and Shan 2008, Zhang and Chen 2009, Zhang, Chen et al. 2010, Zhang, Meng et al. 2013) have performed theoretical analysis on the DNA hybridization induced cantilever deflections. They established multi-scale analytical model to consider the influence of the inhomogeneous distribution of net charge and flexibility of elastic properties of DNA biofilm. They concluded that with high immobilization density, hydration forces are the dominate interactions, while with low immobilization density, the conformational entropy dominates. Moreover, they developed an energy model for deflection predictions to determine the influence of the distribution of the DNA molecules on the cantilever surface, and concluded that the stochastic effect on the chain separations is greater than that of the elastic modulus.

Strey et al. (Strey, Parsegian et al. 1997, Strey, Parsegian et al. 1999) proposed a liquid crystal model to represent the hybridized dsDNA molecules immobilized on the surface of microcantilevers, and established pairwise potential models for dsDNA molecular interactions

for both electrostatic interactions and hydration forces. While Zhang et al. (Zhang, Tan et al. 2011) investigated the theories related to interactions of ssDNA immobilized on microcantilevers. In their report, they conclude that when the immobilization density of ssDNA is low, the interaction energy between neighboring molecules will be too weak to be dominant.

CHAPTER 3. DETECTION OF CANTILEVER DEFLECTION DUE TO MALACHITE GREEN/APTAMER BINDING

Modified from a paper to be submitted

Yue Zhao, Tianjiao Wang, Marit Nilsen-Hamilton, Pranav Shrotriya

Abstract

Microcantilever based sensors can be used for quantitative analysis of the nanomechanical response associated with conformational change and the corresponding charge transduction during molecular interaction. A specific aptamer is used for Malachite Green (MG) recognition, and two different immobilization methods are investigated, single thiolation and double thiolation. The surface stress changes due to the aptamer-ligand binding are measured with differential interferometry techniques and the sensitivity of the two different methods are compared. The findings show that the double thiolation method has a significant improvement on the threshold sensitivity of the sensing system.

Introduction

Microcantilever based sensors are widely studied for their capability for transducing chemical reactions on the sensor to mechanical signals and therefore can act as sensors in chemical and biological sensing. The surfaces of the microcantilevers are coated with a film of receptor molecules which can react with target analyte molecules with certain sensitivity and

specificity. The analyte molecules can be detected by observation of the cantilever deformation due to the binding of target molecules on the functionalized surfaces of the sensors.

Thundat and his colleagues (Thundat, Warmack et al. 1994, Thundat, Wachter et al. 1995) first reported their finding on the Atomic Force Microscope (AFM) cantilever deflection due to changes of relative humidity, which revealed the potential of the AFM cantilevers to work as chemical and biological sensors. Unlike chemical reactions (Su and Dravid 2005, Kadam, Nordin et al. 2006), the sensors with receptor/analyte binding suffer from low sensitivity and detection thresholds (Ji and Armon 2010), because the deflection magnitudes and surface stress changes are low during the binding. For example, surface stress changes of approximately 2 to 40 mN/m have been reported for hybridization of 9-mer to 30-mer ssDNA oligonucleotides (Fritz, Baller et al. 2000, Wu, Ji et al. 2001, Alvarez, Carrascosa et al. 2004, Biswal, Raorane et al. 2006, Stachowiak, Yue et al. 2006, Zhang, Lang et al. 2006).

The weak nature of these intermolecular interactions results in low magnitude of mechanical deformation and consequently, limits the sensitivity and detection limit associated with target analyte. This low sensitivity becomes an obstacle for microcantilever sensors to be the use of biomolecular recognition (Ji and Armon 2010). Consequently, many attempts have been made to improve the threshold sensitivity and selectivity of the sensing platform by controlling sensing environments (Mertens, Rogero et al. 2008), adding new materials (Weizmann, Patolsky et al. 2004), or inventing new structures (Pei, Lu et al. 2010).

In this chapter, we report the investigation on the difference of surface stress changes due to different immobilization methods for malachite green (MG) and malachite green aptamers (MGA). The different immobilization schemes are schematically illustrated in Figure 1, and surface stress changes are captured by a differential sensor based on laser interfere technology.

The immobilization density of different immobilization methods are also measure based on the fluorescent behavior of MG.

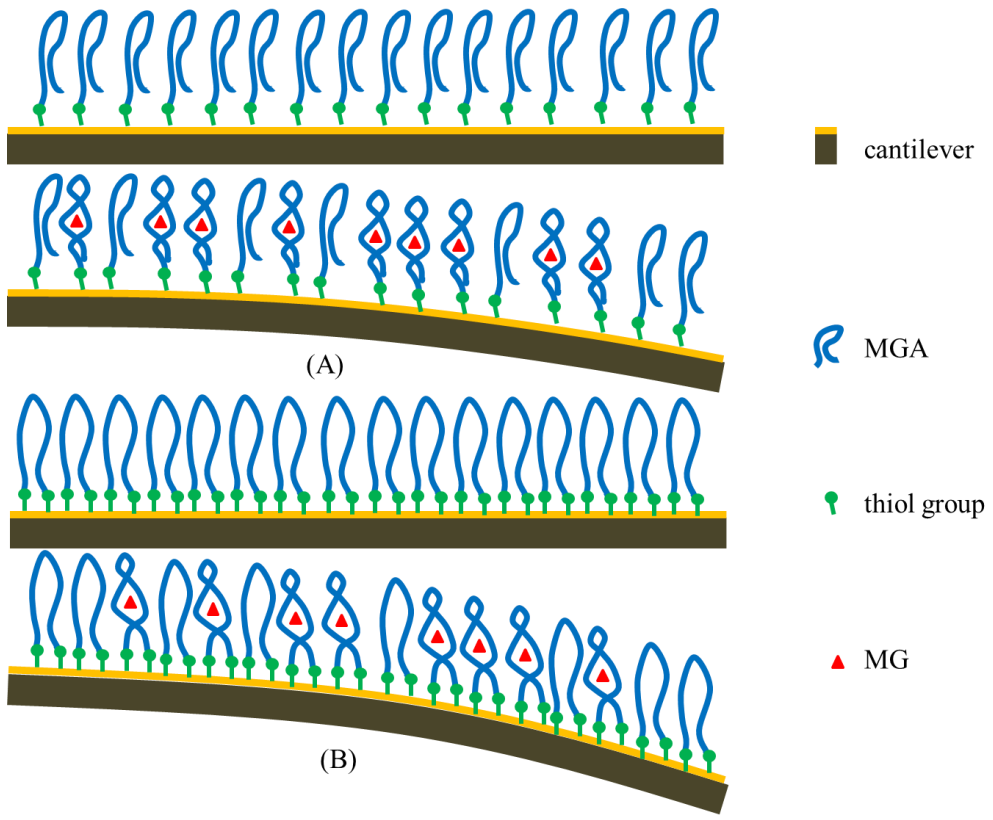

Figure 1. Schematic illustration of different immobilization methods. (A) Single thiolated MGA immobilization; (B) Double thiolated immobilization.

Materials and Methods

MGA/MG binding pairs

The malachite green aptamers (MGA) are short single-stranded RNA molecules which bind specifically to malachite green (MG) molecules. Structural analyses of the MGA/MG binding pairs (Wang, Hoy et al. 2009) show that the aptamers have a tertiary structure and form a binding pocket for the MG molecules to sit in. The MGA and MG molecules both change their

structures during binding. To be specific, the MG molecule becomes flatter and the MGA twists in structure.

The thiolated MGA oligonucleotides were synthesized by Integrated DNA Technologies, Inc. (Coralville, IA) with the reported sequences as listed: thiol – 5' – GGAUCCCGA CUG GCG AGA GCC AGG UAA CGA AUG GAU CC – 3' (– thiol) (The second thiol group is optional for different sensor preparation). MG molecules were purchased from Sigma (St. Louis, MO)

Micro-cantilever specification and sensor preparation

High aspect ratio tipless AFM cantilevers used in the sensor system were purchased from Nanoworld, Switzerland. The cantilevers used were 500 µm long, 20 µm wide and 1 µm thick, and coated with 5 nm of titanium and 30nm of gold film.

In the sensor system, a sensing/reference pair of micro-cantilever were used. The sensing cantilever was immobilized with the thiolated MGA molecules and the reference cantilever was immobilized with scrambled DNA molecules that do not bind with the target MG molecules. Two different types of sensing cantilevers were prepared, one immobilized with MGA with one thiolgoup at 5' end, and the other immobilized with MGA with thiol groups at both 3' and 5' ends.

Differential interferometer

The micro-cantilever based detection assay (Figure 2) was performed with a differential interferometer. In the sensing system, two laser beams were generated and hit on the sample and

reference cantilevers respectively. The reflected signals were collected and interfered, and the intensity of the interfered fringe pattern was monitored.

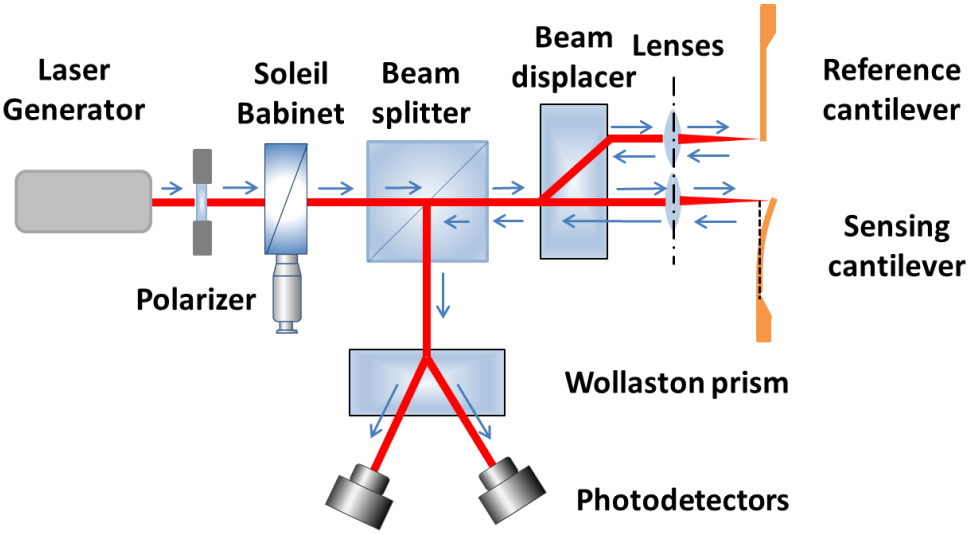

Figure 2. Schematic presentation of cantilever based surface stress sensor

A Wollaston prism is placed at 45° relative to the merged reflective beam, and the intensity of the two beams coming out is detected and converted to electric signals I_1 and I_2 by two photodiodes. The photodiodes signals are

$$I_1 = \frac{1}{4}\left[I_s + I_r + 2\sqrt{I_s I_r}\cos\varphi\right],\ I_2 = \frac{1}{4}\left[I_s + I_r - 2\sqrt{I_s I_r}\cos\varphi\right], \tag{4}$$

where I_s (I_r) is the light intensity of the reflected beams from sensing and reference cantilever respectively, φ is the phase difference between the reflected beams. As a result, we can monitor the change of the phase difference between reference and sensing beams by

$$\cos\varphi = k\frac{I_1 - I_2}{I_1 + I_2}, k = (I_s + I_r)/2\sqrt{I_s I_r} \tag{5}$$

When the MG solution was introduced to the cantilever pair, a differential surface stress change were generated during binding, and a differential cantilever deflection Δl was induced.

As a result, the path length difference travelled by the two reflected laser beam were shifted by a value of $2\Delta l$, and a corresponding phase change of $2\Delta l/\lambda$ was observed. The intensity of the interfered fringe was monitored and recorded during the whole procedure of protein introduction till the signal got stable. By analyzing the interfered signal, the differential deflections could be calculated as $\Delta l = \lambda\Delta\varphi/4\pi$.

Experimental Procedures

In preparation of the experiments, all the micro-cantilever were cleaned with piranha solution (70% H_2SO_4 and 30% H_2O_2) for 1 minute, and rinsed in deionized water. The thiolated MGA were diluted to 0.5 uM concentration with the immobilization buffer (50mM Tris-HCl, 150mM NaCl, 5mM $MgCl_2$, pH 7.4), and heated up to 60°C to break any disulfide bonds. The sensing cantilevers were immersed in the MGA solution for 3 hours for functionalization, and then treated with 3 mM 6-mercapto-1-hexanol solution to wash away all non-immobilized MGA molecules that stayed on the cantilever surface. The reference cantilever is prepared in the same procedure except with the scrambled DNA solution.

Surface coverage density tests

Before the surface stress experiments were taken with the sensor, the coverage densities of the sensing cantilever with both single and double thiolated MGA were determined with fluorescence tests (Demers, Mirkin et al. 2000). After the immobilization of the sensing cantilever, it was merged in the etching buffer (12mM β-mercapthoethanol) for 48 hours. The immobilized MGA molecules were etched into the buffer during the procedure and the etched buffer were used to complete the fluorescence tests based on the fluorescent behavior of MG.

Surface stress experiments

The binding experiments were carried out for both single- and double thiolated sensors with different concentrations of MG in the binding buffer (10 mM HEPES, 100 mM KCl, 5 mM $MgCl_2$, pH 6.0). The sensing and reference cantilever were mounted in the interferometer system, and submerged in the binding buffer. The MG solution was introduced to the system and the reflected interfered signals were monitored during the differential deflection development. Three different sets of experiments were carried out with three different types of sensing cantilevers. (1) The sensing cantilevers were immobilized with single thiolated MGA; (2) the cantilevers were immobilized with double thiolated MGA; and (3) the cantilevers were first immobilized with the binding complex of double thiolated MGA and MG, and then the MG molecules are washed away by DI water of 80˚C.

Results

Surface coverage density

Three measurements were taken for both single- and double thiolated immobilization. Fluorescence signal was observed to be 7.114 – 8.653 for single thiolated MGA immobilization, while it was 6.135 – 7.532 for double thiolated case. The surface coverage densities were then found to be 0.06 – 0.15 nm^{-2} and 0.04 – 0.12 nm^{-2} for single and double thiolated immobilization respectively, with a 90% confidence interval.

Surface stress change

The surface stress tests were conducted with injections of MG solutions with different concentrations. Figure 3 shows a typical profile of the surface stress development during the

binding of MGA and MG molecules. Surface stress changes developed after the injection of the MG solution into the system, and reached the saturation state within 15 to 20 minutes in average. A surface stress change of 14.5 mN/m was observed with single thiolated MGA and MG at final concentration of 100 nM.

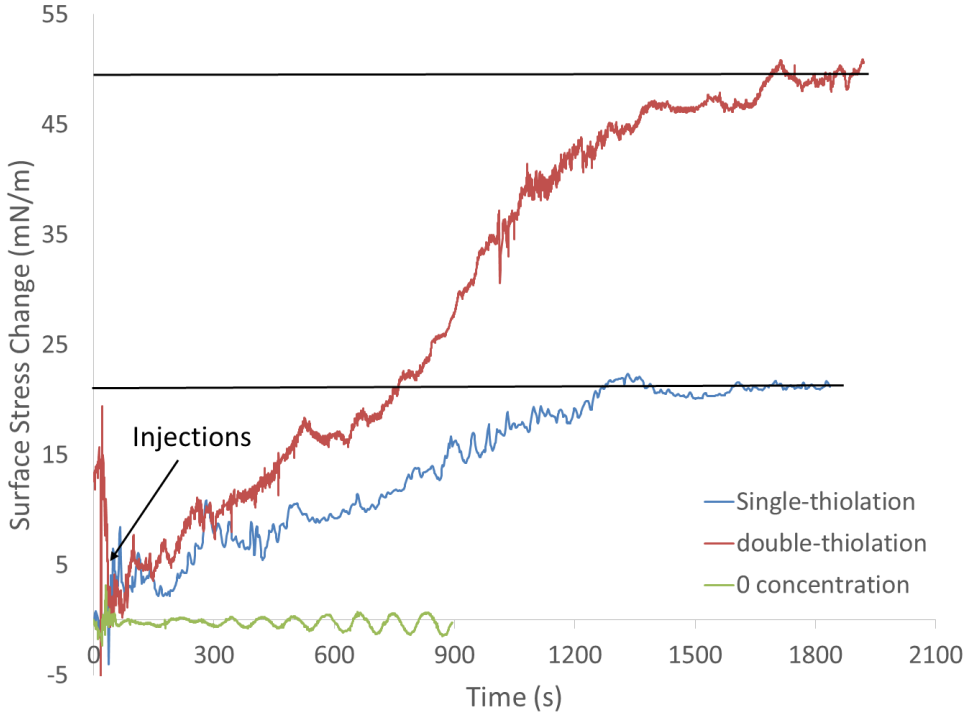

Figure 3. Typical profile of surface stress development during MGA/MG binding with a final concentration of 100nM.

Changes in surface stress during the binding of MG and MGA were captured with different concentrations. The results for experiments set 1 with single thiolated MGA turned to be 10 to 53 mN/m (Figure 4), and the concentration range MG solution is from 50 to 5000 nM. For experiments set 2 with double thiolated MGA, the surface stress change was 9 to 70 mN/m with MG concentration of 5 to 5000 nM; and experiments set 3 showed the surface stress of 14 to 85 mN/m also with 5 to 5000 nM MG solutions.

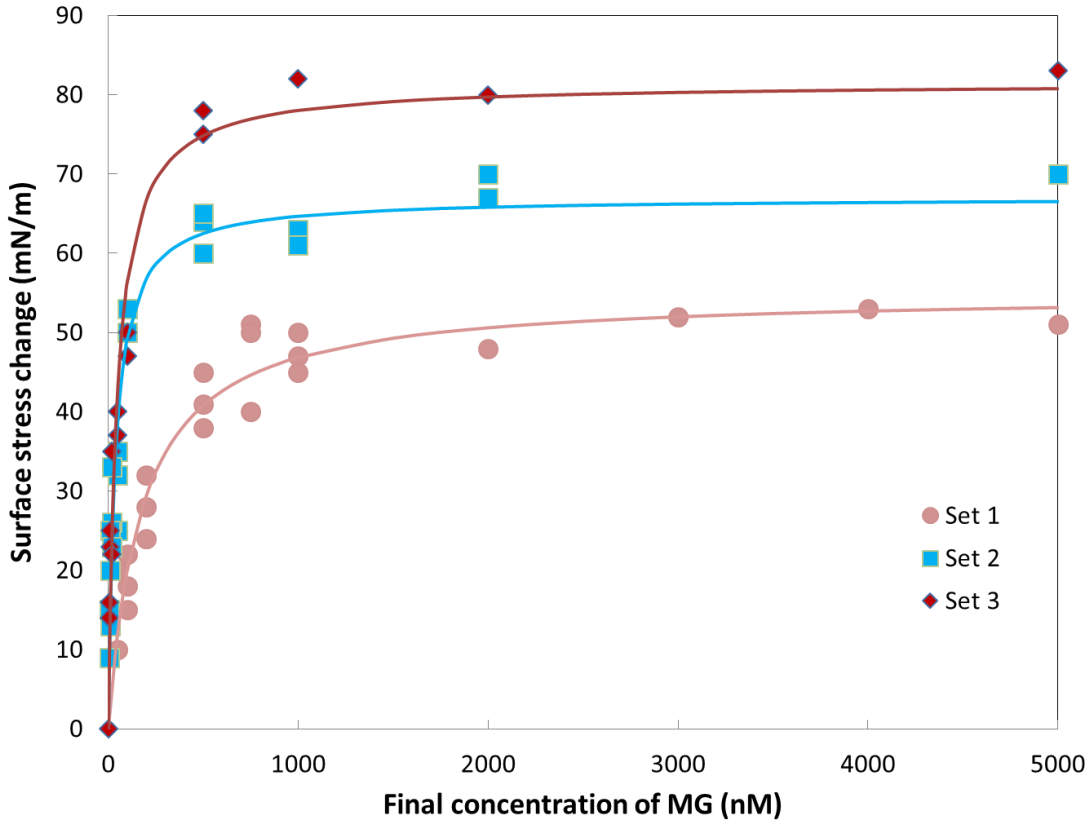

Figure 4. Surface stress change vs. MG concentration for 3 different immobilization methods.

Discussions

Surface coverage tests showed that the coverage densities for both single- and double thiolated MGA immobilization turned to be of the same magnitude, in average 0.09 and 0.08 molecules/nm^2 respectively, which measured in the salt concentration of 150 mM. The results of surface coverage agreed with others' report with similar salt concentration, and therefore obtained high degree of reliability in the tests. In addition, the average separations between immobilized molecules were calculated to be 3.4 and 3.9 nm respectively based on the hexagonal closed pack assumption.

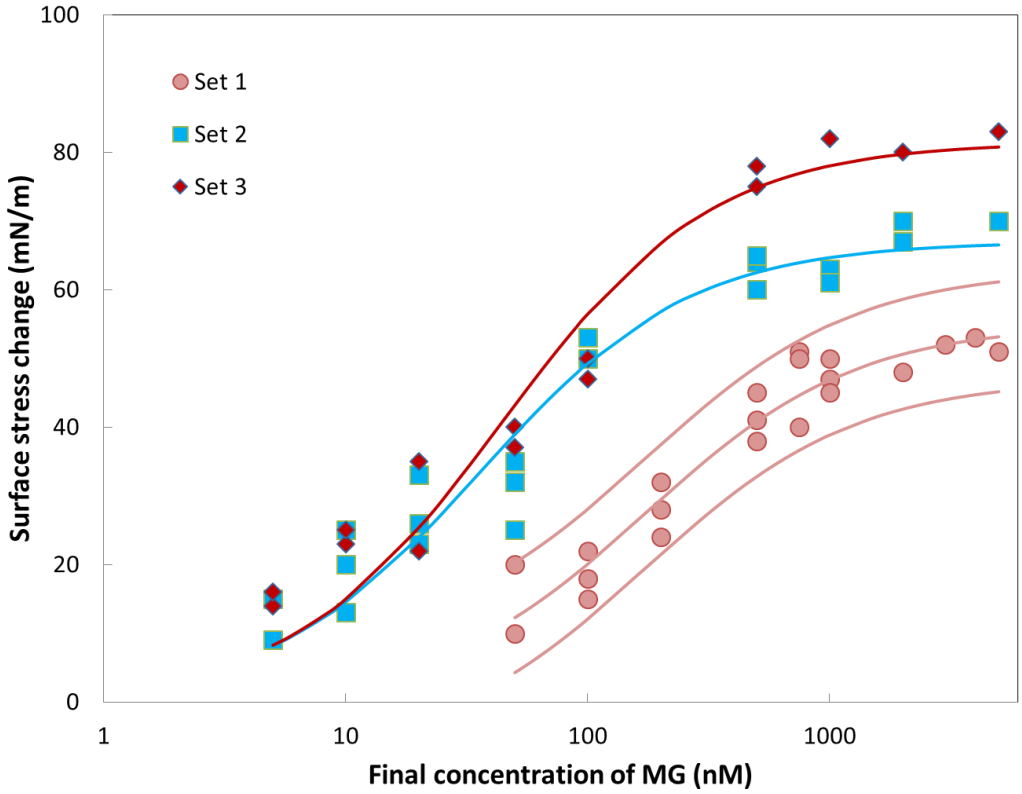

Figure 5. Comparison between 3 different sets on the threshold sensitivity, with 90% confidence interval.

The surface stress measurements associated with binding of the three different immobilization methods of MGA were plotted and compared in Figures 4 and 5. The measurements results showed that, with the same MG concentration injected, the double thiolated cases resulted in higher surface stress changes than those of single thiolated cases, and experiments set 3 provided the highest surface stress change when saturated among the three different types of immobilization. At low concentrations, the double thiolated cases (sets 2 and 3) induced much greater surface stress changes, and the threshold sensitivity was increased by about 10 times (from ~50 mM to ~5 mM). However, the surface stress changes will saturate at lower MG concentration with double thiolated sets (500 nM for set 2, 1000 nm for set 3) compared to single thiolated set (~2000 nM for set 1).

The equilibrium reaction of the binding and the corresponding disassociation constant (k_d) are studied. According to early study, single thiolated DNAs have pairwise interactions which lead to a second order relationship between surface stress changes and binding efficiencies. And with the definition of disassociation constant, we could get

$$\sigma = K\left(\frac{c}{c + k_d}\right)^2 \tag{6}$$

where c is the concentration of the MG molecules, K is the strength constant. The disassociation constant turns out to be 73 nM. The surface binding efficiencies corresponding to each concentration can be determined with the determined binding affinity, and the surface stress changes were plotted with the binding efficiency for all three sets of measurements in Figure 6.

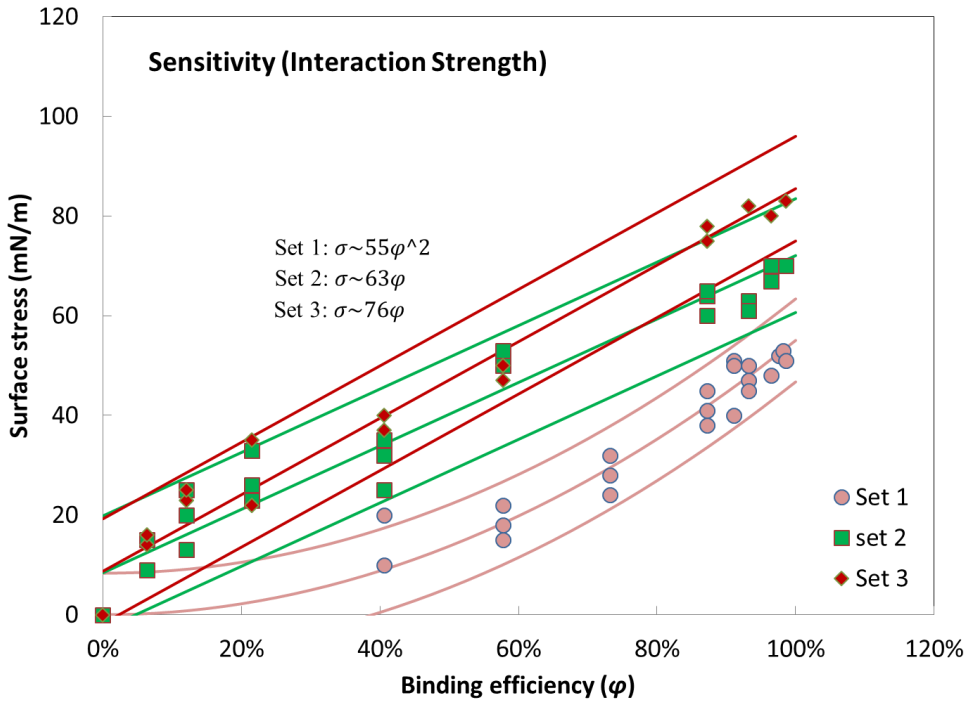

Figure 6. Interaction strength for all 3 sets of measurements.

The results showed that the sensitivity to binding efficiency for single thiolated case (set 1) was increasing as more aptamers bind with MG molecules. While for double thiolated cases

(sets 2 and 3), the surface stress changes are linear with the binding efficiency, and sensitivities are constant (74 and 88 mN/m respectively), which are 7 to 8 times of the sensitivity of set 1 at low binding efficiencies (less than 10%).

It is generally assumed that the surface stress change is induced by the pairwise potential due to the conformational change of the molecules after binding with the targets. The possible potentials include electrostatic repulsions due to deprotonation, conformational entropy along with repulsive steric interactions, and counterion osmotic pressure. Earlier studies showed that among all these potentials, the hydration forces due to disturbance on the hydration bonding network are the dominant factor for the surface stress generation (Strey, Parsegian et al. 1999, Hagan, Majumdar et al. 2002, Mertens, Rogero et al. 2008), and simulations based on that can reasonably predict the surface stress change for single thiolated case, and the magnitude depends on the surface coverage density or the inter-molecular separations.

The surface coverage tests showed that the immobilization densities are similar for all three different immobilization types, which confirms that the differences in surface stress changes for different measurement set are irrelevant to the surface coverage or the molecular separations. As a result, the surface stress changes with double thiolated sets (sets 2 and 3)were assumed to be due to some alternative origins. Since the double thiolated immobilization will bond both ends of MGA onto the surface of the cantilever, the immobilized molecules are pulled closer to the surface, the electrostatic effects resulted from the molecular conformational change will have greater influence on the gold sensing surface. The conformational changes of the MGA before and after binding with the MG have been studied and observed that the MGA molecules will have a significant twisting on the molecular structure. The twisting force couple will

transmit to the sensing surface, and the surface will suffer reconstructions, which will possibly lead to cantilever deflections, and result in a greater surface stress signal and higher sensitivity.

Though the threshold sensitivity was improved by one order of the magnitude, the effective range of sensing was also reduced to 500 nM (set 2) from 2000 nM (set 1). This was possibly due to that when immobilizing both ends of MGA, some of the molecules would be restricted in some structures which were difficult to bind with MG. Set 3 was designed to improve this by immobilizing the surface with MGA molecules which were already bound with MG and washing the MG away afterwards. In this manner, most MGA molecules immobilized onto the surface were in the structure readily to bind with MG. The measurements showed that the effective range was improved to 1000 nM with set 3.

Conclusion

Efforts were made to improve the sensitivity of the micro-cantilever based sensors. A new immobilization method was designed to achieve this goal. Instead of having thiol groups on one end of the MGA molecules which were immobilized on the sensor surface, they were attached with thiol groups on both ends before immobilization. Results showed that this immobilization method can greatly increase the sensitivity for lower concentrations and improve the threshold by one order of magnitude.

One side effect of the double thiolated treatment is that the sensitive range is greatly reduced due to the fixed molecular structure. Simple adjustment is conducted to reduce the side effect by immobilizing with double thiolated MGA which are bound with MG. With this modification, most MGA immobilized on the surface would be ready to adsorb MG. And the sensing limit is increased and the threshold sensitivity is still low.

The new immobilization method is capable to improve the sensitivity and the sensing threshold for the micro-cantilever based sensor, but the surface coverage density measurements showed similar immobilization densities. Therefore, the stronger response of the sensor should due to some stronger interactions induced by the MG/MGA binding, which is still not clearly understood. Reports on MGA structure study showed that MGA molecules were twist when bound with MG, which would possibly induce centers of rotation on the sensor surface. In addition, when both ends were bonded on the surface, the receptor molecules would be closer to the surface and have stronger influence to the surface. Therefore, the new immobilization method tends to induce stronger surface reconstructions on the sensor and lead to greater surface stress changes.

CHAPTER 4. MECHANISM STUDY ON CANTILEVER DEFLECTION DUE TO ALKANETHIOL SELF-ASSEMBLED MONOLAYER IMMOBILIZATION ON CANTILEVER SURFACE

Modified from a paper to be submitted

Yue Zhao, Kyungho Kang, Pranav Shrotriya

Abstract

Experimental results show that the adsorption of the self-assembled monolayers (SAMs) on a gold surface induces surface stress change that cause a deformation of underlying substrate. Multiscale computational models based on Molecular dynamic (MD) simulations are applied to study the mechanism governing surface stress change. Alkanethiols chains are chemisorbed on the gold surfaces due to bond formation between gold and sulfur atoms. Two different mechanisms for adsorption induced surface deformation are investigated. In the first mechanism, inter-chain repulsion between the alkanethiol molecules is assumed to drive the surface deformation; however the simulation results show that this mechanism has little contribution to the surface stress change. In the second mechanism, surface reconstruction caused by the gold-sulfur interaction during alkanethiol chemisorption is assumed to induce the surface stress change. Two different inter-atomic potential, embedded atom method (EAM)(Daw and Baskes 1983, Daw and Baskes 1984, Foiles, Baskes et al. 1986) and surface embedded atom method (SEAM)(Haftel and Rosen 1995), are used in the MD simulations to study the reconstruction induced surface stresses. According to first principle calculation by Andreoni et al. (Gronbeck

and Andreoni 2000), the gold-sulfur interaction will cause an expansion in the nearest gold atoms with inter-atom separation changing from 2.88 to 3.45 Å. This reconstruction is modeled through a modified potential for gold atoms by changing the electron density function of the gold atoms nearest to sulfur in EAM and SEAM potentials. Simulations based on modified EAM potentials show that, each gold atom will lose nearly 0.8 electrons to sulfur atom in order to match the surface reconstruction. While simulations based on modified SEAM potential give a more reasonable value that each gold atom loses 0.2 electrons to the sulfur for the required reconstruction, which is also in good agreement with results from first principle calculations by Beardmore et al. (Beardmore, Kress et al. 1997). Results of the simulations based on modified potentials are used in a multi-scale continuum framework (Kukta, Kouris et al. 2003) to predict the associated surface stress. A surface stress range of 0.12 – 4.38 N/m with respect to the surface coverage change from 0.006 to 0.139 $Å^{-2}$ is obtained. Comparison of the predicted surface stress changes with observed experimental response indicate that the modified SEAM based multiscale models can capture the surface stress changes observed during alkanethiol self-assembled layer formation.

Introduction

Microcantilever based sensors have shown great potential to detect the presence of chemical and biological species by transduction of the molecular interaction to a measurable mechanical deformation. Thundat et.al (Thundat, Warmack et al. 1994) reported the deflection of atomic force microscope (AFM) cantilevers due to changes in relative humidity and thermal heating and thus opened a myriad of possibilities for the use of AFM cantilever deflection technique for chemical and biological sensing. Berger et al. (Berger, Delamarche et al. 1997) reported microcantilever bending associated with formation of alkanethiols self-assembled

monolayers. Their results showed that the immobilization of the SAMs will cause a downward bending of the micro-cantilever. Surface stress range of 0.05 to 0.25 N/m were observed for alkanethiols with chain lengths of 4 to 14 methyl groups. Measured surface stress change was found to increase linearly with chain length of the alkanethiol molecules.

Since the first report of SAM formation induced surface stress change (Berger, Delamarche et al. 1997), SAMs have been used as test system to validate most of cantilever based sensing techniques. Experiments have been conducted to study response of the cantilever based sensor to different materials and end groups (Lang, Berger et al. 1998, Fritz, Baller et al. 2000, Cyganik, Buck et al. 2005, Zhai, Wang et al. 2012), measurement theory (Godin, Tabard-Cossa et al. 2001, Dareing and Thundat 2005, Zhao, Ganapathysubramanian et al. 2012), and cantilever properties(Dannenberger, Buck et al. 1999, Lachut and Sader 2007). Alkanethiol SAMs ($HS\text{-}(CH_2)_{n-1}\text{-}CH_3$) are one of the commonly studied SAMs, because they are relatively easy to prepare, form well-ordered close packed films and offers possibilities of variations in chain lengths, end groups and ligand attachments.

Godin et.al (Godin, Williams et al. 2004) hypothesized that the SAM formation progresses through three different phases as the surface coverage density of the alkanethiol molecule increases. These phases are the unstacked lying-down phase, stacked lying-down phase and standing-up phase. Their experimental results showed that kinetics of absorption and final surface coverage density of the SAM on gold-coated cantilevers depended on the grain size of the gold films. For larger grain size and lower surface roughness, the SAM formation progressed through all three phases and finally formed a close packed standing-up pattern that corresponded to surface stress change of 15.9± 0.6 N/m. While, for smaller grain size and greater surface

roughness, SAM formation stopped in the stacked lying down phase leading to a smaller surface stress change of 0.51±0.02 N/m.

Desikan and coworkers (Desikan, Lee et al. 2006, Desikan, Armel et al. 2007) measured surface stress changes associated with SAM formation for a range of alkanethiol chain lengths on cantilevers with different surface roughness. They observed surface stress change of approximately 0.09 - 0.15 N/m when the RMS roughness of cantilevers changed through three orders of magnitude from 1.32 to 12.8 nm for alkanethiol SAM. In addition, the measured surface stress changed from 0.7 to 1.2 N/m with alkanethiol chain length of n = 8, 12, and 18 for a cantilever with surface roughness RMS of about 10nm.Based on the experimental observation, they concluded that the alkanethiol SAM induced surface stress change is not sensitive to the surface roughness and the chain length.

Surface stress generation during SAMs formation has been attributed to number of different mechanisms such as intermolecular repulsion between the alkanethiol chains, electrostatic repulsion between adsorbates and surface stresses due to surface reconstructions. Godin et.al(Godin, Tabard-Cossa et al. 2010) performed experiments which showed barely any difference of surface stress induced by SAMs of different length. They also conducted molecular simulations that showed that intermolecular Lennard-Jones and electrostatic forces can only generate relatively small surface stresses (0.001-0.05 N/m), and argued that the dominant affect may be the surface charge redistribution.

Andreoni et al. (Gronbeck and Andreoni 2000) used first principle calculations based on density functional theory to show that absorption of thiolated molecules on gold surface leads to redistribution of the charge density and the gold atoms closest to the sulfur atom undergo a surface expansion with interatom separation changing from 2.88 to 3.45 Å. Beardmore et al.

(Beardmore, Kress et al. 1997) also conducted first principle quantum calculation for thiol-gold bond and showed that the gold atoms participating in the gold-thiol bond become more positive while the sulfur atoms become more electronegative. Some recent groups have utilized first principle based approaches to determine

In this paper, the surface stress generated during the formation of self-assembled monolayers is investigated using a combined experimental and computational approach. A differential surface stress sensor is utilized to measure the surface stress generated due to alkanethiol SAM formation of gold coated micro-cantilevers. All-atom molecular dynamics (MD) simulations of alkanethiol chains on gold surface were performed to study the surface stress induced by interchain interactions and electrostatic interactions. Modified embedded atom potentials are derived to model the gold surface reconstruction due to gold-sulfur bond formation. The modified embedded potentials are utilized in multiscale framework to predict the alkanethiol SAM induced surface stress changes. The results of simulations are compared with experimental reports to test the validity of the modeling assumptions.

Surface Stress Measurements

A differential surface stress sensor consisting of two adjacent cantilevers, a sensing/reference pair, where only the sensing surface is activated for adsorption of chemical or biological molecules was utilized for measuring the surface stress generated due to Alkanethiol SAM formation on gold surfaces. Optical circuit for the surface stress sensor is shown in Figure 7. Kang et al. (Kang, Nilsen-Hamilton et al. 2008, Kang and Shrotriya 2008) have reported the principle and details of differential surface stress measurement. Measurement of differential surface stress ensures that detected signal is proportional to specific absorption of analyte species

on the sensing cantilever and eliminates the influence of environmental disturbances such as nonspecific adsorption, changes in pH, ionic strength, and especially the temperature.

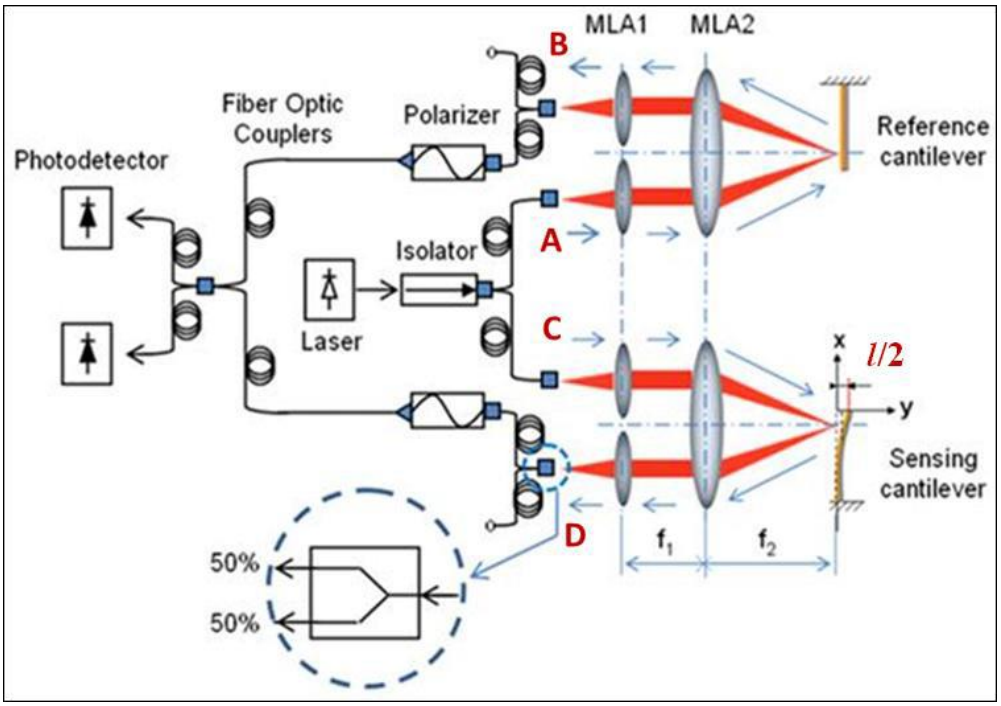

Figure 7. Optical circuit of the surface stress sensor.

Cantilever

In the sensor system, two adjacent rectangular tipless silicon cantilevers (480 μm long, 80 μm wide, and 1 μm thick) with a top side coating of 5nm titanium and 30nm gold film. (Nanoworld, Switzerland) were used as sensing/reference pair. AFM cantilevers are batch produced with large variation of dimensions and mechanical properties from the manufacture's quote (Sader and White 1993, Sader, Chon et al. 1999). In order to accurately measure surface stress development, the thickness of each cantilever is calculated based on the experimentally measured spring constant with the material constants (Sader, Chon et al. 1999). Microstructure

and surface roughness of the gold film on the cantilever were determined using contact mode atomic force microscope imaging.

Experimental procedure

Liquid octanethiol [$CH_3(CH_2)_7SH$] was selected as alkanethiol solution and purchased from Sigma-Aldrich. All the AFM cantilevers were cleaned by immersing for 3 minutes in piranha solution (70% H_2SO_4, and 30% H_2O_2 by volume) and were then rinsed in deionized water and dried in the gentle N2 flow. Only the reference cantilevers were incubated in pure octanethiol solution for 12 hours to ensure the formation of a self-assembled monolayer (SAM) on the gold film. Formation of a stable SAM on the reference cantilever ensures that alkanethiol molecules are only absorbed on the sensing cantilever during subsequent experiments.

Surface stress development associated with alkanethiol SAM formation was measured in three steps. In the first step, reference and sensing cantilever were mounted in the sensor and stability of the interferometer was first checked to ensure that measured signal is not affected by drift and ambient noise. In the second step, 20mL of pure liquid octanethiol was injected into a beaker placed near the two cantilevers. The vapors of alkanethiol solutions were confined near the cantilevers and interferometer was utilized to measure the deflection of sensing cantilever associated with deposition and formation of alkanethiol SAMs. Differential surface stress which is proportional to the cantilever deflection is then calculated by using Stoney's Formula(Stoney 1909) with obtained spring constant and geometry of the cantilever.

After the exposure to alkanethiol, both the sensing and reference cantilevers are expected to be covered with alkanethiol SAM; therefore, reintroduction of alkanethiol vapors should not cause further differential bending of the cantilevers. In the last step, sensing and reference

cantilevers were again exposed to alkanethiol vapors to ensure that measured surface stress change is associated with only alkanethiol formation.

Experimental Results

Gold film on the cantilever was imaged using contact mode and grain size was determined to be 40 ± 10 nm (Figure 8). The mean square roughness of the gold surface was 2.07±0.23 nm for the 750 nm scan size. The stiffness of the cantilever was found to be in the range of 0.16-0.18 N/m resulting in a calculated thickness of approximately 1.7- 1.8 μm.

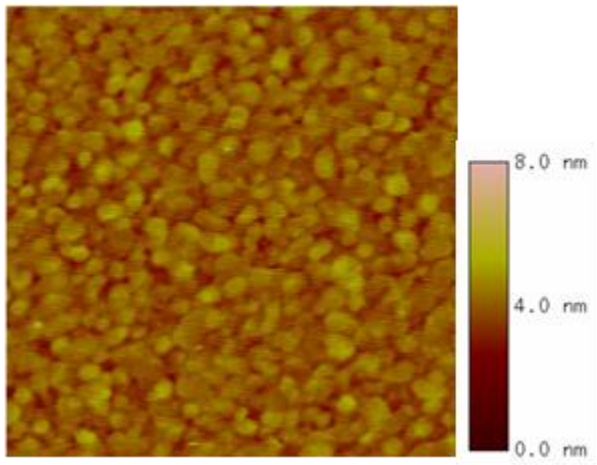

Figure 8. AFM image (750nm×750nm) of gold film microstructure on AFM cantilevers

Experimental measurements of surface stress induced due to vapor phase deposition of alkanethiol during a typical run are plotted in Figure 9. As soon as alkanethiol solution is injected, the microcantilever undergoes an initial tensile surface stress change before the compressive surface stress development. Initial tensile surface stress development has been previously reported by other researchers as well and is thought to be associated with knocking off of surface adsorbed species by individual alkanethiol molecules(Berger, Delamarche et al.

1997). After the initial knock-off phase, the alkanethiol molecules get adsorbed on the surface and arrange into self-assembled monolayers. According to Figure 9, alkanethiol SAMs rapidly form in the early stages, 10 minutes after injection, but it took about 50 minutes to complete SAM formation (final saturation). In the initial phase, plot of surface stress change closely resembles a Langmuir adsorption isotherm. The second development of surface stress change in Figure 9 is due to slow saturation of closely packed SAM on sensing cantilever. In addition, the distance of cantilever to the location where alkanethiol droplets are introduced was 10 cm away. As a result, final surface stress change was 0.28 ± 0.02N/m and the corresponding differential bending was 180 ± 10 nm at grain size of gold surface was 40 ± 10 nm.

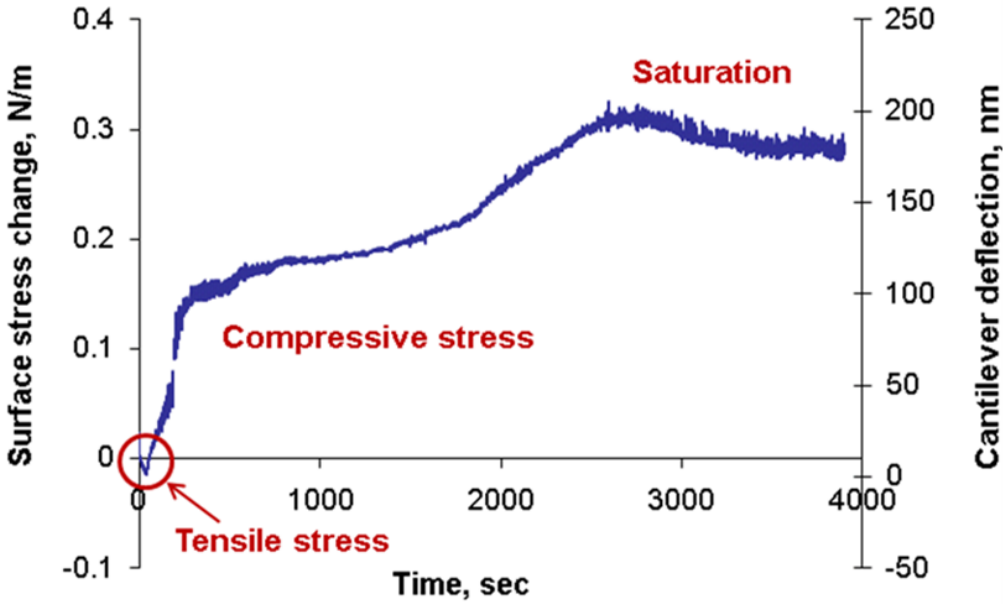

Figure 9. A typical result on cantilever deflection and surface stress change during the adsorption of alkanethiol SAM.

After the SAM formation on the sensing cantilever, sensor was again exposed to alkanethiol vapors. A minimal surface stress change during re-introduction of the alkanethiol vapors indicates that both sensing and reference cantilever are covered with alkanethiol SAM.

Furthermore, it indicates surface stress change observed during the first introduction is unambiguously associated with SAM formation on sensing cantilever. Previous reports(Godin, Williams et al. 2004) have indicated that distance of cantilever to the location where alkanethiol droplets are introduced, condition of gold surface like cleanliness and roughness, and grain structure of the gold on the cantilever's surface affects the kinetics and magnitude of surface stress development. Among those conditions, the microstructure of gold film significantly influences the development of the surface stress during the formation of Alkanethiol SAMs(Godin, Williams et al. 2004).

Measured surface stress changes for alkanethiol SAM formation in the current experiments is compared to other reports in Table 1 as a function of grain size, surface roughness and alkanethiol chain length.

Table 1. Surface stress change reports with different parameters

specimen type	Alkanethiol Chain length	Roughness on 750nm scan size	Grain Size	Surface stress (N/m)	Source
cantilever	4 C - 12 C	-	not reported	0.1-0.25	(Berger, Delamarche et al. 1997)
	12 C	0.3 nm	large	15.9	(Godin, Williams et al. 2004)
	12 C	0.9 nm	small	0.51	(Godin, Williams et al. 2004)
	6 C - 10 C	Not reported	large	6.3	(Godin, Tabard-Cossa et al. 2010)
	12 C	1.32-12.8 nm	not reported	0.09-0.15	(Desikan, Lee et al. 2006)
	8, 12, 18 C	10 nm	not reported	1.2-0.7	(Desikan, Armel et al. 2007)
	8 C	2.07 nm	small	0.28	This work
plate	18 C	1.92 nm	small	0.12-0.15	(Shrotriya, Karuppiah et al. 2008)

Overall Energy of the System due to SAM Adsorption

The mechanism of the cantilever bending due to SAM formation is still not well understood, however it is generally agreed that the adsorbed molecules are responsible for the compressive stress that develops during the adsorption procedure on the surface. The relationship between the cantilever deflection and surface stress is given by Stoney's formula(Stoney 1909),

$$\sigma_s = \frac{Eh^2}{6R(1-\nu)} \tag{7}$$

where σ_s is surface stress, h is the cantilever thickness, R is the radius of curvature due to bending, and E and ν are Young's modulus and Poisson ratio of the cantilever.

The SAM-cantilever system consists of three parts: the SiN_x base layer, the gold layer for SAM adsorption, and the thin layer of SAM chains (Figure 10). According to the reported results from earlier experiments and simulations(Poirier and Pylant 1996, Andreoni, Curioni et al. 2000, Gronbeck and Andreoni 2000), the gold layer is with Au(111) orientation and the sulfur atoms preferentially bind to gold surface on the fcc sites(Gronbeck and Andreoni 2000). In this study, we assume that the SiN_x base is not affected by the SAM absorption since it is far enough from the absorption part and the interactions will be minimum. Therefore the surface stress changes associated with SAM formation are only due to two dominant origins, the adsorbed alkanethiol layer and the gold substrate.

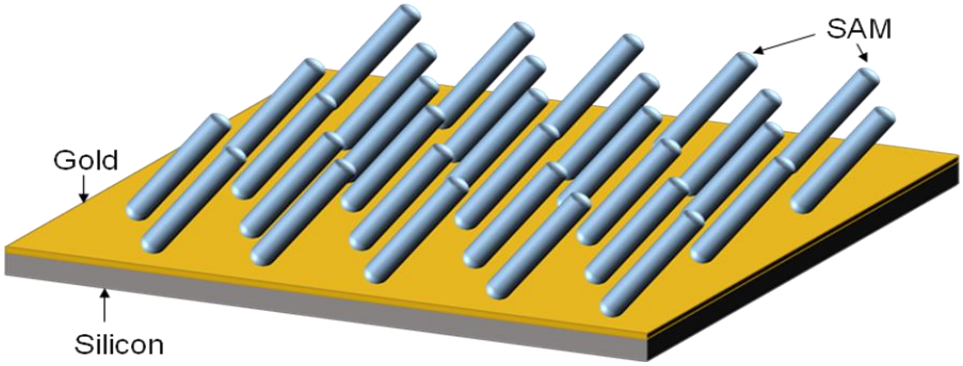

Figure 10. Structure of the microcantilever with alkanetiol adsorption.

The surface stress is defined as the first derivative of the total surface energy change of the system (E_s) with respect to the surface strain (ε_s). The total surface energy change during the alkanethiol SAM formation process is considered to be due to two dominant parts: the energy change within the alkanethiol SAM ($E_{s,SAM}$), and the energy change of the gold substrate associated with the SAM formation ($E_{s,substrate}$). Accordingly, the surface stress induced by SAM formation also consists of two components (SAM layer and gold substrate):

$$E_s = E_{s,SAM} + E_{s,substrate}$$

$$\sigma_s = \frac{\partial(E_s)}{\partial \varepsilon_s} = \frac{\partial(E_{s,SAM})}{\partial \varepsilon_s} + \frac{\partial(E_{s,substrate})}{\partial \varepsilon_s} = \sigma_{s,SAM} + \sigma_{s,substrate} \quad (8)$$

The effects of $\sigma_{s,SAM}$ and $\sigma_{s,substrate}$ are investigated respectively, and the results are compared to determine which component is more dominant in surface stress generation due to alkanethiol SAM formation.

Energy models Associated with Alkanethiol SAM Layer

During the SAM formation, the energy change associated with SAM layer ($E_{s,SAM}$) may come from various origins, including the bonding energy of the covalent chemical bonds within molecules (E_{bond}), the Lenard-Jones potential associated with the van-der-Waal forces between unbonded atoms (E_{L-J}), the interaction energy of gold-sulfur interactions (E_{Au-S}), and the Coulomb energy associated with electrostatic forces between charged molecules (E_{Coul}).

$$E_{s,SAM} = E_{bond} + E_{L-J} + E_{Au-S} + E_{Coul} \quad (9)$$

All these different types of energies are investigated and considered in the energy model. The bonding energy (Xia, Jian et al. 1992, Bosio and Hase 1997) includes the harmonic potentials for bond stretching (stretch), bond bending (bend), and the bond twisting (dihedral) (equation 10(a)). The Lenard-Jones potentials (Jiang 2002) were used to model the interactions between atoms that were not bonded to each other (equation 10(b)). For gold-sulfur interaction, based on a united atom model, Zhang et al. (Zhang, Goddard et al. 2002) employed the Morse potential to depict the interaction, since it can mimic the bonding from a partially covalent bond (equation 10(c)). Partial charges for C, H atoms were obtained from previously reported charge analysis(Franzen 2003), and the Coulomb potentials for the interactions between charged molecules are utilized. These intramolecular and intermolecular potential function parameters have been previously reported to accurately capture the equilibrium conformations, vibrational frequencies, and excess enthalpies of the simulated molecules (Rappe, Casewit et al. 1992, Vemparala, Karki et al. 2004).

$$E_{bond} = \sum_{stretch} \frac{k_r(\alpha - \alpha_0)^2}{2} + \sum_{bend} \frac{k_\theta(\theta - \theta_0)^2}{2} + \sum_{dihedral} \sum_{n=1}^{3} \frac{k_n[1 + cos(n\varphi - \varphi_n)]}{2} \quad (10(a))$$

$$E_{L-J} = 4\varepsilon\left[\left(\frac{\gamma}{r}\right)^{12} - \left(\frac{\gamma}{r}\right)^{6}\right] \quad (10(b))$$

$$E_{Au-S} = De\left\{exp\left[-S\left(\frac{r}{r_e} - 1\right)\right] - 2exp\left[-\frac{S}{2}\left(\frac{r}{r_e} - 1\right)\right]\right\} \quad (10(c))$$

where all the parameters ($k_r, k_\theta, k_n, \alpha_0, \theta_0, \varphi_n, \varepsilon, \gamma, De, S, r_e$) are previously reported.

Energy models Associated with Gold Substrate

Besides the interchain and intrachain effects within the molecular layer of alkanethiol SAM, the surface stress changes may also be due to the gold substrates. The alkanethiol

molecules are chemisorbed on the surface with the sulfur atom forming a strong bond with gold atoms and induce remarkable surface reconstructions. The gold-sulfur bond may result in changes in the electron clouds and the separations of Au atoms. Andreoni et al. (Gronbeck and Andreoni 2000) used first principle calculations based on density functional theory to show that absorption of thiolated molecules on gold surface leads to redistribution of the charge density, and the gold atoms closest to the sulfur atom undergo a surface expansion with interatom separation changing from 2.88 to 3.45 Å. Beardmore et al. (Beardmore, Kress et al. 1997) also conducted first principle quantum calculation for gold-sulfur bond and showed that the gold atoms participating in the bonding become more positive charged while the sulfur atoms become more electro-negative.

Two empirical potentials were modified and utilized to model the energy of the gold substrate associated with surface reconstructions due to gold-sulfur bonds during the SAM formation, the embedded atom method (EAM) (Daw and Baskes 1983, Daw and Baskes 1984, Foiles, Baskes et al. 1986) and surface embedded atom method(Haftel and Rosen 1995) (SEAM). Both two empirical potentials have been widely applied to model gold bulk and surface properties, and have the following form:

$$E_i = F\left(\sum_{j\neq i}\rho(r_{ij})\right) + \frac{1}{2}\sum_{j\neq i}\phi(r_{ij}) \qquad (11)$$

where F is the embedding function that depends only on the local electron density from the surrounding atoms, ρ is the electron density function from a single atom at a distance r, and ϕ is the pair potentials between atoms as a function only of the separation between two atoms.

In these potentials, the embedding function provides the cohesive interaction or attractive force between the atoms while the shielded electrostatic interactions results in a repulsive force between the atoms. Interatomic spacing and the lattice arrangement of the atoms is determined by the balance of cohesive and repulsive forces. The first principle calculations(Andreoni, Curioni et al. 2000) suggest that during alkanethiol SAM formation, sulfur atoms occupy fcc sites on Au (111) surface and the three nearest gold atoms become more positive as they bind to the sulfur atoms. In order to model the surface reconstruction, we assumed that the electron density $\rho(r_{ij})$ of the gold atoms triplet nearest to sulfur atoms is reduced, leading to reduction in cohesive forces and consequently increase in the interatomic spacing between them. EAM/SEAM can solve problems for metals or alloys with different component, but not for metals with surface attachment with adatoms such as sulfur. To solve this problem, we took a modification to the potential models to represent the electron loss of atoms, by changing the electron density function. The electron density of gold triplet binding to sulfur atoms is described as:

$$\rho'(r_{ij}) = k\rho(r_{ij}) \tag{12}$$

where the *k* is reduction factor.

Simulation Models and Surface Stress Predictions

The influences of the energy changes associated with SAM layer and gold substrate are investigated separately with the energy models described above. Molecular dynamics (MD) simulations were conducted with an open source shared parallel code – LAMMPS (http://lammps.sandia.gov/).

For energy investigation with SAM layer, simulation box containing 24×24alkanethiol molecules are utilized (Figure 11). The close packed alkanethiol (S-$(CH_2)_{15}$-CH_3) chains are hexagonally arranged at full coverage density on fcc sites on Au (111) plane with an approximate 30° initial tilt angle with respect to the normal vector of the surface. Two layers of gold atoms are utilized to present the gold substrate, and in order to simulate the energies coming from the SAM molecules alone, the gold atoms are kept fixed and the interactions associated with gold atoms are neglected.. The simulation box is periodic along the in-plane directions (*x* and *y*) and with fixed boundary conditions in *z* direction.

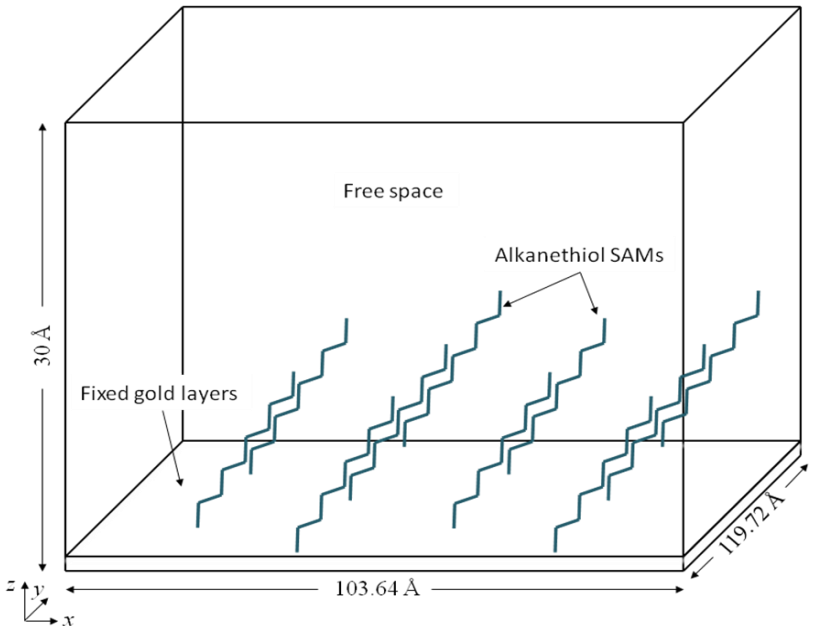

Figure 11. Schematic illustration of the simulation box, periodic boundaries along in-plane directions.

For energy investigation with the gold substrate, simulation box containing 36×60×60 gold atoms are utilized with Au (111) lattice, and lines of gold triplet atoms on the top surface are selected to have the reduction of the electron density to present the gold atoms that interact with the sulfur atoms of the adsorbed SAM molecules (Figure 12). Bottom layer of the gold

atoms was held fixed and the *z* dimension was chosen to be larger than extent of gold lattice in order to simulate the free surface. The simulation box is with periodic *y* and fixed *z* boundary conditions, and two different boundary conditions are applied to *x* direction, periodic (direct computation) and fixed (continuum elasticity based computation), for different analysis approaches.

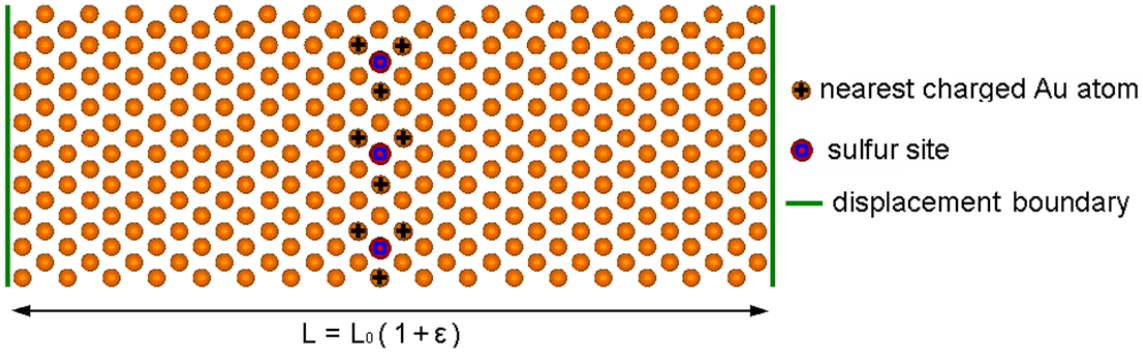

Figure 12. Top view showing the gold triplet atoms on the surface of gold substrate.

Surface stress changes associated with SAM layer and gold substrate during the SAM formation are analyzed based on the energy observations from the simulations. The energy components are evaluated with respect to different strain values applied to the simulation box. Strains are applied by stretching or compressing the simulation box by certain ratio, and the energies associated with SAM layer and gold substrate are calculated accordingly. With all the simulation results, the energies can be plotted as a function of the applied strain, and the surface stress changes are analyzed with the relationship between the energies and the strain.

Two different approaches, direct computation and continuum elasticity based computation, were applied for surface stress analysis associated with SAM formation. The

surface energy changes were calculated as the difference between energy computation with and without the SAM immobilization (equation (13)).

$$E_{s,SAM} = E_{w/\ SAM} - E_{w/o\ SAM} \tag{13}$$

With the direct computation approach, the surface stress are simply predicted with the definition (equation (8)) based on the energy/strain relationship. The first derivative of the energy with respect to strain is taken for surface stress prediction.

The continuum elasticity computation approach was also utilized to investigate the surface stress based on the Elastic interaction between the strain fields imposed due to adsorption of alkanethiol chains on the surface. Following Kukta et al.(Kukta, Kouris et al. 2003), the elastic field induced by an adsorbed alkanethiol molecule is approximated by a force dipole acting on the surface. Absorption induced energy change associated with gold substrate is modeled as a quadratic function of surface strain as:

$$E_{s,SAM} = E_{w/\ SAM} - E_{w/o\ SAM} = a_0 + a_1\varepsilon + \frac{1}{2}a_2\varepsilon^2 \tag{14}$$

where a_1 is the strength of the force dipole induced due to atom adsorption and a_2 determines dependence of induced force dipole on the surface strain to first order. For a two dimensional geometry, the surface stress change due to molecule adsorption is expressed as(Kukta, Kouris et al. 2003):

$$\sigma_{s,SAM} = -\frac{3\eta a_1}{3 - \pi^2\eta^2 C a_2} \tag{15}$$

where $C = (1-\nu)/\pi\mu$ is a positive constant related to substrate Poisson's ratio (ν) and the shear modulus (μ); η is the density of molecules on the surface.

Modeling results and Discussions

In order to determine the energy associated with SAM layer at the equilibrium state in the room temperature, three steps were taken with 1fs time step in MD simulations with LAMMPS code. The system was first set to a very low temperature (0.45 K) with NVT ensembles (fixed number of atoms, volume, and temperature. After the energy was relaxed and stabilized, the temperature of the system was raised and kept fixed at room temperature (300 K) with NVT ensembles until equilibrium state was achieved. Extra charges of the CH_3end groups were applied to all SAM molecules, and the temperature was also kept at 300 K until the equilibrium. In all three steps, the simulation continued with NVE ensembles (fixed number of atoms, volume, and energy) for a period of time (100 ps) to exact statistical information.

Strains (-0.2% to 0.3%) were applied by stretching or compressing the simulation box, and corresponding energies were collected. The energy changes (differences between configurations with and without applied strain) associated with SAM layer in the three steps were plotted with respect to the strain (Figure 13). Surface stress is investigated through direct computation with the relationship of the strain as the definition (equation (8)). However, the simulation results showed that in all three steps, the energies have no obvious trend with respect to strain, which would lead to an insignificant surface stress observation. In details, compared to the short-term and thermal energies, the long term energies which contributed to inter-chain interactions such as the Lenard-Jones potentials, and Coulomb energy between molecules were too small to affect the energy trend line. Thus the surface energy change associated with SAM layer was negligible, and was not the dominant origin of the surface stress generation due to SAM formation.

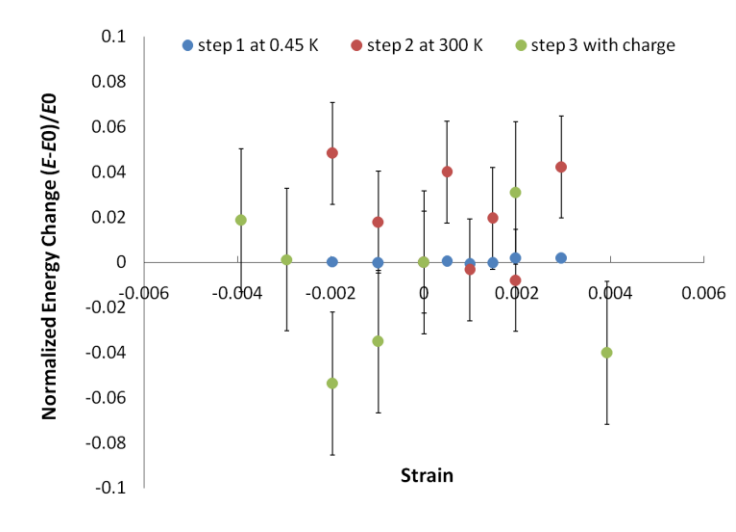

Figure 13. Normalized energy changes with respect to strain

Investigations on modified EAM and SEAM empirical potentials were conducted with increasing electron loss in order to match the surface expansion results with reported first principle calculation observations(Andreoni, Curioni et al. 2000). The surface expansion results are shown in Table 2 with corresponding electron density reduction factor for EAM and SEAM potentials. k = 0.8 and 0.2 were found to achiever the reported expansion of 3.45 Å for EAM and SEAM models respectively, that is, each gold atom need to lose 0.8 electrons for EAM potential, while 0.2 electrons for SEAM potential. Therefore, in EAM model observation, a total amount of 2.4 electrons were lost to a sulfur atom, while in SEAM model, only 0.6 were lost. Beardmore et al.(Beardmore, Kress et al. 1997) reported residual atomic charges of (3×0.17) obtained by fits to the electrostatic potential and dipole moments for SAM formation. As a result, the SEAM gave a better performance in surface stress problem to simulate the electron loss, and we chose to use modified SEAM empirical potential in the simulations of surface stress generation associated with the surface reconstructions in this study.

Table 2. Surface expansion results with EAM and SEAM potentials

reduction factor (*k*)	EAM expansion (Å)	reduction factor (*k*)	SEAM expansion (Å)
0	2.88	0	2.88
0.5	3.19	0.05	2.92
0.7	3.38	0.1	3.21
0.8	3.46	0.2	3.47
1	5.87	0.3	5.14

With the modified SEAM potential, direct computation and continuum elasticity based computation, were both applied for energy calculation and surface stress calculation associated with gold substrate. In the direct computation approach, different number of lines of gold triplet atoms ((1, 2, 3, 4, 6, 12 lines) were utilized to present different coverage densities of SAM, and the energy change (per area) was found to be proportional to the number of lines of gold triplet atoms. Energy changes per line of gold triplet atoms associated with different densities are plotted in Figure 14 as a function of applied strain (-0.5% to 0.5%). The relationship between the surface energy and strain was analyzed and the surface stress was calculated as the first derivative of the energy with respect to the strain (equation (8)). Secord order relationship was obtained between the surface energy and surface strain, thus the surface stress change was linear dependent of strain in this calculation. Surface stress was plotted as a function of the coverage density of SAM with the applied strain of 0, and was found to be proportional to the coverage density (Figure 15), the negative values suggested compressive surface stress on the cantilever.

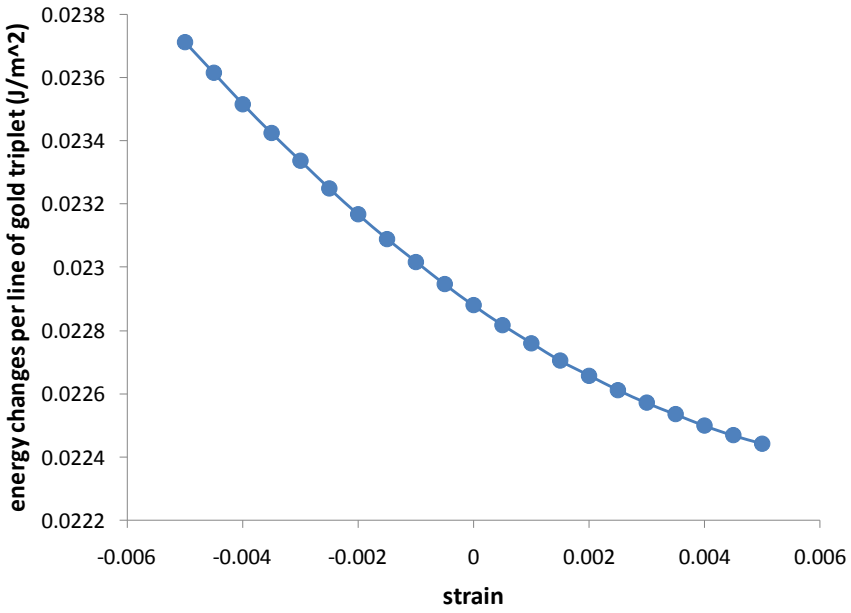

Figure 14. Direct computation approach: surface energy change per line of gold triplet vs. strain

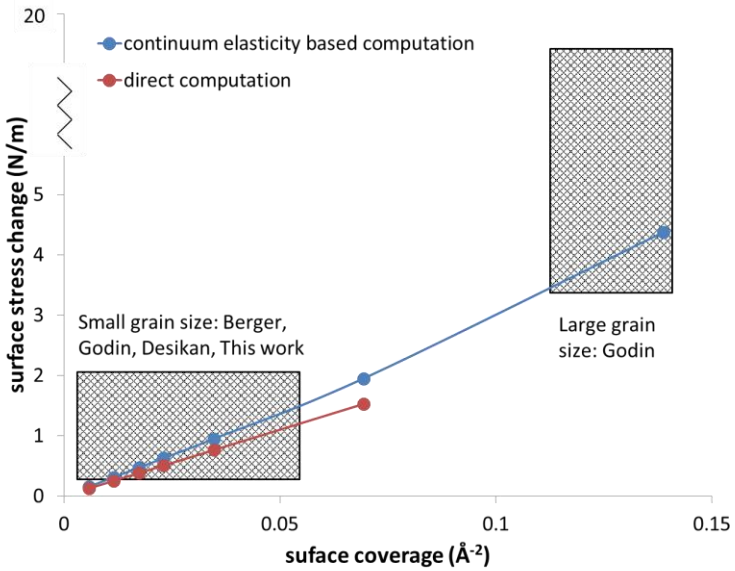

Figure 15. Surface stress change prediction vs. coverage density and comparison with experimental reports

In the continuum elasticity based computation, surface energy change was computed with 1 line of gold triplet atoms and was plotted in Figure 16 as a function of strain (-0.5% to 0.5%). Second order relationship was applied to fit the curve, and the fitted parameters were used for surface stress predictions (equation (16)). The surface stress predictions were plotted in Figure 16 with respect to the surface coverage density. Non-linear influences of the coverage density were observed due to the consideration of the second order term in the energy/strain relationship.

$$E_{s,SAM} = (1.2\varepsilon^2 - 1.63\varepsilon + 0.285) \times 10^{-9},$$

$$\sigma_{s,SAM} = -\frac{4.89\eta}{3 \times 10^9 - 7.8 \times 10^{-11}\eta^2} \quad (16)$$

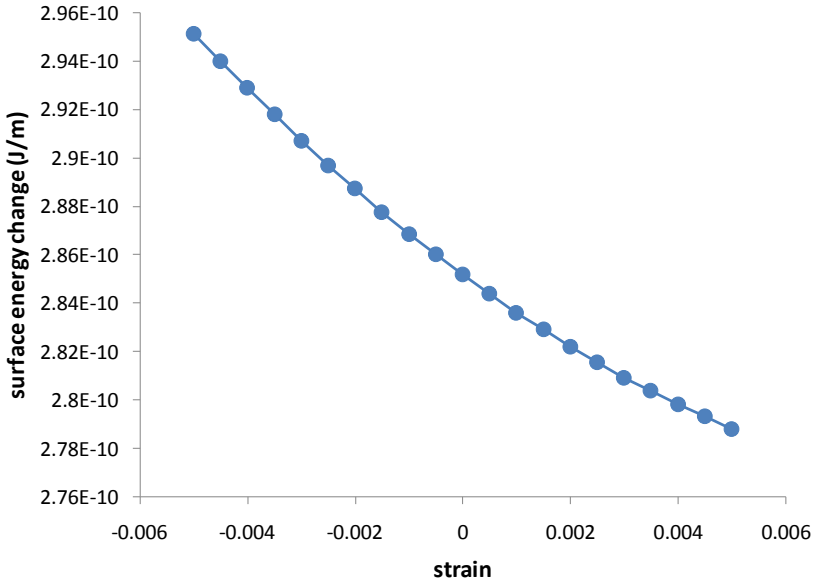

Figure 16. Continuum elasticity based computation: energy change vs. strain

Comparison of Numerical Predictions with Experimental Reports

Since the surface stress change due to the SAM layer is negligible, the dominant origin of the surface stress change during the SAM formation is from the surface reconstruction of the

gold substrate. Two models, direct simulation computation and continuum elasticity based computation, are established to study and confirm the surface stress change with respect to the immobilization density of the SAMs. The direct computation predicted a stress range of 0.12 to 3.06 N/m which was proportional to the immobilization density, and the continuum elasticity based computation provided a stress range of 0.16 to 4.38 N/m. These two models generally predicted the surface stress change of similar magnitude, while continuum elasticity based computation provided a little higher stress changes due to the nonlinear effects.

Both direct computation and continuum elasticity based computation provided surface stress predictions that cover the range of the reported experimental results. As in Godin's report (Godin, Williams et al. 2004), grain size and roughness condition of the gold coating has significant effects on the surface stress changes. The SAMs adsorption on to surfaces with large and flat grains would have high quality monolayers, and vice visa SAMs on small-grained surface would have incomplete adsorption and thus have lower immobilization density and less dense packing. As a result, larger gain and smaller roughness will provide higher immobilization density. The comparison between simulation and experimental results are plotted in Figure 15 that most experiments were performed with small grained surface which lead to low immobilization densities, and according to Godin's work (Godin, Williams et al. 2004), they all form SAMs with lying-down phases.

Conclusions

Separate simulations were performed to study the influences of the energy changes associated with SAM layer on the surface and gold substrate on the surface stress change due to the immobilization of the alkanethiol SAMs. The simulations with SAM layer showed the

surface stress change due to interchain and intra chain interactions of SAM molecules was negligible, and the surface stress associated with the surface reconstruction of the gold substrate was strong dependent of the surface coverage density. The results suggested that the surface reconstructions of the gold substrate were the dominant origin of the surface stress generation. As a result the chain length takes very little influences on the surface stress change during the SAM formation.

The modified SEAM and EAM potentials were first introduced to the SAM study with electron loss considerations, and the results showed that to achieve the same surface expansion, EAM had to suffer more electron loss than it was required for SEAM. In this work, SEAM provided more reasonable electron loss per gold atom (0.2) compared to that of EAM (0.8).According to the results, we suggested that SEAM would be more suitable when analyzing the surface problems with SAM studies.

Both direct computation and continuum elasticity based computation approaches provided similar ranges of surface stress predictions with modified SEAM potential. The predictions increased with the surface coverage density, and the total range of the predictions covered the reported experimental results. According to Godin's work, the surface stress observations were greatly affected by the grain size of the gold substrate. Larger grains may lead to better immobilization and higher immobilization density which will induce higher surface stress, while smaller grains may on contrast lead to lower surface stress change.

CHAPTER 5. CANTILEVER DEFLECTION ASSOCIATED WITH HYBRIDIZATION OF MONOMOLECULAR DNA FILM

Modified from a paper submitted to Journal of Applied Physics

Yue Zhao, Baskar Ganapathysubramanian, Pranav Shrotriya

Abstract

Recent experiments show that specific binding between a ligand and surface immobilized receptor such as hybridization of single stranded DNA (ssDNA) immobilized on a microcantilever surface leads to cantilever deflection. The binding induced deflection may be used as a method for detection of biomolecules such as pathogens and biohazards. Mechanical deformation induced due to hybridization of surface immobilized DNA strands is a commonly used system to demonstrate the efficacy of microcantilever sensors. To understand the mechanism underlying the cantilever deflections, a theoretical model that incorporates the influence of ligand/receptor complex surface distribution and empirical interchain potential is developed to predict the binding induced deflections. The cantilever bending induced due to hybridization of DNA strands is predicted for different receptor immobilization densities, hybridization efficiencies and spatial arrangements. Predicted deflections are compared with experimental reports to validate the modeling assumptions and identify the influence of various components on mechanical deformation. Comparison of numerical predictions and experimental results suggest that at high immobilization densities, hybridization induced mechanical deformation is determined primarily by immobilization density and hybridization efficiency

whereas at lower immobilization densities, spatial arrangement of hybridized chains need to be considered in determining the cantilever deflection.

Introduction

Microcantilever based sensors are an intriguing new alternative for conventional chemical and biological sensors because of their extremely high sensitivity and miniature sensing elements. The sensing strategy involves coating one surface of a micromachined cantilever with a receptor species that has high affinity for the analyte molecule. Binding of the ligand on the sensitized surface induces a mechanical deformation of the microcantilevers thus transducing the surface chemical reaction into a measurable quantitative signal. Thundat and his colleagues (Thundat, Warmack et al. 1994) made the seminal observation that Atomic Force Microscope (AFM) cantilevers deflect due to changes in relative humidity and thus opened a myriad of possibilities for the use of AFM cantilevers for chemical and biological sensing. They predicted possibilities of adsorbate detection of the order of picograms and immediately followed up with another study in which they detected mercury adsorption on cantilever from mercury vapor in air with picogram resolution (Thundat, Warmack et al. 1994, Thundat, Wachter et al. 1995). Since these initial reports, microcantilever-based sensors have been investigated for sensing of chemicals (Tamayo, Humphris et al. 2001, Lavrik, Sepaniak et al. 2004), DNA hybridization (Fritz, Baller et al. 2000, Hansen, Ji et al. 2001, Wu, Ji et al. 2001, Alvarez, Carrascosa et al. 2004, Stachowiak, Yue et al. 2006, Kang, Nilsen-Hamilton et al. 2008, Jin, Shin et al. 2009, Kang, Nilsen-Hamilton et al. 2009), explosives (Thundat, Pinnaduwage et al. 2004, Zuo, Li et al. 2007, Seena, Rajoriya et al. 2010), biomolecules (Ilic, Czaplewski et al. 2001, Raiteri, Grattarola

et al. 2001, Wu, Datar et al. 2001, Arntz, Seelig et al. 2003) , and markers for cancer (Hood, Heath et al. 2004, Ferrari 2005, Sengupta and Sasisekharan 2007).

DNA hybridization is a simple and prominent example of biomolecular recognition and detection, since it is fundamental to most biological process. Fritz et al. (Fritz, Baller et al. 2000) monitored hybridization of surface immobilized single stranded DNA (ssDNA) with oligonucleotide length of 12 nt, and with 3 different concentration values of the target ssDNA molecules (80nM, 400nM, and 2000nM). Cantilever deflections of about 3 nm, 15 nm, and 21 nm were reported respectively. Cantilever deflection was also found to be different for hybridization of ssDNA with strands that had single base-pair mismatch, indicating that microcantilever based sensors have intrinsic sensitivity to detect single nucleotide polymorphisms. Since this work, cantilever deflection due to ssDNA hybridization has been utilized as an validation experiments for new techniques, and cantilever deflection signal up to ~100 nm have been reported for those experiments (Wu, Ji et al. 2001, McKendry, Zhang et al. 2002, Stachowiak, Yue et al. 2006, Kang, Nilsen-Hamilton et al. 2008, Kang, Nilsen-Hamilton et al. 2009) .

Hansen et al. (Hansen, Ji et al. 2001) also demonstrated that hybridization induced cantilever deflection can be used to discriminate base-pair mismatches with 20- and 25-mer probe DNA molecules. They used 10-mer DNA oligonucleotides as complementary target molecules which contain one or two internal mismatches. The results showed that the number and position of mismatch pairs will affect the deflection of the cantilever.

Stachowiak and co-workers (Wu, Ji et al. 2001, Stachowiak, Yue et al. 2006) conducted experiments to investigate the influence of ssDNA strand length, immobilization density and hybridization efficiency on the hybridization induced microcantilever deformation. The salt

concentrations in immobilization and hybridization buffer were varied to achieve different immobilization density and coverage of hybridized molecules, respectively. Changing the salt concentrations from 0 to 1000 mM resulted in an increase in immobilization density from 0.06 to 0.12 nm^{-2} and similar change of salt concentration in hybridization buffer resulted in an increase of hybridization efficiency from 30% to 80%. Three different molecular lengths of 10 nt, 20 nt, and 30nt were used and both immobilization density and coverage of hybridized molecules decreased as the chain length increased. Hybridization induced cantilever deflections corresponding to different chain lengths, immobilization densities and hybridization efficiencies collapsed on to a single curve when expressed as a function of the coverage of hybridized chains. These results indicated that the effects of the immobilization density, hybridization efficiencies and chain length are coupled and the cantilever deflection primarily depends on the surface coverage of hybridized chains.

In order to explain the underlying mechanism for hybridization induced deflection, Fritz (Fritz 2008) hypothesized that the cantilever deflection is result of two competing mechanism: electrostatic repulsion between negative charges on the DNA strands and relaxation of steric hindrance as disordered ssDNA transition to ordered DNA strands. The increase in negative charges during hybridization results in an expansion of the cantilever surface due to the electrostatic repulsion and consequently, bending of the cantilever. Alternatively, when surface bound single stranded oligonucleotide undergo hybridization, conformational changes from a disordered strand to rod-like double helix result in relaxation of the steric hindrance and contraction of the surface. The competing mechanisms were proposed to explain cantilever bending observed during hybridization experiments. During the initial phase of DNA hybridization the relaxation of steric hindrance leads to relaxation of cantilever bending but as

the hybridization proceeds, the surface starts expanding due to buildup of charge interactions among neighboring molecules. However, it is important to note that the DNA hybridization experiments are performed in buffers with high salt concentrations. The positive ions in the solutions may shield the electrostatic repulsion between the strands and the magnitude of inter-chain repulsion may depend on the ionic composition of the hybridization buffer.

Besides the electrostatic effects, hydration forces between the chains may also lead to hybridization induced cantilever deflection (Strey, Parsegian et al. 1997, Strey, Parsegian et al. 1999, Hagan, Majumdar et al. 2002). To study the effect of the hydration forces, Mertens et al. (Mertens, Rogero et al. 2008) conducted experiments to investigate the influence of relative humidity on deflection of micro-cantilevers immobilized with ssDNA and double stranded DNA (dsDNA). Deflection of cantilevers with ssDNA and dsDNA strands increased to about 500 nm and 600 nm, respectively as the relative humidity was changed from 0 to 100%. These results indicate that hydration forces play an important part in determining cantilever deflection.

Hagan et al. (Hagan, Majumdar et al. 2002) modeled the hybridization induced cantilever deflections based on both electrostatic repulsions and hydration forces between DNA strands. The microcantilever was modeled as a membrane and the DNA strands were modeled as straight rods immobilized on the membrane surface. Repulsive interactions between the DNA strands lead to increase in their spacing and rotation of rods, resulting in cantilever bending. Cantilever deflections due to a high immobilization density of 0.17 chains/nm^2 and hybridization efficiency of 100% were investigated. Based on the numerical results it was concluded that the cantilever deflection induced by uniformly distributed DNA strands is much smaller in magnitude compared to experimental observations. However, numerical prediction based on disordered

arrangement of DNA strands and 100% hybridization efficiency was found to match the experimental observations.

In this paper, we report a model for hybridization induced bending of micro-cantilever based on the minimization of energy functional that accounts for cantilever bending energy and DNA inter-chain interactions. Influence of different immobilization densities, hybridization efficiencies and chain distribution on the cantilever bending is considered. Cantilever is idealized as a beam while the energy of DNA is estimated using interaction potentials that account for both electrostatic and hydration forces. Predicted results are compared to experimentally reported deflections to identify the influence of immobilization density, hybridization efficiency and chain distribution on cantilever deflection.

Theoretical Model

The microcantilever is modeled as a slender multilayer beam as schematically represented in Figure 17 and consists of three layers: the SiN_x base layer, the gold (Au) layer for biomolecule immobilization and the immobilized DNA strands. The total energy of the DNA-cantilever system is consisted of two major parts, the bending energy of the cantilever and the inter-chain energy between DNA molecules.

$$E_{total} = E_{bend} + \sum_{all\ molecule\ pairs} F^i \qquad (17)$$

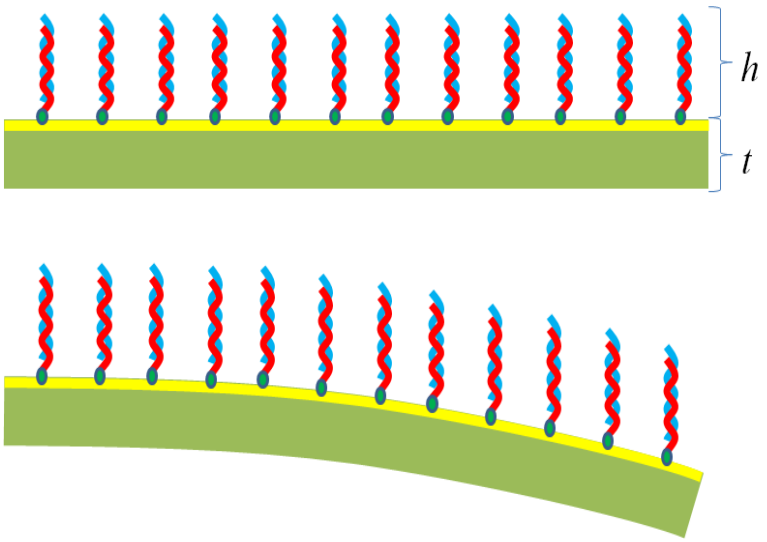

Figure 17. Cantilever bending model in the simulation.

The gold film thickness is much smaller than overall thickness and in addition elastic modulus of gold is of the same order of magnitude as that of the base silicon nitride therefore the cantilever is modeled as a monolithic linear elastic material in order to simplify the bending energy expression. The bending energy of the cantilever, denoted by E_{bend}, can be expressed as a function of the equilibrium radius (R) with the cantilever plane stain elastic modulus and thickness (t) (Ibach 1997)

$$E_{bend} = \frac{Et^3}{12R^2(1-\nu^2)} \tag{18}$$

where $R = \frac{L^2}{2\delta}$, E is the modules, L is the length of the cantilever, ν is the Poisson Ratio, δ is the cantilever deflection.

The total energy of DNA molecules is modeled as the sum of the pair interaction energy, and thus is a function of three groups: the interaction between hybridized dsDNA molecules (*D*-*D*), between hybridized ds DNA and ssDNA (*D*-*S*), and between ssDNAs (*S*-*S*).

$$F = F(D-D) + F(D-S) + F(S-S) \tag{19}$$

Strey et al. (Strey, Parsegian et al. 1997, Strey, Parsegian et al. 1999)showed that the energy of *D-D* interaction is far higher than that of *D-S* and *S-S* interactions. As a result, the energy from *D-S* and *S-S* interactions is neglected, and the total energy of DNA molecules is simplified to be a function only of *D-D* interactions.

$$F = F(D-D) \tag{20}$$

Strey et al. (Strey, Parsegian et al. 1997, Strey, Parsegian et al. 1999) proposed the functional form for the interaction energy based on the analysis of nematically ordered polymers. The function form was derived considering the direct interactions $\mathrm{F}_0^{\mathrm{i}}$ between molecules and the harmonic entropic fluctuation part.

$$F^i = F_0^i(d^i) + ck_BTk_c^{-1/4}\sqrt{\frac{\partial^2 F_0^i}{\partial d^2} - \frac{1}{d}\frac{\partial F_0^i}{\partial d}} \tag{21}$$

where $\mathrm{k_B}$ is the Boltzmann constant, T is the temperature, $\mathrm{l_p}$ is the persistence length of the DNA molecules, $\mathrm{k_c = k_B T l_p}$ denotes the intrinsic bending stiffness of the DNA molecules, and the parameter *c* is an empirical determined dimensionless constant of order 1. The free energy F_0 is the summation of all molecular interaction between DNA molecules as a result of the solvent-mediated interactions (hydration forces) and electrostatic repulsions.

A systematic study of the electrostatic energy between two rod-like molecules with surface charges has been reported by Brenner et al. (Brenner and Parsegia.Va 1974). They did theoretical calculations for two molecules with different configurations and at all mutual angles. Following their analysis, the functional form of the free energy per unit length between hybridized DNA molecules resulting from the electrostatic repulsions is expressed in equation (22).

Hydration forces are attributed to hydration bonding network between neighboring DNA strands in water. Leikin et al (Leikin, Parsegian et al. 1993) reported that dsDNA is surrounded by at least two hydration shells which contain about 20 water molecules per base pair. This leads to a strong repulsion between DNA molecules when the separation is within several decay length. They also suggested that the free energy per unit length due to hydration forces between rod–like molecules should be of the same form as the electrostatic repulsions.

The DNA molecules used in the cantilever experiments are usually less than 50 nucleotide long (< 17 nm) and are considerably short compared to the persistence length of double strand DNA (Smith, Cui et al. 1996). As a result, the hybridized DNA molecules can be treated as rods or cylinders standing on the surface of the micro-cantilever. With the parallel rods assumption, the energy of electrostatic repulsion and hydration forces per unit length can be written as (Brenner and Parsegia.Va 1974)

$$F_{EL}^{i} = a\sqrt{\frac{\pi}{2}}\frac{exp\left(-d^{i}/\lambda_{D}\right)}{\sqrt{d^{i}/\lambda_{D}}} \qquad (22)$$

where λ_D and d^i are the decay length and the axial separation between molecules respectively, a is determined by the salt concentration in the solution experimentally. Similarly, the expression for the hydration force induced interactions is expressed as:

$$F_{H}^{i} = b\sqrt{\frac{\pi}{2}}\frac{exp\left(-d^{i}/\lambda_{H}\right)}{\sqrt{d^{i}/\lambda_{H}}} \qquad (23)$$

where λ_H (~0.29 nm) is the correlation length (decay length) of water, and b is also determined empirically. So the final free energy for a pair of DNA molecules (F_0 in Strey's equation (Strey, Parsegian et al. 1997, Strey, Parsegian et al. 1999)) is written as:

$$F_0^i(d^i) = a\sqrt{\frac{\pi}{2}}\frac{exp(-d^i/\lambda_D)}{\sqrt{d^i/\lambda_D}} + b\sqrt{\frac{\pi}{2}}\frac{exp(-d^i/\lambda_H)}{\sqrt{d^i/\lambda_H}} \quad (24)$$

The DNA molecules are initially considered to be standing parallel on the surface of the cantilever. As the separation between DNA chains is increased, F_0 decays exponentially. Since the DNA strands are only immobilized on the top surface of the cantilever, increase in DNA separation will lead to cantilever bending. Since the length of DNA strands (h = several nm) is two order of magnitude smaller than the cantilever thickness (t = 500-1000 nm), cantilever deflections of the order of 10-100 nm will only result in small rotations of the DNA strands. Therefore, the DNA strands are assumed to stay nearly parallel throughout the cantilever deflections. The relation between inter chain separation and radius of curvature of the bent cantilever is expressed as

$$d^i = d_0^i\left(1 + \frac{t}{2R}\right) \quad (25)$$

where d_0^i is the initial separation before cantilever bending, and i denotes the ith molecule pair.

As a result, the total energy of the system which is the summation of the cantilever bending and total free interaction energy is a function of the initial ensemble of hybridized DNA molecules and equilibrium radius of the cantilever.

$$E_{total} = E_{bend}(R) + \sum_{DNA\ pairs} F\left(d_0^i, R\right) = E_{total}(d_0, R) \quad (26)$$

The total energy is minimized to determine the equilibrium radius of curvature for different ensembles to investigate the effect of different immobilization and hybridization efficiencies.

Initial DNA Ensembles

In the cantilever bending experiments, the ssDNA molecules are first immobilized on the cantilever with a certain immobilization density. Subsequently, a certain percentage of ssDNA chains (quantified by the hybridization efficiency) bind with the complementary targets forming hybridized dsDNA chains leading to cantilever bending. The number of the hybridized dsDNA chains on the surface is determined by the immobilization density and hybridization efficiency while their arrangement will depend both on the spatial distribution of DNA chains during immobilization and hybridization steps. The immobilization density and hybridization efficiency may be experimentally determined but it is hard to directly measure the chain arrangement on the cantilever surface. For a given hybridization and immobilization efficiency, four different ensembles of hybridized DNA chains are constructed in order to determine the influence of spatial arrangements on the hybridization induced cantilever bending. Each ensemble consisted of 1600 DNA chains.

In the first ensemble (average spacing), the hybridized chains were assumed to be arranged in a hexagonal close packed arrangement with uniform spacing. Hexagonal closed pack arrangement were created from the given immobilization density (d_0) and hybridization efficiency (φ). The interchain spacing was computed to match coverage of hybridized chains (d), calculated according to the following equation:

$$d^i = d_0^i/\sqrt{\varphi} \tag{27}$$

Close-packed hybridized dsDNA ensembles were generated for the desired coverage of hybridized chains and the cantilever deflections were computed through minimization of bending and hybridized dsDNA interaction energy.

Although the close-packed distribution of hybridized dsDNA is easy to construct, it neglects most details in the real experiments. The first ensemble simply combines the two steps together and may not represent the real surface arrangement of hybridized dsDNA chains. The immobilization and hybridization steps were considered separately in generating the next three ensembles of hybridized dsDNA chains.

In the second ensemble (random selected), the ssDNA were assumed to be immobilized on the surface with hexagonal closed pack spacing. Distribution of hybridized dsDNA was generated assuming that all the immobilized ssDNA chains have equal probability for hybridization. A certain proportion of the ssDNA chains were randomly selected and converted to hybridized dsDNA in order to match the required hybridization efficiency. Random selection is the simplest way to make an ensemble which has high degree of disorder due to the hybridization. Five hundred different ensembles were generated for each immobilization and hybridization efficiency and the cantilever deflections were computed for each ensemble through minimization of the bending and hybridized dsDNA interaction energy.

In the third ensemble (Monte-Carlo selected), the ssDNA were again assumed to be immobilized on the surface with hexagonal closed pack spacing however the hybridized dsDNA distributions were generated assuming that hybridized sites will be distributed on the surface such that interaction energy between the ssDNA chains is minimized. A Monte-Carlo method based procedure was used to identify the distribution of hybridized dsDNA sites that have the lowest interaction energy for hybridized dsDNA chains. In each step of the energy minimization procedure, a single hybridized and non-hybridized site were selected for exchange and this exchange was accepted or rejected depending on the change in interaction energy and acceptance probability. This process was repeated for approximately 10^6 steps till the total interaction

energy does not have any further reduction. The hybridized dsDNA distributions corresponding to minimum interaction energy were used to compute the cantilever deflections for different immobilization densities and hybridization efficiencies.

In the fourth ensemble (Gaussian disordered), the chain distributions computed through Monte-Carlo based energy minimization were perturbed by imposing a random displacement at each hybridized dsDNA sites. The random displacements followed a Gaussian distribution with a mean value of zero and a range specified as fraction of interchain separation. In the random selected and the Monte-Carlo selected ensembles (discussed above) ssDNA chains are assumed to immobilize in a hexagonal close packed arrangement on the cantilever. Therefore, ensembles with different range of perturbations were used for computing the cantilever deflection in order to investigate the influence of disorder magnitude on hybridization induced bending.

Cantilever Bending Computation

Cantilever deflections are computed through minimization of the total bending and hybridized dsDNA interaction energy given in equation (17). A function minimization program is taken to minimize the total energy and the stable state is achieved (Shor 1985). The cantilever deflections are computed for hybridized dsDNA strands of three different lengths, 10-, 20-, and 30-nt, immobilization densities varying from 0.046 to 0.171 nm^{-2}, and hybridization efficiencies varying from 10% to 100%. The combination of chain lengths, immobilization densities and hybridization efficiencies are specified in Table 1. For each case, cantilever deflections were computed for all the different ensembles of hybridized dsDNA (discussed above) In order to obtain statistically significant trends, 500 different realizations were generated for random

selected and Gaussian disordered arrangements and the average cantilever deflection were used to eliminate the influence of random selection.

Simulation Results and Discussions

Representative distribution of hybridized dsDNA chains corresponding to immobilization density of 0.13 nm^{-2} generated and hybridization efficiency of 50% for the four different ensembles are presented in Figure 18. In order to quantify the chain distributions and to verify the underlying assumptions for the different ensembles, the average occupation density of nearest neighbor sites by hybridized dsDNA chain was calculated as the ratio of hybridized dsDNA chains to the total number of possible sites at that neighbor level and is plotted in Figure 19 for each of the ensembles.

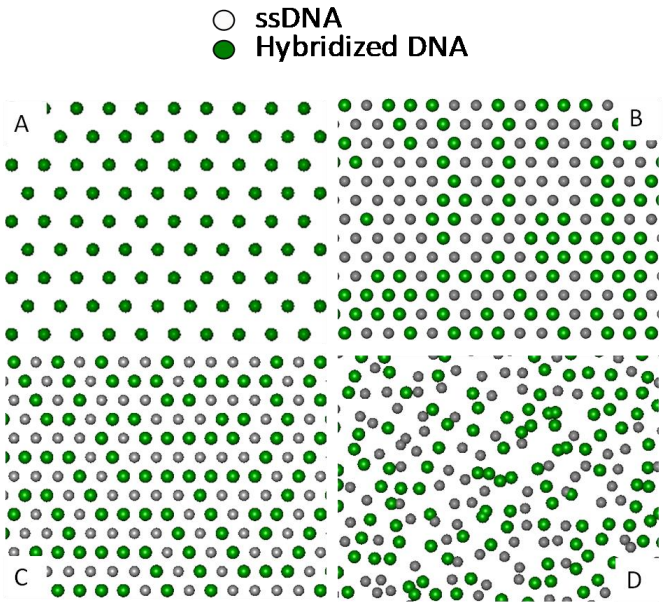

- Figure 18. Representative realization of hybridized DNA ensembles for hybridization efficiency of 50%: A) average spacing ensemble; B) random selection ensemble; C) energy minimization ensemble; D) Gaussian perturbation ensemble.

In first ensemble shown in Figure 18(a), all the hybridized DNA strands are arranged in hexagonal closed packed manner. Since the first ensemble is based on combining the immobilization and hybridization procedures together, all the neighbor sites are filled as shown in Figure 19 and we refer to this ensemble as "average spacing" ensemble. The nearest neighbor distances decrease with increase in hybridization efficiency as shown in Equation (27).

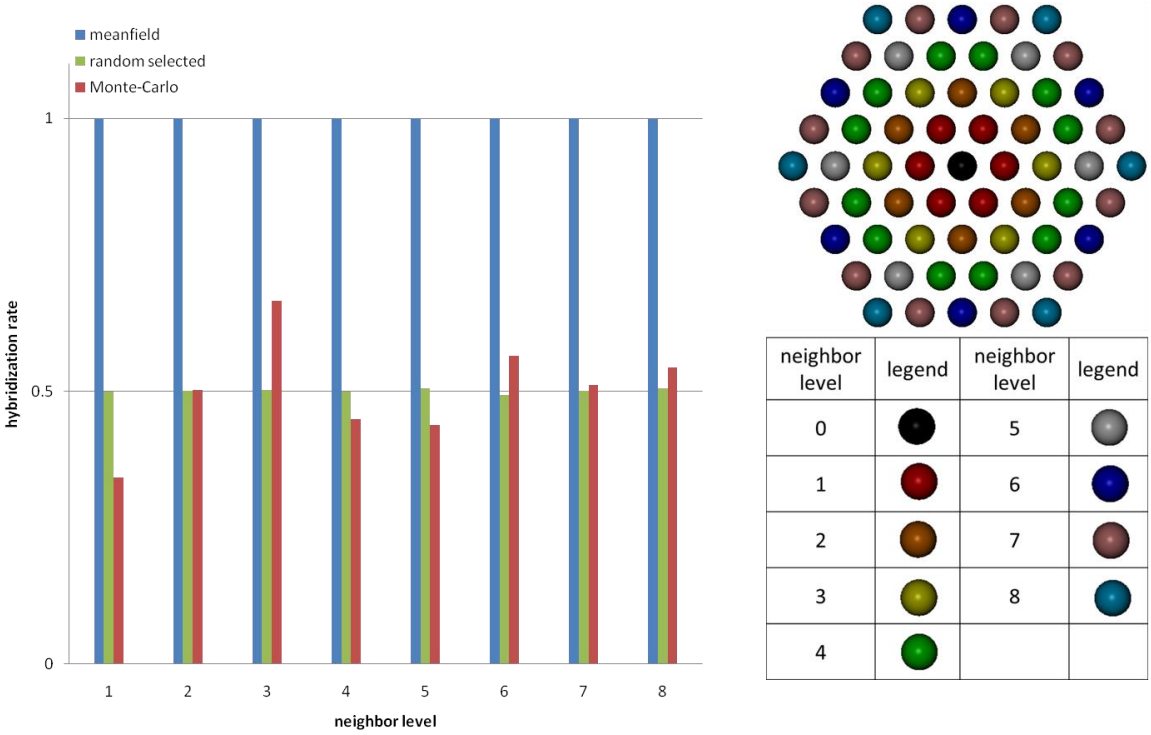

Figure 19. occupation density for each neighbor level for three ensembles with hybridization efficiency of 50%.

The second ensemble (random selected) shown in Figure 18(b) is generated assuming a uniform immobilization of ssDNA and equal probability of hybridization for all the sites. The generated ensembles show clusters of hybridized chains which results in a range of interchain separations. The occupation density of neighbor sites plotted in Figure 19 is uniform for all

hybridization efficiencies confirming the modeling assumption that all sites have equal probability for hybridization.

The third ensemble (Monte-Carlo selected) shown in Figure 18(c) is generated based on assumption that ssDNA chain will hybridize in a manner that minimizes the interaction energy between the hybridized strands. The energy minimization produces a more ordered pattern of hybridized dsDNA distribution in comparison to the second ensemble with a similar range of interchain separations. The neighborhood occupation density shown in Figure 19 is lower for the close neighbors and increases for higher order neighbors.

The fourth ensemble (Gaussian disordered) is generated through spatial perturbations of hybridized chain positions calculated in the third ensemble. Representative ensemble plotted in Figure 18(d) corresponds to a perturbation of 20% of the ensemble plotted in Figure 18(c). Similar ensembles with different range of spatial distribution were generated to investigate the influence of spatial disorder on the hybridization induced bending. The perturbed hybridized dsDNA arrangement does not have a clear definition of neighbor orders and neighbor separation values, therefore the neighborhood occupation density was not calculated for this arrangement.

Table 3. Parameters used in cantilever deflection predictions

ensembles	immobilization density (nm^{-2})	hybridization efficiency	length of DNA	number of simulations	standard deviation
average spacing	0.046 - 0.171	10% - 100%	10-, 20-, and 30-nt	1	N/A
Monte-Carlo selected				1	
random selected				500	
Gaussian disordered				500	5% - 25%

According to the experiment reports, in our simulations we considered immobilization density range of 0.046 – 0.171 nm^{-2}, hybridization efficiency range of 10-100%, and a chain

length range of 10-30 nucleotides. The standard deviation values of the Gaussian disorder ensembles are taken from 5% to 25% of the initial separation values.

In our computational framework, predicted cantilever bending is linearly dependent on the chain length because the DNA strands are assumed to stay nearly parallel throughout the cantilever deflections. Predicted cantilever bending is normalized with DNA chain length in order to simplify the discussion of computational results.

Normalized cantilever bending calculated for immobilization density of 0.13 nm^{-2}, is plotted as a function of hybridization density in Figure 19(a) for the four different ensembles. In addition, the normalized bending predictions for hybridization efficiency of 50% are plotted as a function of immobilization densities in Figure 19(b) for the four different ensembles. In the case of random selected and Gaussian disordered ensemble, average of bending predictions from 500 different ensembles is plotted and error bars correspond to total range of the spread in the predictions.

In all cases, cantilever deflection increases with increase in hybridization efficiency. Initial immobilization density is one of the dominant factors that affect the induced cantilever deflection. When the immobilization density is small, the hybridized chains have large separations and the predicted deflections are almost negligible for all the four ensembles. As the immobilization density increases, the deflection results increase exponentially with increase in immobilization density.

Predictions from first three ensembles are similar in magnitude with the smallest deflection predicted for fully packed hexagonal arrangement of hybridized chains (average spacing ensemble) and largest deflections for random selected ensemble in which single stranded chains have equal probability for hybridization. Predictions corresponding to Monte-Carlo

selected ensemble that corresponds to hybridization of single stranded chains with minimum interaction energy lie in the middle of the first two ensembles. The interaction potential due to hydration and electrostatic repulsion has an exponential dependence on the hybridized chain spacing and thus the bending results are dominated by chains in close proximity to each other. The bending predictions are higher for ensembles that have large range of intrachain spacing. At low hybridization density, the predictions from Monte-Carlo selected ensemble are close to that of average spacing ensemble as the hybridized chains are spaced apart but at the high hybridization density, the predictions from random selected and Monte-Carlo selected ensemble start converging as hybridized chains have to be in closer proximity. Cantilever predictions corresponding to the first three ensembles converge to same value as the hybridization efficiency approaches 100% because at full coverage all three ensembles are exactly the same.

For all hybridization efficiencies and immobilization densities, predictions based on the Gaussian disordered ensemble are consistently higher than all other ensembles. Random spatial perturbations used to generate the fourth ensemble increase the range of intrachain spacing and ensure that significant number of hybridized chains is within one decay length of the interaction potential. As shown in the Figures 20(a) and (b), bending predictions are strongly dependent on the range and distribution of hybridized chain spacing in an ensemble. For the same immobilization density and hybridization efficiency, the ensemble with perfect arrangement has the smallest predicted displacements and the predicted displacement increase as the chain distribution becomes more disordered from third to second and fourth ensemble. The disordered ensembles predict much higher deflection values than the non-disordered ensembles due to the large entropy in hybridized chain arrangement.

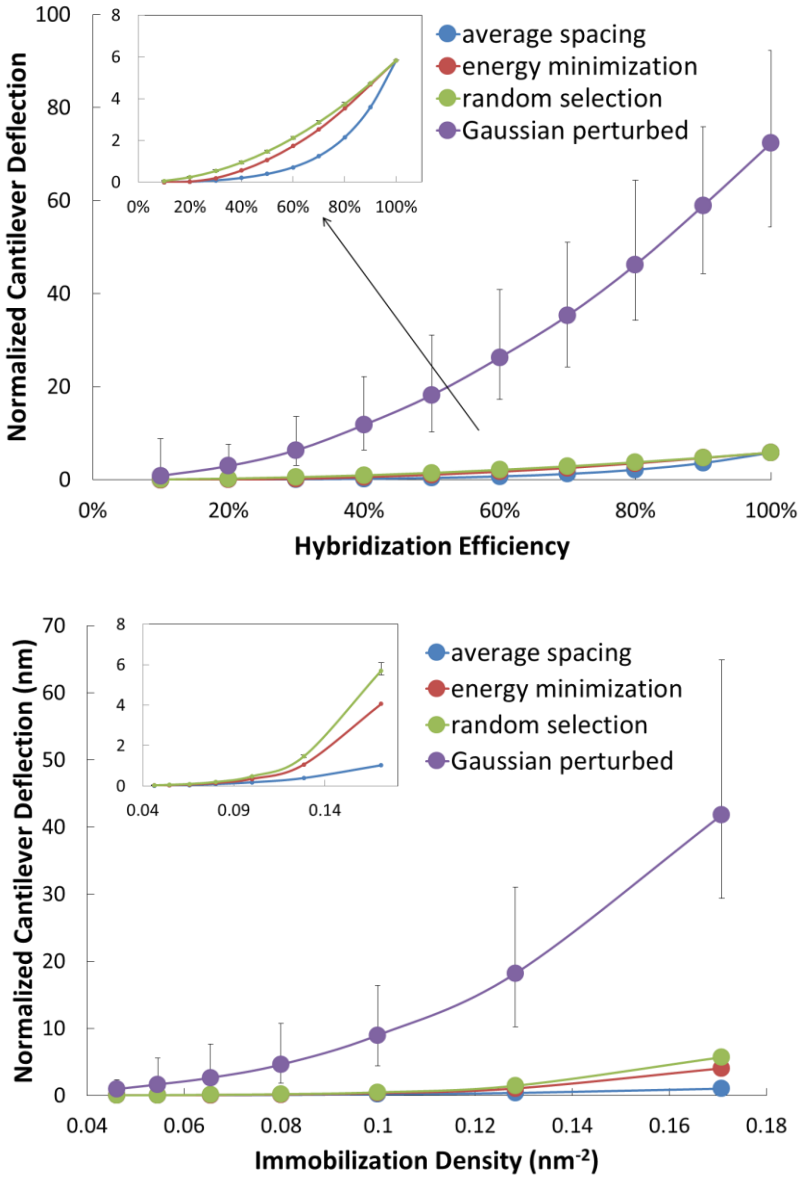

Figure 20. Normalized deflection predicted for the four different ensembles. (a) Deflections as a function of hybridization efficiency for immobilization density at 0.13 nm^{-2}; (b) Deflections as a function of immobilization density for hybridization efficiency at 50%

In order to further examine the influence of arrangement disorder on the predicted deflection, the ratio of predicted displacements from spatially perturbed ensemble (Gaussian disordered) and unperturbed ensemble (Monte-Carlo selected) are plotted as a function of the reciprocal of immobilization density in Figure 21 for different range of spatial perturbations. As

shown in the Figure 21, increasing the range of spatial perturbations or disorder in the hybridized chain arrangement increases the predicted displacement. The increase in predicted displacement is also strongly dependent on the initial immobilization density. For smaller immobilization density, increasing the range of perturbation from 5% to 25% of immobilized chain separation, increases the predicted displacement from about 5 times to 200 times the deflection predicted for third ensemble. However for larger immobilization density, increasing the range of perturbation from 5% to 25%, results in increased displace from about 5 times to 30 times the deflection predicted for third ensemble. In addition, the increase in predicted displacements has a linear dependence initial separation of ss DNA chains for a fixed range of spatial perturbations as indicated by the linear fit plotted in Figure 21. The slope of linear fits increases with range of spatial perturbations imposed on the ensembles. The increase in displacements clearly highlights the importance of disorder in chain arrangement on the predicted displacements.

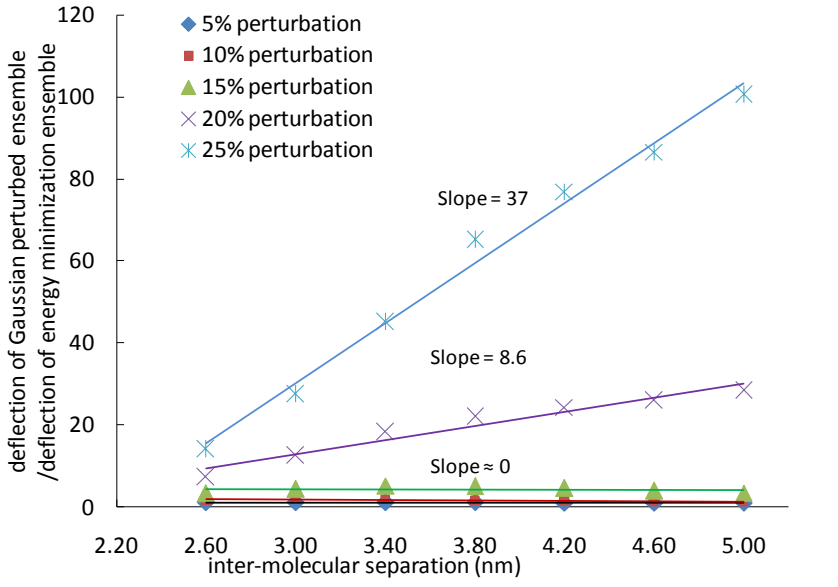

Figure 21. Influence of spatial perturbation on predicted cantilever deflections.

Comparison of Numerical Prediction with Experimental Reports

Numerical predictions of cantilever bending are compared to the reported experimental measurements for different immobilization densities, hybridization efficiencies and chain lengths in order to demonstrate the efficacy of our modeling assumptions. Early reports on experiments gave high immobilization densities in the range of 0.13 – 0.17 chains/nm^2 (Strey, Parsegian et al. 1999, Wu, Ji et al. 2001), the displacement predictions corresponding to these densities are compared to experimental measurements reports (Fritz, Baller et al. 2000, Wu, Ji et al. 2001, McKendry, Zhang et al. 2002, Alvarez, Carrascosa et al. 2004, Stachowiak, Yue et al. 2006) in Table 4. With large immobilization densities (> 0.13 nm^{-2}), all three non-disordered ensembles can predict cantilever deflections that are comparable to experimentally measured displacements.

Table 4. Comparison of Numerical Predictions with Experimental Reports

	Experimental results	Immobilization density (nm^{-2})	DNA length	$\delta(h/L)^2$ (10^{-5}nm)	Simulation predictions $\delta(h/L)^2$ (10^{-5}nm)			
					Average spacing	Random selected	Monte-Carlo selected	Gaussian disordered
High density	Fritz et al (Fritz, Baller et al. 2000)	~0.2	12-nt	~3	~1.5	~5.5	~4.5	-
			16-nt	~6	~2	~7.3	~5.5	-
	Mckendry et al (McKendry, Zhang et al. 2002)	~0.13	12-nt	~2	~1.4	~5	~4	-
			20-nt	~3	~2.4	~9	~6	-
	Wu et al (Wu, Ji et al. 2001)	~0.15	20-nt	~3.5	~2.4	~9	~6.5	-
			30-nt	~8.5	~3.7	~1.4	~1	-
	Alvarez et al (Alvarez, Carrascosa et al. 2004)	~0.13	12-nt	~2.5	~1.4	~5	~4	-
Low density	Stachowial et al (Stachowiak, Yue et al. 2006)	0.01 - 0.1	10-nt	8.5~18.5	~0.05	~0.1	~0.08	7~17
			20-nt	4~12	~0.095	~0.2	~0.17	5~12
			30-nt	1~3	~0.15	~0.35	~0.25	5~8

The simulations gave a deflection range of 2.0 – 6.2 nm (30% hybridization efficiency) to 78.30 – 116.48 nm (80% hybridization efficiency) for 10nt DNA. Though no hybridization

efficiencies were reported for large immobilization densities, we can predict the experimental results within this range.

Although the simulations can predict the experimental results with large immobilization densities, it failed to agree with the reports when immobilization densities are low (< 0.13 nm^{-2}) due to the exponential drop of the interaction free energy with immobilized chain separation larger than the decay length. Stachowiak et al reported systematic results on the cantilever deflection with the immobilization density and hybridization efficiency. When the initial immobilization densities are smaller than 0.13 nm^{-2}, the simulations with non-disordered ensembles (First, Second and Third) failed to predict deflections comparable to experimentally measured values. At this immobilized chain separation, the interactions between neighboring molecules become weak, and it is expected that hybridized DNA may possibly arrange in more disordered arrangements. As a result, the influence of spatial perturbations was considered to predict the cantilever deflection.

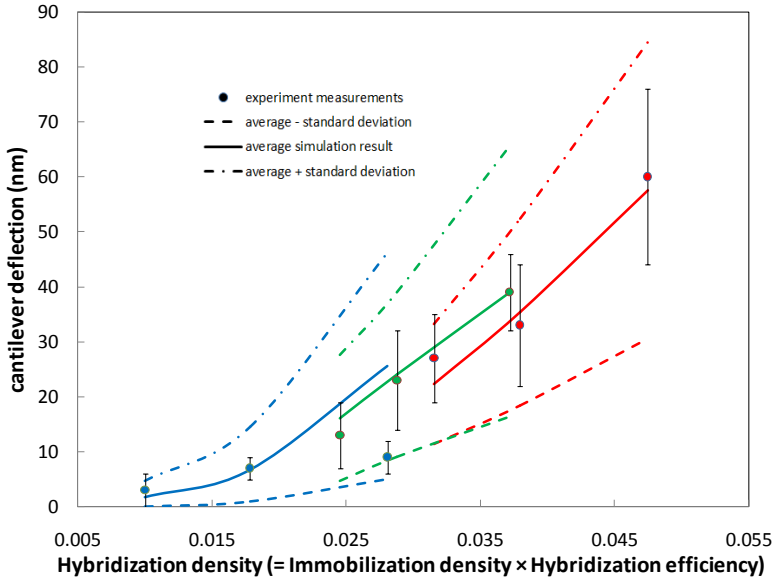

Figure 22. Comparison of predicted displacement of Gaussian perturbed ensemble with reported experimental measurements. [11]

Cantilever deflections were predicted for ensembles with increasing spatial perturbations in order to match the experimentally measured values for the reported immobilization densities and hybridization densities. Comparison with experimental result indicated the ensembles with spatial perturbation ranging from 19% to 21% of immobilized ssDNA separation result in bending predictions comparable to measured deflections. Numerical predictions corresponding to disordered ensembles with spatial perturbations of 19%, 20%, and 21% are compared to experimental measurements reported in Stachowiak et al. (Stachowiak, Yue et al. 2006). Comparison of the numerical predictions and experimental results demonstrates that disordered ensembles can be used to predict the cantilever bending for low surface immobilization densities. Another observation from the Figure 22 is that smaller magnitude of spatial perturbations are required to match the experimental results corresponding to longer chain lengths: 19% for 30 nt DNA, 20% for 20 nt, and 21% for 10 nt. Spatial perturbation imposed in the ensemble simulate the disorder induced in the surface chain arrangement during immobilization of the ssDNA molecules. When the ssDNA molecules are longer, the gyration radius, which is function of the number of nucleotides of ssDNA, becomes larger. Therefore for the same immobilization density, the free space between molecules is expected to be smaller for longer DNA chains and consequently, the chain arrangement are expected to be less disordered for longer sequences in comparison to shorter DNA sequences.

Comparison of the bending predictions and experimental measurements show that when the immobilized chain separation is larger than a threshold (here we picked 3.0 nm, 10 times of the decay length), the Gaussian disordered ensemble is needed to be considered due to the large free space between molecules. This implies at smaller immobilization densities, the disorder in

the hybridized dsDNA arrangement is a dominant factor in determining the cantilever bending. For low immobilization density experiments, the spatial disorder may also be influenced by the number of nucleotides in the DNA strands and thus more disordered arrangements are required to predict deflections for shorter nucleotides.

For larger immobilization densities ensembles that account for disorder generated during hybridization of a closed packed ssDNA are sufficient to predict the deflection range reported by Fritz et al. (Fritz, Baller et al. 2000)and Wu et al. (Wu, Ji et al. 2001). Our calculations show that with large immobilization densities, the entropy induced by the hybridization method play an important role.

For all the cases, the ensembles based on hexagonal closed packing of hybridized chains do not predict cantilever deflections that match reported experimental results. This strong dependence of cantilever deflection on spatial arrangement disorder has important implications for the design of experiments that employ surface adsorbed receptor molecules. The self-assembly of immobilized molecules must be carefully controlled for reproducibility and reliability of the experiments.

Conclusions

We presented a model to examine deflections of micro-cantilever resulting from DNA hybridization in this paper. An empirical interaction potential for hybridized DNA chains was used in the simulation to predict hybridization induced bending. Cantilever bending was predicted based on four different ensembles of hybridized DNA chains arrangement. Hexagonal close packing of hybridized DNA is the simplest ensemble to generate but it neglects the immobilization and hybridization induced disorder in the chain arrangements. Consequently, the

hexagonal close packed ensemble results the smallest predictions of cantilever deflections. Hybridized DNA ensemble produced through either random selection or ensuring minimum interaction energy during hybridization of hexagonally closed packed single stranded DNA resulted in larger prediction of cantilever bending. Random selected ensemble has more disordered arrangement of chains and higher predicted cantilever deflection in comparison to the minimum interaction energy ensemble. Introducing spatial perturbations in the hybridized dsDNA arrangement leads to larger predictions for cantilever bending. Comparison of numerical predictions with reported experimental results indicates the importance of immobilization density in determining the arrangement of hybridized DNA chains on the surface as well as the hybridization induced bending. At larger immobilization densities or smaller interchain separation, predictions based on ensembles with initial uniform immobilization and partial hybridization of DNA chains, are able to predict deflections similar to experimental measurements. At smaller immobilization densities or larger interchain separation, only predictions based on ensembles with spatial perturbation of hybridized DNA strands can match the experimentally measured cantilever deflections. Comparison of numerical predictions and experimental results highlights the importance of immobilization density and spatial disorder imposed during immobilization and hybridization on the hybridization induced cantilever bending.

Acknowledgements

This research was supported by National Science Foundation Career Award (CMMI 0547280.

CHAPTER 6. INFLUENCES OF MOLECULAR CONFIGURATION AND CONFORMATION ON CANTILEVER DEFLECTION ASSOCIATED WITH DNA HYBRIDIZATION

Modified from a paper to be submitted

Yue Zhao, Kyungho Kang, Pranav Shrotriya

Introduction

In recent years, Microcantilever based biosensors have been widely studied as label-free chemical and biological sensors for molecular detections and recognitions since the initial reports(Fritz, Baller et al. 2000, Wu, Ji et al. 2001). The low cost, fast response and high sensitivity of the microcantilever based sensor make it a platform for analysis with DNA hybridization(Fritz, Baller et al. 2000, Wu, Ji et al. 2001, Hagan, Majumdar et al. 2002, Alvarez, Carrascosa et al. 2004, Stachowiak, Yue et al. 2006, Zhang and Chen 2009, Kim, Cho et al. 2010, Pei, Lu et al. 2010, Zhang, Chen et al. 2010, Kang 2011, Zhang, Lang et al. 2012, Ghosh, Mishra et al. 2014), ligand-receptor binding(Osawa, Takase et al. 2009, Torres-Chavolla and Alocilja 2009, Seena, Rajoriya et al. 2010, Urwyler, Schift et al. 2011, Zhai, Wang et al. 2012), drug discovery(Kang, Nilsen-Hamilton et al. 2008, Kang, Nilsen-Hamilton et al. 2009), and cancer cell detection(Hood, Heath et al. 2004, Ferrari 2005, Zhang, Lang et al. 2006, Sengupta and Sasisekharan 2007, Shekhawat and Dravid 2013, Wang, Chen et al. 2013) .

Hybridization of ssDNA molecules with their complementary oligonucleotides has become a simple and prominent example in biomolecular recognition and detection since it is fundamental to most biological process. Experimental observations on cantilever deflection associated with DNA hybridization were reported by many groups with different experimental conditions and different parameters used in the experiments(Fritz, Baller et al. 2000, Wu, Ji et al. 2001, Hagan, Majumdar et al. 2002, McKendry, Zhang et al. 2002, Alvarez, Carrascosa et al. 2004, Stachowiak, Yue et al. 2006, Pei, Lu et al. 2010, Kang 2011). The reported results have different magnitude due to different immobilization densities and hybridization efficiencies.

Although it has been years since the first report by Fritz et al. (Fritz, Baller et al. 2000) on the cantilever deflection associated with DNA hybridization, the origin of the bending is still not clarified. Based on the experimental reports with different conditions, the cantilever deflection may derive from hydration forces(Hagan, Majumdar et al. 2002, Stachowiak, Yue et al. 2006, Mertens, Rogero et al. 2008), conformational entropy(Wu, Ji et al. 2001), physical steric crowding(McKendry, Zhang et al. 2002), and the covalent attachment to the surface(Alvarez, Carrascosa et al. 2004).

Strey et al. (Strey, Parsegian et al. 1997, Strey, Parsegian et al. 1999) proposed a liquid crystal model to represent the hybridized dsDNA molecules immobilized on the surface of microcantilevers, and established pairwise potential models for dsDNA molecular interactions for both electrostatic interactions and hydration forces. While Zhang et al. (Zhang, Tan et al. 2011) investigated the theories related to interactions of ssDNA immobilized on microcantilevers. In their report, they conclude that when the immobilization density of ssDNA is low, the interaction energy between neighboring molecules will be too weak to be dominant.

We modeled the DNA hybridization induced cantilever deflection considering the distribution of DNA strands(Zhao, Ganapathysubramanian et al. 2012). A beam bending model was proposed for the system with the microcantilever modeled as a beam and the dsDNA strands modeled as straight rods immobilized on the beam surface with designated distributions. Four different distributions of DNA ensembles were proposed and investigated: average-spacing, random selected, Monte-Carlo selected, and Gaussian disordered. We showed with simulations that the influence of the molecular distribution of immobilized DNA on the surface of the microcantilevers. The commonly used average spacing distribution underestimated the importance of the disorder and provided deflection predictions lower than actual observations. The two-step determined distributions were more suitable, and the magnitude of the disorder was affected by the immobilization density and hybridization efficiency of the system.

In this paper, we report an energy model for DNA hybridization induced bending of microcantilevers. Influence of different immobilization densities, hybridization efficiencies, and molecular configurations on the cantilever bending is considered. Predicted results are compared to experimentally reported deflections to identify the influence of different factors on the cantilever deflection.

Experimental Observations

Since the initial reports(Fritz, Baller et al. 2000, Wu, Ji et al. 2001) on the cantilever deflection induced by the hybridization of immobilized ssDNA, ssDNA hybridization has been utilized as a validation experiments for new techniques. Many experiments have been reported by different groups with different immobilization densities, hybridization efficiencies, and molecular conformations(Wu, Ji et al. 2001, McKendry, Zhang et al. 2002, Stachowiak, Yue et al.

2006). Typically the procedure of the DNA hybridization induced deformation experiments are conducted as two steps: sensor functionalization and DNA hybridization (Figure 23). ssDNA molecules are immobilized on the cantilever surface in the functionalization step, and complementary ssDNA molecules with certain concentrations are introduced to the sensors. During the hybridization procedure, the surface stress of the microcantilever will change and the bend the cantilever accordingly with Stoney's formula(Stoney 1909).

$$\sigma = \frac{Et^2}{6R(1-\nu)}, \qquad R = \frac{L^2}{2\delta} \tag{27}$$

where E is the modules, ν is the Poisson Ratio, R is the equivalent radius of the curvature, t and L are the thickness and length of the cantilever respectively, and δ is the cantilever deflection.

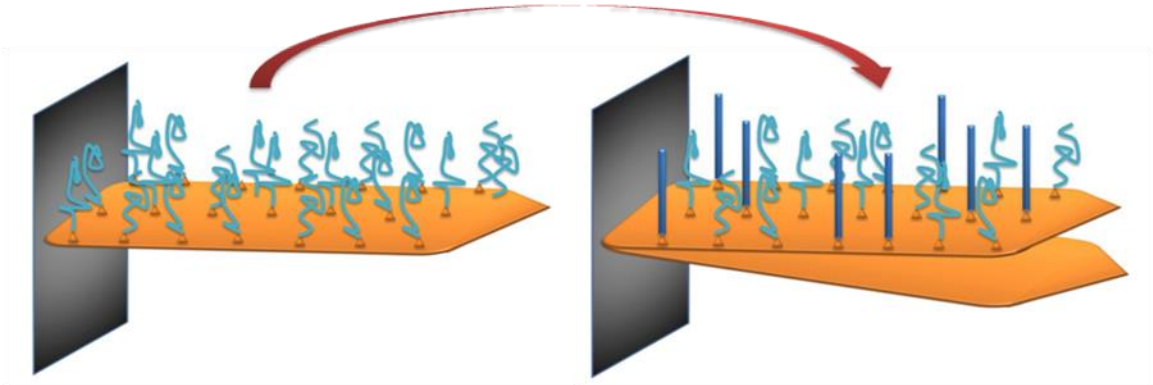

Figure 23. Illustration of cantilever functionalization and DNA hybridization procedures of microcantilever based sensor

Different magnitudes of surface stress change observations are collected with different target concentrations among groups (Figure 24(a)). Large variations of surface stress results are reported among groups and confirm that the target concentration is not the factor driving different magnitudes. It is generally accepted that the cantilever deflection is due to the DNA hybridization on the surface so that the number of hybridized DNA molecules should be

essential. Therefore deflection results are studied with respect to the hybridization densities (Figure 24(b)). Four groups of experimental results are categorized based on different magnitude of hybridization densities. In each group the surface stress change is increasing with the hybridization density, but in a bigger map, lower hybridization density will lead to higher surface stress change. Since it is widely accepted that the cantilever deformation is due to the interactions associated with hybridized DNA molecules, higher surface stress changes would be expected when higher hybridization densities are reported. However, Figure 24(b) shows that the overall trend is opposite among the four different groups with greater surface stress change at lower hybridization densities.

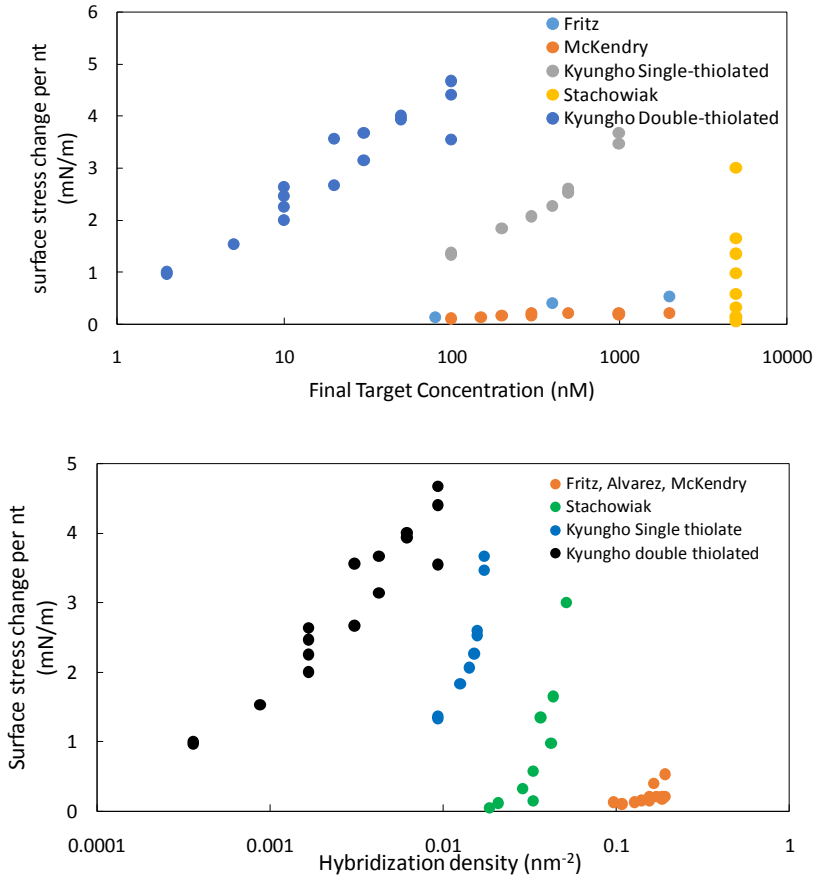

Figure 24. Collections of experimental observations: (a) surface stress change vs. final target concentration; (b) surface stress change vs. hybridization density.

Distributions and Configurations of Hybridized DNA

Godin et al. (Godin, Williams et al. 2004) reported their observations on molecular configurations of alkanthiol self-assembled monolayers on gold-coated surface associate with immobilization density that immobilized molecules will rest in different phases, lying-down or standing-up phases, according to the magnitude of immobilization density. As a result, the molecular separation and length scales of DNA molecules are essential to the configurational study. Based on this consideration, molecular configurations are investigated associated with distributions and length scales of hybridized DNA to understand the mechanism underlying DNA hybridization induced deformation.

Molecular separations between hybridized DNA molecules are related to the distribution of DNAs which is controlled by two major factors, immobilization density and hybridization efficiency. We (Zhao, Ganapathysubramanian et al. 2012) have reported the investigation on four ensembles of different spatial considerations: average spacing, random selection, energy minimization, and Gaussian perturbed ensembles. Hexagonal closed-packed arrangement was considered as the baseline of all ensembles. The average spacing ensemble assumes uniform spacing for all hybridized dsDNAs for given hybridization density. All the other three ensembles considered two steps, immobilization and hybridization, separately to generate DNA ensembles. ssDNAs were assumed to be immobilized on the surface with hexagonal closed packed arrangement, and distribution of hybridized dsDNA was then generated. The ds DNA distribution of the random selection ensemble assumes that all immobilized ssDNA have equal probability for hybridization, while that of energy minimization ensemble assumes that hybridized dsDNA will be distributed such that the chain-chain interaction energy is minimized. The Gaussian

perturbed ensemble perturbs the chain distribution of energy minimization ensemble by using a random displacement at each hybridization dsDNA site.

All four ensembles are evaluated with different immobilization densities and hybridization efficiencies (Figure 25). Average spacing ensemble is simplest to generate but neglects the immobilization and hybridization induced disorder in chain arrangement. Both ensembles produced through either random selection or energy minimization are more reasonable and provide better predictions for experiments with high immobilization densities. When the immobilization density gets lower, the initial spatial separation become larger and DNA molecules are more possible to move near the desired positions. Therefore, a Gaussian spatial perturbation of hybridized dsDNA will be required to present the greater disorder in the ensemble.

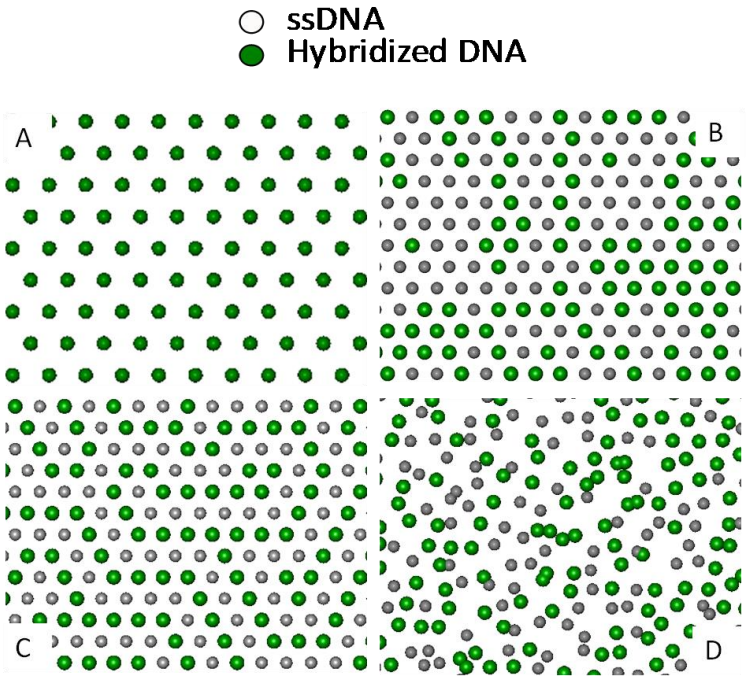

Figure 25. Four typical DNA ensembles used in DNA hybridization simulations: (A) average spacing, (B) Random selection, (C) Energy minimization, and (D) Gaussian-perturbed

The configurations of dsDNA on the cantilevers surface are controlled by immobilization methods and molecular separation between DNAs (Figure 26). The regular immobilization approach which is most used is the single-thiolated approach, i.e. the receptor ssDNAs are functionalized with thiolgroups on only one end of the molecules and then immobilized on the surface. An alternative approach, double-thiolated approach(Kang 2011) is that the receptor molecules are functionalized with two thiolgroups on both ends of the ssDNAs and immobilized on the surface on both ends. The hybridized dsDNA molecules will have different configurations with different immobilization approaches. The dsDNAs with double-thiolated approach are restricted close to the surface and have little freedom to move, while dsDNAs with single-thiolated approach have only one end attached to the surface and the other end is free to move. Thus the single-thiolated dsDNAs are more flexible and have different configurations according to the immobilization densities. When the immobilization density is low and the molecular separations are large, the molecules will prefer to rest in the lying-down phase due to the surface-molecule attractions, and when the immobilization density is high and the molecular separations are small, the dsDNA molecules will be pushed up to form standing-up configurations due to the strong repulsions from the surrounding molecules (Figure 26).

The determination of the ensembles and molecular configurations is controlled by the molecular length scales of DNA molecules, including the diameter (D_{DNA}) and length of the hybridized dsDNAs (L_{DNA}). When the ratio of the smallest separation (d) and molecular diameter of dsDNA (d/D_{DNA}) is small, the molecules are too close and have no sufficient space to move, therefore the hybridized DNA molecules are more likely to form distributions of random selection and energy minimization ensembles. While when d/D_{DNA} is large, the molecules will have enough space to move and form distributions of Gaussian perturbed ensembles. When d

increases to even larger and is comparable to the molecular length of hybridized dsDNA ($d/L_{DNA} \sim 1$), the dsDNA molecules will be far enough to form lying-down configurations.

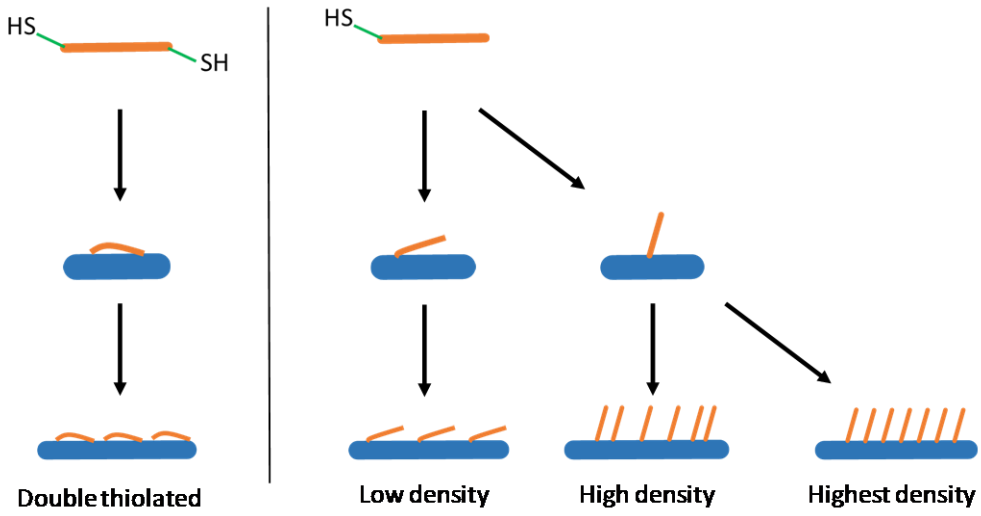

Figure 26. Molecular configurations of hybridized dsDNA molecules due to different immobilization conditions

Energy Models and Cantilever Bending Predictions

The microcantilever system is modeled as a beam consists of three layers: the SiN_x base layer, the gold (Au) layer, and the immobilized DNA molecules. The total energy of the overall system consists of the energy of the cantilever and that from the immobilized DNA layer. During the hybridization procedure, the energy change in the system may come from various origins, including the elastic bending energy of the cantilever (E_{bend}), the chemical energy relaxation due to DNA hybridization (ΔE_{hybr}), the surface energy change of surface reconstruction caused by DNA (ΔE_{recon}), and the energy associated with chain-surface interactions ($\Delta E_{chain-surface}$) and chain-chain interactions ($\Delta E_{chain-chain}$) respectively.

$$\Delta E_{total} = E_{bend} + \Delta E_{hybr} + \Delta E_{recon} + \Delta E_{chain-surface} + \Delta E_{chain-chain} \quad (28)$$

In order to simplify the cantilever system and the bending energy expression, the layer of gold film can be negligible, since the thickness of gold film (~20 nm) is far smaller than the overall thickness (1000 nm) and the elastic modulus of gold is of the same order of magnitude as that of SiN_x. As a result, the bending energy of the cantilever can be expressed as(Ibach 1997)

$$E_{bend} = \frac{Et^3}{12R^2(1-\nu^2)}, \qquad R = \frac{L^2}{2\delta} \quad (29)$$

where E is the modules, ν is the Poisson Ratio, R is the equivalent radius of the curvature, t and L are the thickness and length of the cantilever respectively, and δ is the cantilever deflection.

The chemical energy relaxation due to DNA hybridization (ΔE_{hybr}) is the dominant energy change during the hybridization procedure. It describes the energy released from the hybridization of ssDNA into dsDNA, it is the energy driving the reaction to go forward and determines the hybridization efficiency. If the hybridization reaction can produce greater energy relaxation, the ssDNA molecule will be more readily to be hybridized and become dsDNA, and vice versa. As a result, the chemical energy relaxation (ΔE_{hybr}) is a function of the number of hybridized molecules and the chemical energy change of each hybridization reaction.

The surface energy change of surface reconstruction caused by DNA (ΔE_{recon}) is induced by the change of the structures of gold surface. Andreoni et al. (Andreoni, Curioni et al. 2000) have reported their observations on the surface reconstructions induced by the alkanthiol SAM formation based on first principle calculations. They observed that the change of the electrons on the surface will lead to the surface expansion and further induce the cantilever deformation. When the ssDNAs are hybridized into dsDNAs, the random-coil like molecules are completely changed to double helix structures and negatively charged outside. Therefore when the dsDNA

molecules are very close to the cantilever surface, the electron density on the surface will also change due to the charge effect, and the surface will have strong surface reconstructions according which will lead to the cantilever deformation.

Kukta et al. (Kukta, Kouris et al. 2003) reported their model on the surface defects induced surface stress change with a second order assumption considering the energy change with respect to the strain. With this assumption, the total surface energy change of surface reconstruction (ΔE_{recon}) is the summation of the surface reconstruction energy change induced by each hybridized dsDNA (F^i_{recon}), which is as a second order function of the surface strain (ε)

$$\Delta E_{recon} = \sum_{hybridized\ dsDNAs} F^i_{recon} \tag{30}$$

$$F^i_{recon} = A(s^i)[a(\varepsilon)^2 + b(\varepsilon) + c], \qquad \varepsilon = \frac{t}{2R} \tag{31}$$

where a and b are the strength factors of the interactions, s^i is the initial separation between immobilized thiolgroups of dsDNA molecule, and $A(s^i)$ is the interaction area which is a function of s^i.

The energy change associated with chain-surface interactions ($\Delta E_{chain-surface}$) is determined by the chain-surface distance. An energy well profile is utilized to describe the chain-surface energy (Figure 27). From the profile, most single-thiolated cases are in the attraction region, and double-thiolated cases are in the repulsion region due to the close distance between molecules and cantilever surface. The chain-surface energy change determines the molecular configurations on the surface. With single-thiolated cases in the attraction region, the molecules are dragged down to the surface as the lying-down configurations because of the interaction when the molecules are far away from each other and cannot provide sufficient repulsions, while

as the molecules get closer with higher density, the molecule will have repulsions strong enough to support the standing-up configurations.

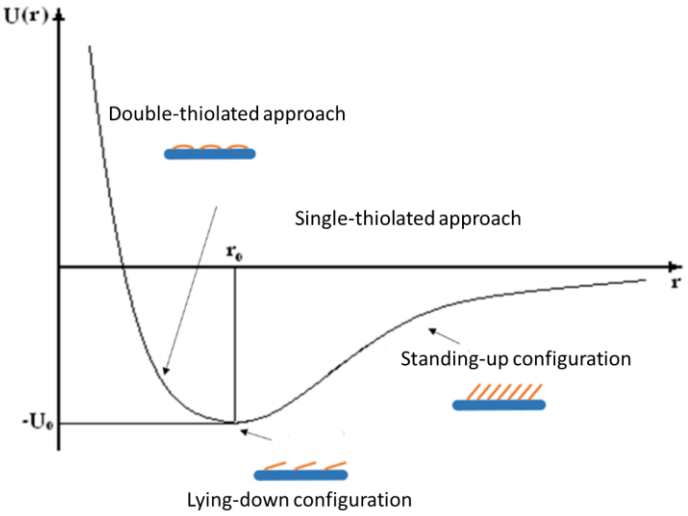

Figure 27. Energy well assumption for interactions between cantilever surface and hybridized dsDNA chains

The energy change associated with chain-chain interactions ($\Delta E_{chain-chain}$) is the summation of the pairwise energy between each pair of DNA molecules ($F^i_{chain-chain}$).

$$\Delta E_{chain-chain} = \sum_{DNA\ pairs} F^i_{chain-chain} \tag{32}$$

Before the hybridization occurred, it is assumed that all the unhybridized ssDNA molecules stay in the random coil structures and have weak interactions denoted as $F(S-S)$. After the introduction of the complementary part of ssDNA in the system, certain percentage of ssDNA molecules are hybridized and form dsDNA molecules, and the rest ssDNA molecules remain unhybridized. Therefore, the total pairwise energy of the DNA ensemble is modeled as the summation of all pairwise interactions between unhybridized and hybridized dsDNA

molecules, which include the interaction between hybridized dsDNA molecules $(D-D)$, between hybridized dsDNA and ssDNA$(D-S)$, and between ssDNAs$(S-S)$.

$$E_{chain-chain} = \sum_{DNA\ pairs} [F(D-D) + F(D-S) + F(S-S)] \tag{33}$$

Strey et al. (Strey, Parsegian et al. 1997, Strey, Parsegian et al. 1999) showed that the interaction energies with unhybridized molecules ($D-S$and $S-S$) are far smaller than that of interactions between hybridized molecules$(D-D)$. Therefore, the total in-film energy of DNAs before hybridization can be neglected and that after hybridization can be simplified to be a function only of interactions between hybridized dsDNA molecules$(D-D)$.

$$\Delta E_{chain-chain} = \sum_{hybridized\ dsDNA\ pairs} F^i_{chain-chain} \tag{34}$$

Strey's potential(Strey, Parsegian et al. 1997, Strey, Parsegian et al. 1999) was applied to observe the pairwise interaction energy between molecules (per unit length).

$$F^i_{chain-chain} = F^i_0(d^i) + ck_BTk_c^{-1/4}\sqrt[4]{\frac{\partial^2 F^i_0}{\partial d^2} - \frac{1}{d}\frac{\partial F^i_0}{\partial d}} \tag{35}$$

$$\text{with} \quad d^i = d^i_0\left(1 + \frac{t}{2R}\right) \tag{36}$$

where d^i is the axial separation between the lying-down molecules, d^i_0 is the initial separation before cantilever bending, k_B is the Boltzmann constant, T is the temperature, l_p is the persistence length of the DNA molecules, $k_c = k_BTl_p$ denotes the intrinsic bending stiffness of the DNA molecules, and the parameter c is an empirical determined dimensionless constant of order 1.

The free energy F_0 consists of hydration forces and electrostatic interactions, both of which can be determined semi-empirically.

$$F_0^i(d^i) = a\sqrt{\frac{\pi}{2}}\frac{exp(-d^i/\lambda_D)}{\sqrt{d^i/\lambda_D}} + b\sqrt{\frac{\pi}{2}}\frac{exp(-d^i/\lambda_H)}{\sqrt{d^i/\lambda_H}} \qquad (37)$$

where λ_D and λ_H are the decay length for electrostatic and hydration forces respectively, *a* and *b*are strength factors which determined by the salt concentration in the solution empirically.

The deflection observation is based on the minimization of the total energy change with respect to the variation of cantilever curvature. The true deflection will be the value when the total energy change reaches the minimized value. Among all the energy components, the chemical energy relaxation (ΔE_{hybr}), as described, is only a function of number of hybridized dsDNAs and the chemical energy change of each hybridization reaction. Since the number of dsDNAs and the chemical energy change do not change with the curvature in the small curvature consideration, the total chemical energy relaxation therefore does not change with the deflection and thus not considered in the minimization of the total energy change. The energy associated with chain-surface interactions ($\Delta E_{chain-surface}$) is determined only by the distance between dsDNA molecules and cantilever surface, which is not influenced by the curvature. Thus the chain-surface energy, though determines the molecular configuration of dsDNAs, is also not considered explicitly in the minimization of the total energy change.

Therefore, the total energy change considered in the minimization procedure is consisted of three components: the elastic bending energy of the cantilever (E_{bend}), the surface energy change of surface reconstruction caused by DNA (ΔE_{recon}), and the energy change associated with chain-chain interactions ($\Delta E_{chain-chain}$). From equations (29), (31), (35) and (36), all these

energy changes are functions of the curvature of the cantilever ($1/R$). The minimization of the total energy change in equation (38) will lead to the final cantilever deflections.

$$\Delta E_{total} = E_{bend} + \Delta E_{recon} + \Delta E_{chain-chain} \quad (38)$$

A function minimization program (Shor 1985) is taken to minimize the total energy given in equation (38) and the stable state is achieved. The influences of both energy change components, surface reconstruction energy (ΔE_{recon})and chain-chain interaction energy ($\Delta E_{chain-chain}$), were examined with respect to different immobilization densities (0.012 to 0.171 nm^{-2}), hybridization efficiencies (10% to 100%), molecular configurations (standing-up and lying-down), perturbation levels (0.5 to 1.0 nm), and dsDNA distribution ensembles (random selection, energy minimization, and Gaussian perturbed ensembles). In order to obtain statistical significant trends, 500 different realizations were generated and the average surface stress was used to eliminate the influence of the randomness.

Model Results

In our computational framework, predicted surface stress change is corresponding to the immobilization approaches and molecular configurations. In the single-thiolated approach, both standing-up and lying-down configurations are applied according to the immobilization density (molecular separation). All dsDNA molecules are assumed to stay parallel throughout the cantilever deflections in both standing-up and lying-down configurations. For predictions with single-thiolated approach, since the dsDNA molecules are generally rest in the attraction region and are away from the cantilever surface with both standing-up and lying-down configurations, the interactions between dsDNA molecules and cantilever surface are too weak to produce surface reconstruction, and thus the surface energy change due to surface reconstruction

(ΔE_{recon}) can be negligible during the cantilever deflection. Therefore, only the elastic energy of the cantilever (E_{bend}) and the energy change due to chain-chain interactions ($\Delta E_{chain-chain}$) is evaluated in simulations with single-thiolated approach. On the other hand, for predictions with double thiolated approach, the immobilization density and the hybridization efficiency are both very low, so the hybridized dsDNA molecules will be far apart and the energy change due to pairwise chain-chain interactions ($\Delta E_{chain-chain}$) will be very weak and negligible, while the surface energy change due to surface reconstructions will be high due to short distance between the cantilever surface and the dsDNA molecules restricted to the surface with both ends. As a result, in simulations with double-thiolated approach we will only consider the elastic energy of the cantilever (E_{bend}) and the energy change due to chain-chain interactions (ΔE_{recon}).

In simulations with single-thiolated approach, the influences of immobilization on surface stress change are investigated with all three ensembles (random selection, energy minimization, and Gaussian perturbed ensembles) and two configurations (standing up and lying down). Surface stress change is plotted as a function of molecular separation in Figure 28 with three different ensembles at a hybridization of 50%. Two standard deviation values (0.5 and 0.866 nm) in Gaussian perturbation are presented, which represent the distances of the first two nearest fcc sites on the Au(111) surface(Andreoni, Curioni et al. 2000). Surface stress predictions are strongly dependent on the molecular separation and distribution of hybridized chains. In all cases, predicted surface stress change decreases with an increase in molecular separation. At the same molecular separation and hybridization efficiency, energy minimization ensembles has smaller predicted surface stress change than the random selection ensembles as the chain distribution of random selection ensembles become more disordered, and Gaussian perturbed ensembles predicted consistently higher surface stress change than the other two ensembles due

to the large entropy in hybridized chain arrangement. In addition the predictions are greater with larger standard deviations in Gaussian perturbed ensembles.

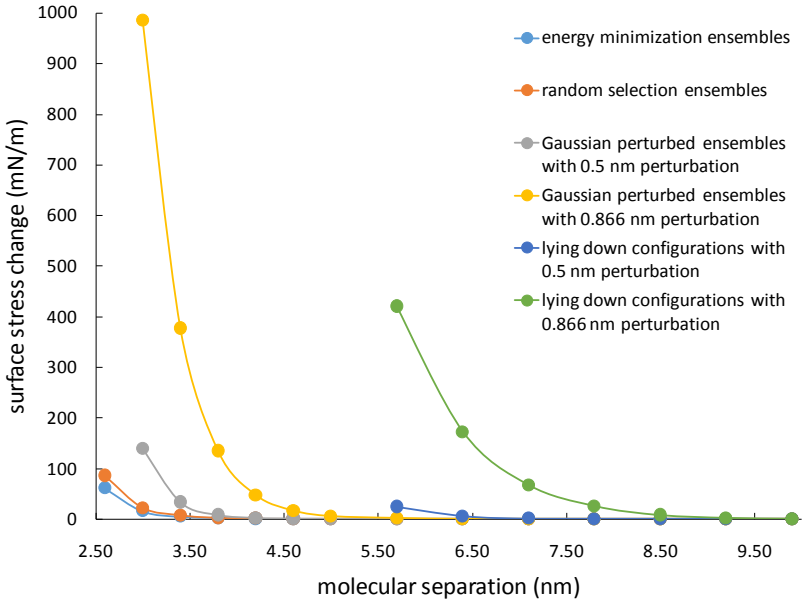

Figure 28. Modeling results of surface stress change with considerations of all molecular ensembles and configurations for single-thiolated approach

The plot is divided into groups according to different ranges of molecular separation based on comparison with length scales of hybridized dsDNA (D_{DNA} and L_{DNA}).When separation is small and $d/D_{DNA} < 1.5$, the Gaussian perturbed ensembles provide very strong surface stress change which indicates the movement of the molecules requires high energy input that the molecules are unlikely to form Gaussian perturbed ensembles in this range. As the separation increases and$d/D_{DNA} > 1.5$, the energy requirement for molecule movement to form Gaussian perturbed ensembles decrease, and molecules are more likely to have greater disorder with larger molecular separation. When the separation further increase, the surface stress predictions drops greatly and all of the three ensembles with standing up configurations predict very small surface stress changes (predictions are close to 0 when $d > 5$ nm). When the separation is comparable to

the chain length of hybridized dsDNA ($d/L_{DNA} > 0.6$), the lying down configurations are achievable. With the lying down configuration, surface stress change predictions are greater than that of standing up configurations with the same immobilization density, hybridization efficiency, and Gaussian perturbation.

In simulations with double-thiolated approach, energy change associated with surface reconstructions are investigated with equations (30) and (31). The influences of the interaction area are simplified to be proportional to the molecular end to end distance of the hybridized dsDNAs. The statistical properties of the distribution of the end to end distance are investigated with a ball-chain model with random-walk assumption in half space. Therefore, the energy change of surface reconstruction can be expressed as equation (39).The energy change is dependent on the total number of hybridized molecules on the surface (*N*), mean value of end to end distances of all hybridized molecules ($\langle s \rangle$), and the strength factors of a single site of surface reconstruction (*a* and *b*).

$$\Delta E_{recon} = \sum s^i \left[a(\varepsilon)^2 + b(\varepsilon) + c\right] = N\langle s \rangle \left[a(\varepsilon)^2 + b(\varepsilon) + c\right] \qquad (39)$$

The total number of hybridized molecules is determined by both immobilization density and hybridization efficiency, or the hybridization density. The distribution of end to end distances are observed with 10^6 realizations of random walk ball chain model in half space, and the probability density function is plotted in Figure 29. For DNA molecules with *n* nucleotides, distribution with an average value of $1.42\sqrt{n}$ nm and a standard deviation of $0.57\sqrt{n}$nm is observed. Therefore if considering all DNA molecules have the same probability to be hybridized, the surface stress prediction is related to the DNA chain length with $\sqrt{n}$.

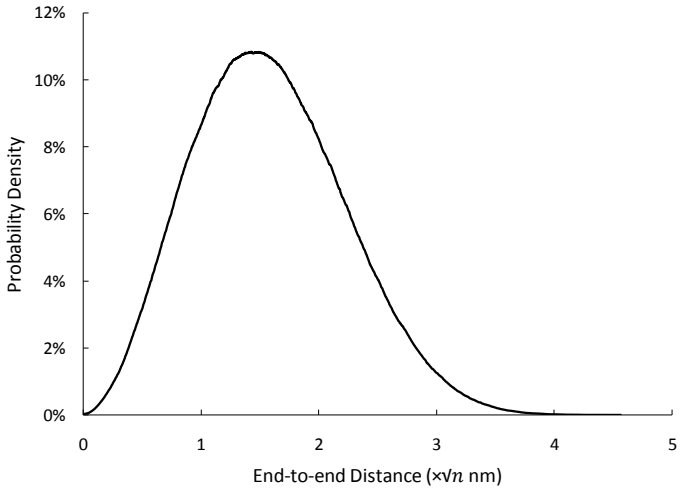

Figure 29. Probability density profile of the distribution of end-to-end distance of ssDNA molecules

The influences of the strength factors of a single site, *a* and *b*, are investigated respectively with DNA molecules with 30 nucleotides, and surface stress changes are plotted with respect to hybridization density in Figure 30. The surface stress predictions are dependent on the hybridization density and the magnitude of the predictions increases as the hybridization density increases in all cases. Strength factor *b* (Figure 30(a)) controls the linear influence on the predictions, and $b < 0$ provides compressive surface stress which drives the cantilever to bend downward. As *b* becomes more negative, the strength of the surface reconstruction induced interaction is stronger, and the surface stress predictions are greater. Strength factor *a* controls the non-linear effects on the surface stress change (Figure 30(b)). When *a* = 0, the predictions will be linear with the hybridization density, while when $a \neq 0$, the non-linear behavior will be obvious. In addition, the sign of *a* determines the slope change of the predictions with respect to hybridization density. If $a < 0$, the surface stress change prediction will be a convex function of hybridization efficiency, while if $a > 0$, it will be a concave function. This means that when $a < 0$, the second order term helps to generate compressive surface stress which will bend the

cantilever down more, and vice versa. The actual values of *a* and *b* in the model will be determined empirically with the reported experimental observations.

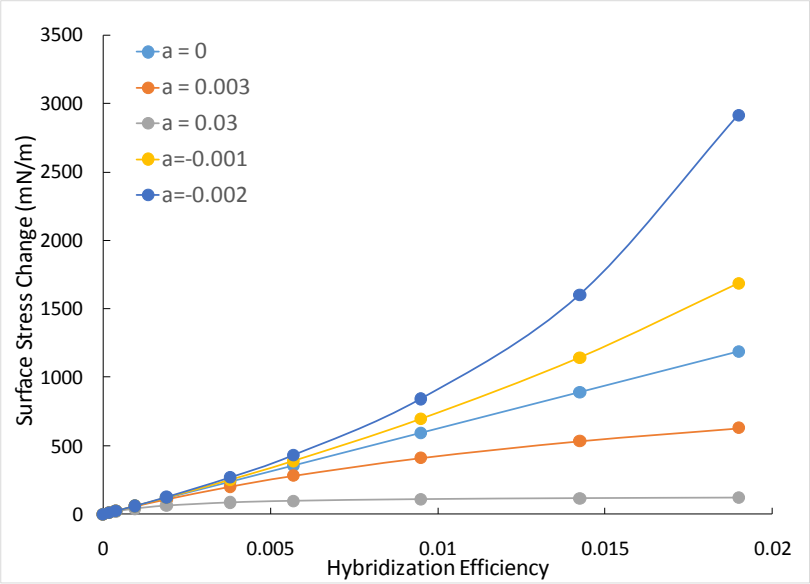

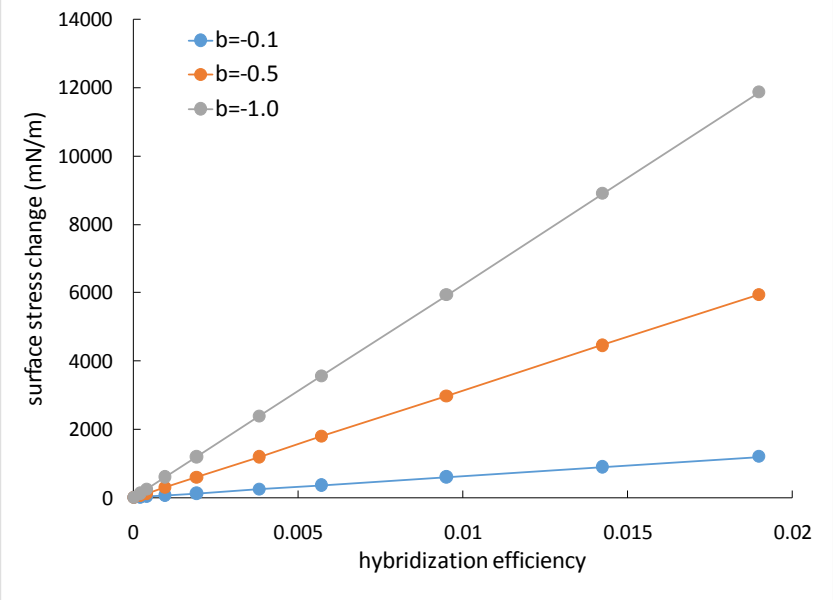

Figure 30. Effects of strength factors (*a* and *b*) on the surface stress predictions: (a) linear effect of *b*; (b) non-linear effect of *a*.

Comparison of Numerical Prediction with Experimental Reports

Numerical predictions of surface stress change are compared to the reported experimental measurements for different immobilization methods, immobilization densities, hybridization efficiencies in order to evaluate our models. The comparison of the surface stress change is plotted in Figure 31 as a function of hybridization density. Most experiments were conducted with single-thiolated approach. Early experimental reports (Strey, Parsegian et al. 1999, Wu, Ji et al. 2001) gave high immobilization densities resulting in molecular separations in the range of 2.6 to 3.0 nm, the corresponding separation/diameter ratio is less than 1.5, and the experiments(Fritz, Baller et al. 2000, Wu, Ji et al. 2001, McKendry, Zhang et al. 2002, Alvarez, Carrascosa et al. 2004, Stachowiak, Yue et al. 2006) observed surface stress change from 1.3 to 6.4 mN/m. The surface stress predictions with these densities are compared to the results. In this separation range ($d/D_{DNA} < 1.5$), random selection and energy minimization ensembles can predict surface stress change that is comparable to the reported measurements. The simulation gave a surface stress range of 0.42-3.1 mN/m (30% hybridization efficiency) to 10-58 mN/m (80% hybridization efficiency) for 10 nucleotides DNA. Though no hybridization efficiencies were reported for these small separation cases, the predictions are of similar magnitude as reported.

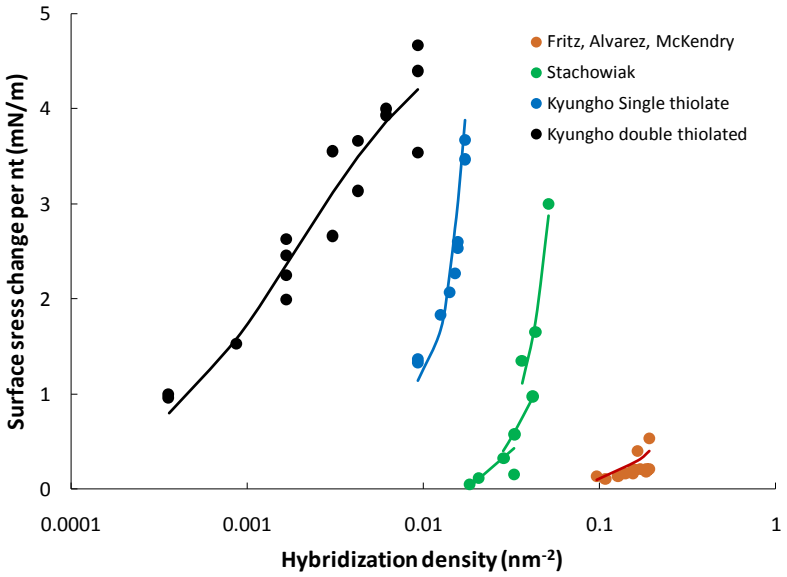

Figure 31. Comparison of numerical predictions with experimental reports for all different immobilization approaches and densities.

When the molecular separation is larger than 3.0 nm, the predictions with random selection and energy minimization ensembles are too small compared to the experimental observations. The large separation correspond to separation/diameter ration greater than 1.5, and in this range, the interactions between neighboring molecules become weak and the space between molecules become large. Therefore it is expected that DNA molecules may be likely to have more disordered distributions, and the influence of spatial perturbation was considered. Predictions with increasing Gaussian perturbation level were conducted in order to match the experimental measurements with reported immobilization densities and hybridization efficiencies. The comparison with reported results by Stachowiak (Stachowiak, Yue et al. 2006) indicated that the ensembles with perturbation from 0.6 to 1.0nm gave best predictions. Another observation is that the perturbation level is controlled by the molecular separation, and the perturbation level is greater as the separation increases. When the separation is small and close to

3 nm, the spatial perturbation is 0.6 nm which means some molecules may only be able to move to the nearest neighboring fcc sites, while when the separation is close to 5 nm, the spatial perturbation is 1.0 nm showing that molecules are able to move up to the third nearest neighboring fcc sites.

When the separation is greater than 6 nm, the simulations with Gaussian perturbed ensembles also fail to predict surface stress changes comparable to experimental reports. The molecules are too far away and the separations are comparable to the chain length of hybridized DNA (($d/L_{DNA} > 0.6$). At this separation, the interactions are very weak between standing up molecules, and the separation is sufficient for molecules to lie down, therefore the influence of the lying-down configuration was considered to predict the surface stress change. Comparison with experimental measurements by Kang(Kang 2011) showed that the Gaussian perturbed ensembles with spatial perturbation of 0.86 nm can best match the reported surface stress values. This perturbation value indicates that with the lying down configurations, the molecules can move up to the second nearest neighboring fcc sites.

For double-thiolated approach, surface stress change were predicted with increasing strength factors (a and b) in order to match the experimentally measured values for reported hybridization densities. Comparison with experimental results(Kang 2011) indicated the strength factors of $a = 0.034$ and $b = -0.127$ result in predictions comparable to measure surface stress change. Comparison of the numerical predictions and experimental results demonstrates that the surface reconstruction model can be used to predict the full range of surface stress change value for double-thiolated approach.

Comparison of the prediction and experimental measurements show that, molecular separation is important for determination of molecular configurations and distributions. When

the molecular separation is small ($d/D_{DNA} < 1.5$), the free space between molecules is small that random selection and energy minimization ensembles with standing up configurations are sufficient to predict the surface stress change reported.

For larger molecular separations ($d/D_{DNA} > 1.5$), a Gaussian perturb ensemble has to be considered due to the large free space between DNA molecules. This indicates that the disorder in the DNA distribution is dominant in surface stress change when separation is large, and the spatial perturbation level can be influenced by the molecular separation that greater perturbations are required for predictions with larger separation.

When the separations are comparable to the chain length of DNA ($d/L_{DNA} > 0.6$), the free space between molecules is sufficient for molecules to lie down. In this separation range, the interactions between molecules are weak that Gaussian perturbed ensembles with standing up molecules fail to predict the surface stress change. Lying down configurations of DNA molecules has to be considered with Gaussian perturbed ensemble that has similar disorder level to that of the standing up configurations.

For double-thiolated approach, the influences of the molecular separation and distribution are negligible due to the low immobilization density and hybridization efficiency. The energy change induced by the surface reconstructions is dominant in determining the surface stress change. The predictions are controlled by the hybridization densities on the cantilever surface, the number of nucleotides in the DNA strands, and the strength of a single hybridized site.

Conclusions

We presented an energy model to examine surface stress change of a microcantilever induced by DNA hybridization in this paper. Different DNA immobilization densities and

hybridization efficiencies are investigated with different DNA distributions and configurations. Molecular separation between molecules is considered to determine the distribution and configuration of hybridized molecules. As the ratio of d/D_{DNA} increases, greater spatial disorder is required to provide higher predictions. When d is comparable to L_{DNA}, lying down configurations are approachable and considered in surface stress predictions. Comparison of numerical predictions and experimental reports indicates the importance of molecular separation in determining the distribution and configurations of DNA molecules as well as the surface stress change. At smaller separations, the random selection and energy minimization ensembles with standing up molecules are able to predict surface stress similar to experimental measurements. At large separations, the Gaussian perturbed ensembles with standing up configurations are required to match the experimental reports. At even larger separations, the lying down configurations are required due to the large free space between molecules. For double-thiolated approach, the interactions between molecules are too weak and energy from surface reconstruction is the dominant origin that drives the surface stress change and cantilever deflections.

CHAPTER 7. CONCLUSIONS

MicroCantilever (MC) based sensors are increasingly being used to detect chemical and biological species in both gas and liquid environments, and these devices could be developed for the use of molecular recognitions. The sensing strategy involves coating one surface of a micromachined cantilever with receptor species that has a high affinity for specific target ligands. The presence of the ligand is detected by resolving the surface stress change associated with absorption/adsorption of receptor molecules immobilized on the sensitized surface. The introduction of cantilevers substantially enriches the portfolio of sensing scenarios that can be used in high performance miniaturized analytical systems.

A miniature sensor consisting of two adjacent micromachined cantilevers (a sensing /reference pair) was utilized for detection of target ligands by measuring the differential surface stress associated with adsorption/absorption of chemical or biological species on the cantilevers. The unique advantages of the surface stress sensor are: 1) differential measurements of surface stress eliminates the influence of environmental disturbances such as nonspecific adsorption, changes in pH, ionic strength, and especially the temperature; and 2) sensitivity of the sensor is independent on the distance between the sensing surface and detectors. Therefore, the sensor is being amenable for miniaturization and enables an array of sensors to be easily fabricated on a single MEMS device.

The threshold sensitivity of the system was improved by utilizing an alternative immobilization approach. There have been many attempts to improve stability and sensitivity of the sensor such as adding polarizers and isolator or selecting microcantilevers with a high aspect-

ratio. Not only did we consider this mechanical or optical aspect of the sensor, but we also designed a new format of a molecular structure to achieve this goal. First attempt was made by attaching a thiol-group on both ends of receptor molecules (ssDNAs) to achieve mechanically rigid and stable immobilization on the gold surface of a sensing cantilever. While binding with target molecules, double-thiolated receptors may give rise to more stress on the cantilever due to configurational change of the receptor molecules and repulsive force between molecules. We verified this improvement by comparing the surface stress generation due to single thiolated and double thiolated receptors with the same immobilization density; DNA hybridization and malachite green (MG)-aptamer binding were utilized as the experiment materials. We observed that the activity of hybridization with the double-thiolated poly Acould reduce the sensitivity as low as two orders of magnitude in surface stress changes compared with the measurement of a single-thiolated poly A, and also reduce the sensitivity by one order of magnitude in surface stress changes with double thiolated MG aptamers compared to the single thiolatedaptamers.

Simulations were carried out to investigate the mechanism underlying the surface stress generation due to different origins, including the immobilization of alkanethiol self-assembled monolayers (SAM), and the hybridization of ssDNAs. Simulation models were investigated to study the dominant influences on the SAM formation. All atom approach was utilized to simulate the potentials of the chemical bonds at atomic level, with bond stretching, bending, and twisting, and the long-range weak van-der-Walls forces. Results of the predictions showed that the inter-chain and intrachain potentials had very small effects on the cantilever bending. And the surface stress change is dominantly due to the surface reconstruction induced by the charge redistribution of the gold atoms on the cantilever surface. When the alkanethiol was immobilized on the gold surface, the sulfur atom would form a strong bond with the gold atoms on the

surface, which would change the electron density of the gold atom, and therefore result in surface reconstructions. Two different modified potential models were utilized in the simulation, the embedded atom method (EAM) and surface embedded atom method (SEAM). The modification of the models were on the electron density, and we assumed the gold atom would lose a certain amount of the electrons due to the Au:S bond. The simulation predictions showed that SEAM was more suitable for surface problem predictions, and provided more reasonable electron loss of the gold atoms. The surface reconstruction was shown to be the dominant effects on the surface stress generation, and the surface stress change increased as the surface coverage density.

In order to investigate the mechanism of the surface stress generation, a beam bending model was established based on the total energy of the system. The overall energy consisted of the bending energy of the cantilever and the interaction energy induced by DNA hybridization. Experimental reports were collected from different groups working with different immobilization densities and hybridization efficiencies. The analysis with the experimental observations showed that, the surface stress changes would fall into different stages based on the immobilization density levels. Three different stages of immobilization were proposed accordingly, the standing-up stage, lying-down stage, and attachment stage. Among the three different stages, the attachment stage was due to alternative immobilization method, with which the molecules were immobilized on to the cantilever surface with both ends and thus dragged to the surface. The standing-up and lying-down stages were determined by the immobilization density. High immobilization density would lead to small molecular distance and strong inter-molecular repulsions which would push the molecules to stand up, while low immobilization density would provide low inter-molecular forces, and have the molecules to lie down closer to the surface. The

molecular distribution of the DNA molecules was proved to be another essential factor on surface stress generation. A two-step model to determine the DNA distribution was proposed. In this model, the ssDNA was assumed to be immobilized on the cantilever surface based on a hexagonal pattern, and the certain amount of DNA molecules were selected to be hybridized afterwards. The results showed that the new model could provide better predictions than the general average spacing model. Another observation was that the randomness would also play an important role in surface stress generation. For high immobilization density, the molecules are close to each other and the distribution of the molecules would follow the hexagonal pattern, while when the immobilization density became low, the distribution would have more randomness, and the randomness came from the distribution of the ssDNA immobilization as well as selected sites for the hybridization. Predictions showed that Gaussian perturbation with 10-20% standard deviation could provide sufficient randomness for the distribution.

Future work of this study is to expand the measurements and simulations to more aptamer/target binding. More sensitive and compact sensor system is desired. The sensor system can be modified to be smaller and even portable which will be more convenient to use, or larger and with higher stability and sensitivity. More experimental materials can be applied to verify the system in other type of chemical or biological reactions. Simulation models can be expanded to investigate mechanisms for different types or chemical and biological reactions besides DNA hybridizations. More potential models need to be find out for different reaction types and environments.

BIBLIOGRAPHY

Allison, D. P., T. Thundat, P. Modrich, R. J. Isfort, M. J. Doktycz, P. S. Kerper and R. J. Warmack (1995). "Mapping Site-Specific Endonuclease Binding to DNA by Direct Imaging with Afm." Ultrasensitive Instrumentation for DNA Sequencing and Biochemical Diagnostics, Proceedings Of **2386**: 24-29.

Alvarez, M., L. G. Carrascosa, M. Moreno, A. Calle, A. Zaballos, L. M. Lechuga, C. Martinez-A and J. Tamayo (2004). "Nanomechanics of the formation of DNA self-assembled monolayers and hybridization on microcantilevers." Langmuir **20**(22): 9663-9668.

Andreoni, W., A. Curioni and H. Gronbeck (2000). "Density functional theory approach to thiols and disulfides on gold: Au(111) surface and clusters." International Journal of Quantum Chemistry **80**(4-5): 598-608.

Arntz, Y., J. D. Seelig, H. P. Lang, J. Zhang, P. Hunziker, J. P. Ramseyer, E. Meyer, M. Hegner and C. Gerber (2003). "Label-free protein assay based on a nanomechanical cantilever array." Nanotechnology **14**(1): 86-90.

Beardmore, K. M., J. D. Kress, A. R. Bishop and N. GronbechJensen (1997). "Ab-initio calculations of the gold-sulfur interaction for alkanethiol monolayers." Synthetic Metals **84**(1-3): 317-318.

Berger, R., E. Delamarche, H. P. Lang, C. Gerber, J. K. Gimzewski, E. Meyer and H. J. Guntherodt (1997). "Surface stress in the self-assembly of alkanethiols on gold." Science **276**(5321): 2021-2024.

Biswal, S. L., D. Raorane, A. Chaiken, H. Birecki and A. Majumdar (2006). "Nanomechanical detection of DNA melting on microcantilever surfaces." Analytical Chemistry **78**(20): 7104-7109.

Biswal, S. L., D. Raorane, A. Chaiken and A. Majumdar (2006). "Nanomechanical motion from microcantilevers as a platform for detecting phase changes of macromolecules." Abstracts of Papers of the American Chemical Society **231**.

Bosio, S. B. M. and W. L. Hase (1997). "Energy transfer in rare gas collisions with self-assembled monolayers." Journal of Chemical Physics **107**(22): 9677-9686.

Brenner, S. L. and Parsegia.Va (1974). "PHYSICAL METHOD FOR DERIVING ELECTROSTATIC INTERACTION BETWEEN ROD-LIKE POLYIONS AT ALL MUTUAL ANGLES." Biophysical Journal **14**(14): 327-334.

Chen, G. Y., R. J. Warmack, T. Thundat, D. P. Allison and A. Huang (1994). "Resonance Response of Scanning Force Microscopy Cantilevers." Review of Scientific Instruments **65**(8): 2532-2537.

Cyganik, P., M. Buck, J. D. E. T. Wilton-Ely and C. Woll (2005). "Stress in self-assembled monolayers: omega-biphenyl alkane thiols on Au(111)." Journal Of Physical Chemistry B **109**(21): 10902-10908.

Dannenberger, O., M. Buck and M. Grunze (1999). "Self-assembly of n-alkanethiols: A kinetic study by second harmonic generation." Journal of Physical Chemistry B **103**(12): 2202-2213.

Dareing, D. W. and T. Thundat (2005). "Simulation of adsorption-induced stress of a microcantilever sensor." Journal of Applied Physics **97**(4).

Daw, M. S. and M. I. Baskes (1983). "SEMIEMPIRICAL, QUANTUM-MECHANICAL CALCULATION OF HYDROGEN EMBRITTLEMENT IN METALS." Physical Review Letters **50**(17): 1285-1288.

Daw, M. S. and M. I. Baskes (1984). "EMBEDDED-ATOM METHOD - DERIVATION AND APPLICATION TO IMPURITIES, SURFACES, AND OTHER DEFECTS IN METALS." Physical Review B **29**(12): 6443-6453.

Demers, L. M., C. A. Mirkin, R. C. Mucic, R. A. Reynolds, R. L. Letsinger, R. Elghanian and G. Viswanadham (2000). "A fluorescence-based method for determining the surface coverage and hybridization efficiency of thiol-capped oligonucleotides bound to gold thin films and nanoparticles." Analytical Chemistry **72**(22): 5535-5541.

Desikan, R., S. Armel, H. M. Meyer and T. Thundat (2007). "Effect of chain length on nanomechanics of alkanethiol self-assembly." Nanotechnology **18**(42).

Desikan, R., I. Lee and T. Thundat (2006). "Effect of nanometer surface morphology on surface stress and adsorption kinetics of alkanethiol self-assembled monolayers." Ultramicroscopy **106**(8-9): 795-799.

Dutta, P., C. A. Tipple, N. V. Lavrik, P. G. Datskos, H. Hofstetter, O. Hofstetter and M. J. Sepaniak (2003). "Enantioselective sensors based on antibody-mediated nanomechanics." Analytical Chemistry **75**(10): 2342-2348.

Ferrari, M. (2005). "Cancer nanotechnology: Opportunities and challenges." Nature Reviews Cancer **5**(3): 161-171.

Foiles, S. M., M. I. Baskes and M. S. Daw (1986). "EMBEDDED-ATOM-METHOD FUNCTIONS FOR THE FCC METALS CU, AG, AU, NI, PD, PT, AND THEIR ALLOYS." Physical Review B **33**(12): 7983-7991.

Franzen, S. (2003). "Density functional calculation of a potential energy surface for alkane thiols on Au(111) as function of alkane chain length." Chemical Physics Letters **381**(3-4): 315-321.

Fritz, J. (2008). "Cantilever biosensors." Analyst **133**(7): 855-863.

Fritz, J., M. K. Baller, H. P. Lang, H. Rothuizen, P. Vettiger, E. Meyer, H. J. Guntherodt, C. Gerber and J. K. Gimzewski (2000). "Translating biomolecular recognition into nanomechanics." Science **288**(5464): 316-318.

Fritz, J., M. K. Baller, H. P. Lang, T. Strunz, E. Meyer, H. J. Guntherodt, E. Delamarche, C. Gerber and J. K. Gimzewski (2000). "Stress at the solid-liquid interface of self-assembled monolayers on gold investigated with a nanomechanical sensor." Langmuir **16**(25): 9694-9696.

Ghosh, S., S. Mishra and R. Mukhopadhyay (2014). "Enhancing sensitivity in a piezoresistive cantilever-based label-free DNA detection assay using ssPNA sensor probes." Journal of Materials Chemistry B **2**(8): 960.

Godin, M., V. Tabard-Cossa, P. Grutter and P. Williams (2001). "Quantitative surface stress measurements using a microcantilever." Applied Physics Letters **79**(4): 551-553.

Godin, M., V. Tabard-Cossa, Y. Miyahara, T. Monga, P. J. Williams, L. Y. Beaulieu, R. B. Lennox and P. Grutter (2010). "Cantilever-based sensing: the origin of surface stress and optimization strategies." Nanotechnology **21**(7).

Godin, M., P. J. Williams, V. Tabard-Cossa, O. Laroche, L. Y. Beaulieu, R. B. Lennox and P. Grutter (2004). "Surface stress, kinetics, and structure of alkanethiol self-assembled monolayers." Langmuir **20**(17): 7090-7096.

Grogan, C., R. Raiteri, G. M. O'Connor, T. J. Glynn, V. Cunningham, M. Kane, M. Charlton and D. Leech (2002). "Characterisation of an antibody coated microcantilever as a potential immuno-based biosensor." Biosensors & Bioelectronics **17**(3): 201-207.

Gronbeck, H. and W. Andreoni (2000). "Gold and platinum microclusters and their anions: comparison of structural and electronic properties." Chemical Physics **262**(1): 1-14.

Haftel, M. I. and M. Rosen (1995). "MOLECULAR-DYNAMICS DESCRIPTION OF EARLY FILM DEPOSITION OF AU ON AG(110)." Physical Review B **51**(7): 4426-4434.

Hagan, M. F., A. Majumdar and A. K. Chakraborty (2002). "Nanomechanical forces generated by surface grafted DNA." Journal of Physical Chemistry B **106**(39): 10163-10173.

Hansen, K. M., H. F. Ji, G. H. Wu, R. Datar, R. Cote, A. Majumdar and T. Thundat (2001). "Cantilever-based optical deflection assay for discrimination of DNA single-nucleotide mismatches." Analytical Chemistry **73**(7): 1567-1571.

Hood, L., J. R. Heath, M. E. Phelps and B. Y. Lin (2004). "Systems biology and new technologies enable predictive and preventative medicine." Science **306**(5696): 640-643.

Ibach, H. (1997). "The role of surface stress in reconstruction, epitaxial growth and stabilization of mesoscopic structures." Surface Science Reports **29**(5-6): 195-263.

Ilic, B., D. Czaplewski, M. Zalalutdinov, H. G. Craighead, P. Neuzil, C. Campagnolo and C. Batt (2001). "Single cell detection with micromechanical oscillators." Journal of Vacuum Science & Technology B **19**(6): 2825-2828.

Ji, H.-F. and B. D. Armon (2010). "Approaches to Increasing Surface Stress for Improving Signal-to-Noise Ratio of Microcantilever Sensors." Analytical Chemistry **82**(5): 1634-1642.

Jiang, S. Y. (2002). "Molecular simulation studies of self-assembled monolayers of alkanethiols on Au(111)." Molecular Physics **100**(14): 2261-2275.

Jin, K. S., S. R. Shin, B. Ahn, Y. Rho, S. J. Kim and M. Ree (2009). "pH-Dependent Structures of an i-Motif DNA in Solution." Journal of Physical Chemistry B **113**(7): 1852-1856.

Kadam, A. R., G. P. Nordin and M. A. George (2006). "Use of thermally induced higher order modes of a microcantilever for mercury vapor detection." Journal of Applied Physics **99**(9).

Kang, K. (2011). "MicroCantilever (MC) based nanomechanical sensor for detection of molecular interactions."

Kang, K., M. Nilsen-Hamilton and P. Shrotriya (2008). "Differential surface stress sensor for detection of chemical and biological species." Applied Physics Letters **93**(14).

Kang, K., M. Nilsen-Hamilton and P. Shrotriya (2009). "Novel Differential Surface Stress Sensor for Detection of DNA Hybridization." Proceedings of the Asme Summer Bioengineering Conference - 2009, Pt a and B: 1159-1160.

Kang, K. G. and P. Shrotriya (2008). "Novel differential surface stress sensor for detection of chemical and biological species." Microelectromechanical Systems - Materials And Devices **1052**: 171-176.

Kim, S. K., H. Cho, J. Jeong, J. N. Kwon, Y. Jung and B. H. Chung (2010). "Label-free and naked eye detection of PNA/DNA hybridization using enhancement of gold nanoparticles." Chem Commun (Camb) **46**(19): 3315-3317.

Kukta, R. V., D. Kouris and K. Sieradzki (2003). "Adatoms and their relation to surface stress." Journal of the Mechanics and Physics of Solids **51**(7): 1243-1266.

Lachut, M. J. and J. E. Sader (2007). "Effect of surface stress on the stiffness of cantilever plates." Physical Review Letters **99**(20).

Lang, H. P., R. Berger, F. Battiston, J. P. Ramseyer, E. Meyer, C. Andreoli, J. Brugger, P. Vettiger, M. Despont, T. Mezzacasa, L. Scandella, H. J. Guntherodt, C. Gerber and J. K. Gimzewski (1998). "A chemical sensor based on a micromechanical cantilever array for the identification of gases and vapors." Applied Physics a-Materials Science & Processing **66**: S61-S64.

Lavrik, N. V., M. J. Sepaniak and P. G. Datskos (2004). "Cantilever transducers as a platform for chemical and biological sensors." Review of Scientific Instruments **75**(7): 2229-2253.

Leikin, S., V. A. Parsegian, D. C. Rau and R. P. Rand (1993). "HYDRATION FORCES." Annual Review of Physical Chemistry **44**: 369-395.

Lim, S. H., D. Raorane, S. Satyanarayana and A. Majumdar (2006). "Nano-chemo-mechanical sensor array platform for high-throughput chemical analysis." Sensors and Actuators B-Chemical **119**(2): 466-474.

Maraldo, D., F. U. Garcia and R. Mutharasan (2007). "Method for quantification of a prostate cancer biomarker in urine without sample preparation." Analytical Chemistry **79**(20): 7683-7690.

Marie, R., J. Thaysen, C. B. V. Christensen and A. Boisen (2003). "A cantilever-based sensor for thermal cycling in buffer solution." Microelectronic Engineering **67-8**: 893-898.

McKendry, R., J. Y. Zhang, Y. Arntz, T. Strunz, M. Hegner, H. P. Lang, M. K. Baller, U. Certa, E. Meyer, H. J. Guntherodt and C. Gerber (2002). "Multiple label-free biodetection and quantitative DNA-binding assays on a nanomechanical cantilever array." Proceedings of the National Academy of Sciences of the United States of America **99**(15): 9783-9788.

Mertens, J., C. Rogero, M. Calleja, D. Ramos, J. A. Martin-Gago, C. Briones and J. Tamayo (2008). "Label-free detection of DNA hybridization based on hydration-induced tension in nucleic acid films." Nature Nanotechnology **3**(5): 301-307.

Moulin, A. M., S. J. O'Shea, R. A. Badley, P. Doyle and M. E. Welland (1999). "Measuring surface-induced conformational changes in proteins." Langmuir **15**(26): 8776-8779.

Mukhopadhyay, R., V. V. Sumbayev, M. Lorentzen, J. Kjems, P. A. Andreasen and F. Besenbacher (2005). "Cantilever sensor for nanomechanical detection of specific protein conformations." Nano Letters **5**(12): 2385-2388.

Osawa, Y., M. Takase, K. Sode and K. Ikebukuro (2009). "DNA Aptamers that Bind to PQQGDH as an Electrochemical Labeling Tool." Electroanalysis **21**(11): 1303-1308.

Pei, H., N. Lu, Y. Wen, S. Song, Y. Liu, H. Yan and C. Fan (2010). "A DNA nanostructure-based biomolecular probe carrier platform for electrochemical biosensing." Adv Mater **22**(42): 4754-4758.

Pei, H., N. Lu, Y. L. Wen, S. P. Song, Y. Liu, H. Yan and C. H. Fan (2010). "A DNA Nanostructure-based Biomolecular Probe Carrier Platform for Electrochemical Biosensing." Advanced Materials **22**(42): 4754-+.

Poirier, G. E. and E. D. Pylant (1996). "The self-assembly mechanism of alkanethiols on Au(111)." Science **272**(5265): 1145-1148.

Raiteri, R., M. Grattarola, H. J. Butt and P. Skladal (2001). "Micromechanical cantilever-based biosensors." Sensors and Actuators B-Chemical **79**(2-3): 115-126.

Raiteri, R., G. Nelles, H. J. Butt, W. Knoll and P. Skladal (1999). "Sensing of biological substances based on the bending of microfabricated cantilevers." Sensors and Actuators B-Chemical **61**(1-3): 213-217.

Rappe, A. K., C. J. Casewit, K. S. Colwell, W. A. Goddard and W. M. Skiff (1992). "UFF, A FULL PERIODIC-TABLE FORCE-FIELD FOR MOLECULAR MECHANICS AND MOLECULAR-DYNAMICS SIMULATIONS." Journal of the American Chemical Society **114**(25): 10024-10035.

Sader, J. E., J. W. M. Chon and P. Mulvaney (1999). "Calibration of rectangular atomic force microscope cantilevers." Review Of Scientific Instruments **70**(10): 3967-3969.

Sader, J. E. and L. White (1993). "Theoretical-Analysis Of the Static Deflection Of Plates for Atomic-Force Microscope Applications." Journal Of Applied Physics **74**(1): 1-9.

Savran, C. A., T. P. Burg, J. Fritz and S. R. Manalis (2003). "Microfabricated mechanical biosensor with inherently differential readout." Applied Physics Letters **83**(8): 1659-1661.

Savran, C. A., S. M. Knudsen, A. D. Ellington and S. R. Manalis (2004). "Micromechanical detection of proteins using aptamer-based receptor molecules." Analytical Chemistry **76**(11): 3194-3198.

Seena, V., A. Rajoriya, A. Fernandes, K. Dhale, P. Pant, S. Mukherji, V. R. Rao and Ieee (2010). FABRICATION AND CHARACTERIZATION OF NOVEL POLYMER COMPOSITE MICROCANTILEVER SENSORS FOR EXPLOSIVE DETECTION. Mems 2010: 23rd Ieee International Conference on Micro Electro Mechanical Systems, Technical Digest**:** 851-854.

Sengupta, S. and R. Sasisekharan (2007). "Exploiting nanotechnology to target cancer." British Journal of Cancer **96**(9): 1315-1319.

Shekhawat, G. S. and V. P. Dravid (2013). "Nanomechanical sensors: Bent on detecting cancer." Nat Nanotechnol **8**(2): 77-78.

Shor, N. Z. (1985). Minimization methods for non-differentiable functions New York : Springer-Verlag.

Shrotriya, P., K. K. S. Karuppiah, R. Zhang, A. Chandra and S. Sundararajan (2008). "Surface stress generation during formation of alkanethiol self-assembled monolayer (SAM)." Mechanics Research Communications **35**(1-2): 43-49.

Smith, S. B., Y. Cui and C. Bustamante (1996). "Overstretching B-DNA: The Elastic Response of Individual Double-Stranded and Single-Stranded DNA Molecules." Science **271**(5250): 795-799.

Stachowiak, J. C., M. Yue, K. Castelino, A. Chakraborty and A. Majumdar (2006). "Chemomechanics of surface stresses induced by DNA hybridization." Langmuir **22**(1): 263-268.

Stoney, G. G. (1909). "The tension of metallic films deposited by electrolysis." Proceedings of the Royal Society of London Series a-Containing Papers of a Mathematical and Physical Character **82**(553): 172-175.

Stoney, G. G. (1909). "The tension of metallic films deposited by electrolysis." Proceedings of the Royal Society of London: A **82**: 172-175.

Strey, H. H., V. A. Parsegian and R. Podgornik (1997). "Equation of state for DNA liquid crystals: Fluctuation enhanced electrostatic double layer repulsion." Physical Review Letters **78**(5): 895-898.

Strey, H. H., V. A. Parsegian and R. Podgornik (1999). "Equation of state for polymer liquid crystals: Theory and experiment." Physical Review E **59**(1): 999-1008.

Su, M. and V. P. Dravid (2005). "Surface combustion microengines based on photocatalytic oxidations of hydrocarbons at room temperature." Nano Letters **5**(10): 2023-2028.

Tamayo, J., A. D. L. Humphris, A. M. Malloy and M. J. Miles (2001). "Chemical sensors and biosensors in liquid environment based on microcantilevers with amplified quality factor." Ultramicroscopy **86**(1-2): 167-173.

Thaysen, J., A. D. Yalcinkaya, P. Vettiger and A. Menon (2002). "Polymer-based stress sensor with integrated readout." Journal of Physics D-Applied Physics **35**(21): 2698-2703.

Thundat, T., L. Pinnaduwage and R. Lareau (2004). Explosive vapour detection using micromechanical sensors. Electronic Noses & Sensors for the Detection of Explosives. J. W. Gardner and J. Yinon. **159:** 249-266.

Thundat, T., E. A. Wachter, S. L. Sharp and R. J. Warmack (1995). "Detection of Mercury-Vapor Using Resonating Microcantilevers." Applied Physics Letters **66**(13): 1695-1697.

Thundat, T., R. J. Warmack, D. P. Allison and K. B. Jacobson (1994). "Critical-Point Mounting of Kinetoplast DNA for Atomic-Force Microscopy." Scanning Microscopy **8**(1): 23-30.

Thundat, T., R. J. Warmack, G. Y. Chen and D. P. Allison (1994). "Thermal and Ambient-Induced Deflections of Scanning Force Microscope Cantilevers." Applied Physics Letters **64**(21): 2894-2896.

Torres-Chavolla, E. and E. C. Alocilja (2009). "Aptasensors for detection of microbial and viral pathogens." Biosensors & Bioelectronics **24**(11): 3175-3182.

Urwyler, P., H. Schift, J. Gobrecht, O. Häfeli, M. Altana, F. Battiston and B. Müller (2011). "Surface patterned polymer micro-cantilever arrays for sensing." Sensors and Actuators A: Physical **172**(1): 2-8.

Vemparala, S., B. B. Karki, R. K. Kalia, A. Nakano and P. Vashishta (2004). "Large-scale molecular dynamics simulations of alkanethiol self-assembled monolayers." Journal of Chemical Physics **121**(9): 4323-4330.

Wang, J., G. Chen, H. Jiang, Z. Li and X. Wang (2013). "Advances in nano-scaled biosensors for biomedical applications." Analyst **138**(16): 4427-4435.

Wang, T. J., J. A. Hoy, M. H. Lamm and M. Nilsen-Hamilton (2009). "Computational and Experimental Analyses Converge to Reveal a Coherent Yet Malleable Aptamer Structure That Controls Chemical Reactivity." Journal Of the American Chemical Society **131**(41): 14747-14755.

Weizmann, Y., F. Patolsky, O. Lioubashevski and I. Willner (2004). "Magneto-mechanical detection of nucleic acids and telomerase activity in cancer cells." Journal of the American Chemical Society **126**(4): 1073-1080.

White, R. J., N. Phares, A. A. Lubin, Y. Xiao and K. W. Plaxco (2008). "Optimization of electrochemical aptamer-based sensors via optimization of probe packing density and surface chemistry." Langmuir **24**(18): 10513-10518.

Wu, G. H., R. H. Datar, K. M. Hansen, T. Thundat, R. J. Cote and A. Majumdar (2001). "Bioassay of prostate-specific antigen (PSA) using microcantilevers." Nature Biotechnology **19**(9): 856-860.

Wu, G. H., H. F. Ji, K. Hansen, T. Thundat, R. Datar, R. Cote, M. F. Hagan, A. K. Chakraborty and A. Majumdar (2001). "Origin of nanomechanical cantilever motion generated from biomolecular interactions." Proceedings of the National Academy of Sciences of the United States of America **98**(4): 1560-1564.

Xia, T. K., O. Y. Jian, M. W. Ribarsky and U. Landman (1992). "Interfacial Alkane Films." Physical Review Letters **69**(13): 1967-1970.

Yue, M., H. Lin, D. E. Dedrick, S. Satyanarayana, A. Majumdar, A. S. Bedekar, J. W. Jenkins and S. Sundaram (2004). "A 2-D microcantilever array for multiplexed biomolecular analysis." Journal of Microelectromechanical Systems **13**(2): 290-299.

Yue, M., J. C. Stachowiak, H. Lin, R. Datar, R. Cote and A. Majumdar (2008). "Label-free protein recognition two-dimensional array using nanomechanical sensors." Nano Letters **8**(2): 520-524.

Zhai, L. J., T. J. Wang, K. Kang, Y. Zhao, P. Shrotriya and M. Nilsen-Hamilton (2012). "An RNA Aptamer-Based Microcantilever Sensor To Detect the Inflammatory Marker, Mouse Lipocalin-2." Analytical Chemistry **84**(20): 8763-8770.

Zhang, J., H. P. Lang, F. Huber, A. Bietsch, W. Grange, U. Certa, R. McKendry, H. J. Guntgerodt, M. Hegner and C. Gerber (2006). "Rapid and label-free nanomechanical detection of biomarker transcripts in human RNA." Nature Nanotechnology **1**(3): 214-220.

Zhang, J., H. P. Lang, G. Yoshikawa and C. Gerber (2012). "Optimization of DNA hybridization efficiency by pH-driven nanomechanical bending." Langmuir **28**(15): 6494-6501.

Zhang, L. Z., W. A. Goddard and S. Y. Jiang (2002). "Molecular simulation study of the c(4x2) superlattice structure of alkanethiol self-assembled monolayers on Au(111)." Journal of Chemical Physics **117**(15): 7342-7349.

Zhang, N.-H. and J.-Y. Shan (2008). "An energy model for nanomechanical deflection of cantilever-DNA chip." Journal of the Mechanics and Physics of Solids **56**(6): 2328-2337.

Zhang, N. H. and J. Z. Chen (2009). "Mechanical properties of double-stranded DNA biolayers immobilized on microcantilever under axial compression." J Biomech **42**(10): 1483-1487.

Zhang, N. H., J. Z. Chen, J. J. Li and Z. Q. Tan (2010). "Mechanical properties of DNA biofilms adsorbed on microcantilevers in label-free biodetections." Biomaterials **31**(25): 6659-6666.

Zhang, N. H., W. L. Meng and Z. Q. Tan (2013). "A multi-scale model for the analysis of the inhomogeneity of elastic properties of DNA biofilm on microcantilevers." Biomaterials **34**(7): 1833-1842.

Zhang, N. H., Z. Q. Tan, J. J. Li, W. L. Meng and L. W. Xu (2011). "Interactions of single-stranded DNA on microcantilevers." Current Opinion in Colloid & Interface Science **16**(6): 592-596.

Zhao, Y., B. Ganapathysubramanian and P. Shrotriya (2012). "Cantilever deflection associated with hybridization of monomolecular DNA film." Journal of Applied Physics **111**(7): 074310.

Zhao, Y., B. Ganapathysubramanian and P. Shrotriya (2012). "Cantilever deflection associated with hybridization of monomolecular DNA film." Journal Of Applied Physics **111**(7).

Zuo, G. M., X. X. Li, Z. X. Zhang, T. T. Yang, Y. L. Wang, Z. X. Cheng and S. L. Feng (2007). "Dual-SAM functionalization on integrated cantilevers for specific trace-explosive sensing and non-specific adsorption suppression." Nanotechnology **18**(25).